STRUCTURAL DYNAMICS OF SINGLE PHOTOACTIVE YELLOW PROTEIN MOLECULE MONITORED WITH SURFACE ENHANCED RAMAN SCATTERING SUBSTRATES

By
KUSHAGRA SINGHAL
Bachelor of Science in Mechanical Engineering
Indian Institute of Technology
Kanpur, U.P. (India)
2006

Submitted to the Faculty of the
Graduate College of the
Oklahoma State University
in partial fulfillment of
the requirements for
the Degree of
MASTER OF SCIENCE
May, 2009

STRUCTURAL DYNAMICS OF SINGLE PHOTOACTIVE YELLOW PROTEIN MOLECULE MONITORED WITH SURFACE ENHANCED RAMAN SCATTERING SUBSTRATES

Thesis Approved:

Dr. Kaan Kalkan

Thesis Adviser

Dr. Raman Singh

Dr. Aihua Xie

Dr. A. Gordon Emslie

Dean of the Graduate College

ACKNOWLEDGMENTS

First and foremost, I would like to acknowledge the efforts and guidance of Dr. Kaan Kalkan. Without his hard work and vision, this thesis would not have been possible. For this and for his patience, I am really grateful to him. Also, without the funding by OSU Regents (OSHRE), none of this would have materialized.

I would also like to thank Dr. Aihua Xie and Dr. Wouter Hoff for not only providing us with PYP samples, but also for their guidance and contribution to the discussions in the study. Besides, I extend my gratitude to Zhouyang Kang for his computational work, which helped us gain more understanding from our SM-SERS spectra. The discussions involving him and Dr. Xie have also been very fruitful.

I am really thankful to my colleague Karthik Bhatt who has been a great help, especially with AFM and providing some out-of-the-box suggestions that were quite helpful. Also, I can't disregard the help by Dr. Susheng Tan in obtaining the AFM scans of substrates. Lately, the discussions with and fresh ideas brought by my colleague Jianting Liu have been of great help too.

Finally, I would like to thank my parents and girlfriend for their patience and support (financially as well as morally) during the study.

Kushagra Singhal

TABLE OF CONTENTS

LIST OF TABLES

LIST OF FIGURES

CHAPTER I. INTRODUCTION

Protein functions in biosystems vary from light sensing in vision to break-down of nutrients in digestion. These functions are performed through a series of transient conformational changes that involve a diversity of pathways and distribution of time scales from one molecule to another. Such heterogeneity is, however, averaged out and masked by ensemble-averaged measurements,[1] thus hinting at the significance of single-molecule (SM) studies. In the present work, high-enhancement factor SERS substrates were developed to study the distinct conformational changes of a single photoactive yellow protein (PYP) molecule during its photo-excitation.

Photoactive Yellow Protein (PYP) is a small (14 kDa) cytosolic photoreceptor protein with 125 amino acid residues.[2, 3] It belongs to the family of Xanthopsins [4] and is responsible for the negative phototactic response of its host organism *Halorhodospira halophila* (thus the wild type PYP is called Hal-PYP).[5] With its high water-solubility and ease of crystallization along with its high chemical- and photo-stability, PYP has emerged as an ideal model for studies in photochemistry and protein-folding.[6] The similarity of PYP in its spectroscopic properties as well as mechanistic functions with other photoreceptor proteins – rhodopsins (vision in animals),[3, 7] phytochromes (light quality analysis in plants),[8, 9] sensory rhodopsins,[10-12] bacterio- and halo-rhodopsins (ion pumps),[13, 14] and bacterial phytochromes[15] – has made it a widely employed tool to study fundamental protein functions.

The present work employs surface-enhanced Raman scattering (SERS) using indigenously prepared “nanometal-on-semiconductor-thin-film” substrates to conduct single molecule studies at low (~10^{-9} M) concentrations of PYP. SERS is a surface-sensitive technique that results in the enhancement of Raman scattering of molecules adsorbed on nano-structured metallic surfaces.[16] Raman scattering, first postulated by Smekal [17] in 1923 and experimentally observed in 1928 by C. V. Raman,[18] measures inelastic scattering of photons as a result of their interaction with the vibronic states (electronic state coupled with a vibrational state) of molecules or condensed matter. The resultant shift in energy of the photon results from a phonon creation (Stokes shift) or annihilation (Anti-Stokes shift), and therefore characterizes a certain vibrational mode (Figure I.1). Figure I.2 shows 3 of such normal modes of vibration in a tri-atomic molecule, which provide information about the molecular structure:[19]

- Stretching between two bonded atoms, which can be further categorized into 2 types - Symmetric and Asymmetric stretching.
- Bending between three atoms connected by two bonds.
- Out-of-plane deformation modes.

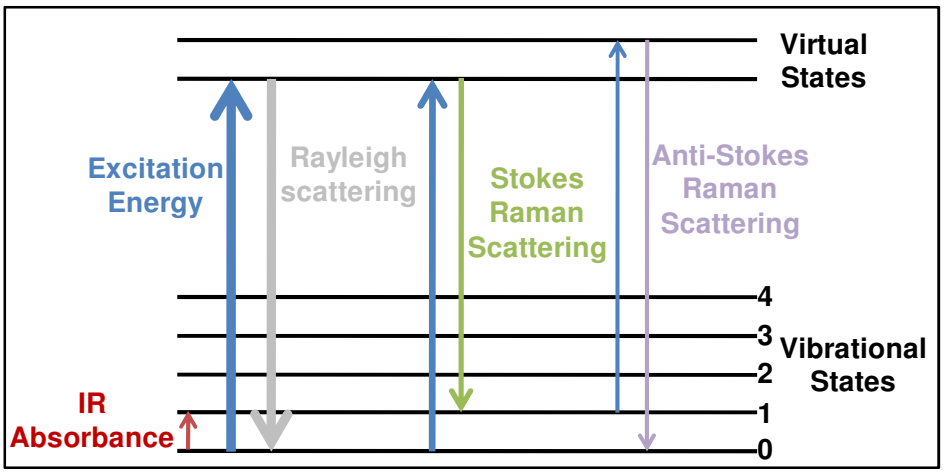

Figure I.1. Energy level diagram to demonstrate Raman scattering. Thickness of lines indicates the signal strength of different mechanisms of scattering.[20]

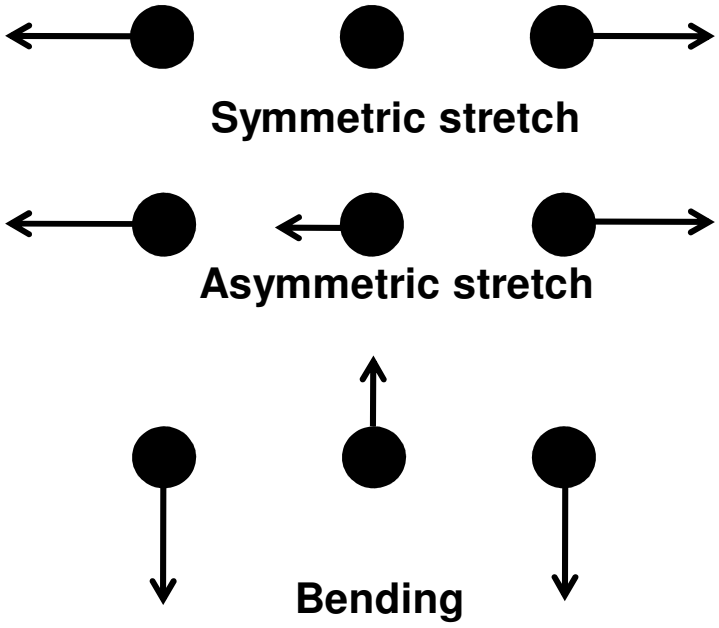

Figure I.2. Normal modes of vibration in a tri-atomic molecule.

Compared to other single molecule techniques like fluorescence spectroscopy, atomic force microscopy (AFM) and FRET, Raman spectrum of a molecule contains a high degree of structural information about it, thus making SERS an efficient single-molecule detection technique. However, realization of single-molecule SERS detection

depends on the employment of efficient and reproducible substrates, which in turn depends on a myriad of factors. First, unless the laser excitation is resonant with electronic excitation of the molecule allowing resonant Raman-effect, the metal surface is required to be agent-free in order to allow electron transfer between the analyte and metal (i.e. chemical enhancement). Further, the surface should be impurity-free, as impurities lead to chemical-interface damping of plasmon modes; and the reduced plasmon lifetime accounts for a dramatic decrease in SERS gain factor (i.e., SERS gain factor $\propto$ (plasmon lifetime)^4).

Second, single molecule sensitivity requires a minimum electromagnetic gain of 10^8 with a resonant Raman contribution of 10^6. However, a single silver nanoparticle can at most provide an electromagnetic enhancement of 10^4. In single molecule SERS, the required gigantic enhancements (i.e., hot spots) are created by higher level nanostructures like dimers, trimers or higher order aggregates. On the other hand, to resolve single molecules, one needs only one molecule trapped in a hot spot at a time. Therefore, the density of hot spots is a crucial parameter. In addition, the density of hot spots, which deliver gains below single molecule sensitivity, should be minimized for lowest ensemble-averaged background. In short, one should engineer the optimum morphology- distribution of nanoparticle sizes and separations. Finally, SERS is only possible if the analyte molecule has affinity for the metal surface.

Thus, one salient feature of the present study is the development of efficient and reproducible SERS substrates that are capable of detecting single molecules with minimal effort and time. Further, we employ these SERS substrates to acquire temporal appearance of SERS peaks of PYP with significant peak-narrowing and spectral shifts

in consecutive scans, and report conformational changes thus captured. These conformational changes are homologous to the conformational steps that are instrumental in the photocycle of PYP, especially isomerization and protonation of the PYP chromophore. This observation suggests that single PYP molecules find high enhancement sites ("hot spots") on our SERS substrates under 514 nm-radiation and exhibit structural changes during photo-excitation, suggesting a possibility of "surface-enhanced photocycle" in single PYP molecules.

The uniqueness of this study lies in the achievement of high throughput single-molecule detection (immediate detection after spotting of analyte) of PYP on novel "nanometal-on-semiconductor" substrates,[21] as well as in the weakly chemisorbed molecules on nanoparticles exhibiting a high SERS effect. At the single-molecule level, SERS yields well-resolved peaks, some of which were not reported earlier. These new modes along with variations in chemisorption configuration of PYP on AgNPs result in a broad spectrum upon statistical averaging of single-molecule spectra. Certain mutually exclusive peak pairs (or groups) have been identified, that can elucidate the molecular structure and configuration using the SERS selection rules. These observations point out the significance of single-molecule SERS studies in allowing us to observe and analyze modes that are otherwise averaged out by high-enhancement modes in ensemble-averaged SERS. Thus, the present work develops a novel approach towards gaining a better understanding of the structural dynamics of the PYP molecule during its photo-excitation.

CHAPTER II. LITERATURE REVIEW

II.1 Photoactive Yellow Protein

In 1985, T.E. Meyer discovered a small (14kDa, 125 amino-acids) yellow-colored protein (Figure II.1) with properties similar to rhodopsin, while attempting to make an inventory of all colored proteins present in an anoxygenic phototrophic bacterium called *Ectorhodospira* (later renamed to *Halorhodospira*) *Halophila*.[2] It was later shown to be photoactive and thus named "Photoactive Yellow Protein."[22]

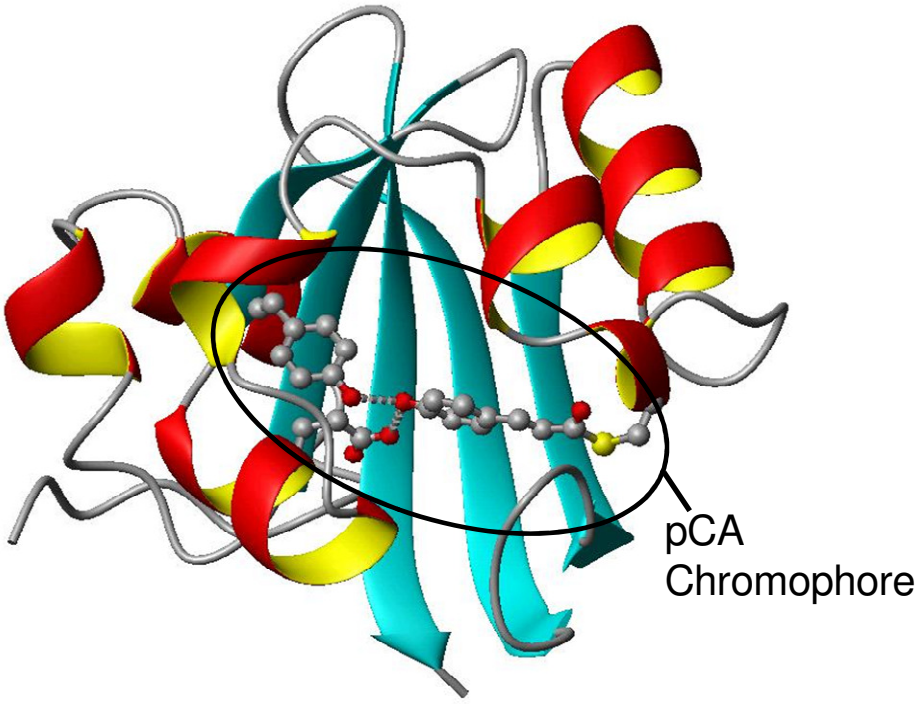

Figure II.1. Helical structure of PYP with the pCA chromophore in the binding pocket.[23]

Subsequent studies showed that PYP has a *para*-coumaric acid (*p*CA) chromophore (Figure II.2)[24, 25] covalently bound to side chain of Cys69 through a thiolester linkage.[26, 27] The X-ray crystallography showed its α/β-fold containing a six-stranded anti-parallel β-sheet as a scaffold, flanked by several helices.[28] The two hydrophobic cores on either side of β-scaffold comprise of N-terminus and "chromophore-binding pocket". In the initial dark (receiver or **pG**) state, the pCA is in trans configuration about the vinyl C7=C8 bond with a deprotonated phenolic oxygen.[25, 29] The carbonyl oxygen is H-bonded to the amide group of Cys69 residue, and phenolic O^- is stabilized by H-bonding network involving Tyr42 and neutral [30] side chain of Glu46.[28] The side-chain oxygen of Thr50 H-bonds both with the main-chain carbonyl oxygen of Glu46 and with the OH group of Tyr42, while its main-chain oxygen forms an H-bond with the side-chain of Arg52.[28, 31]

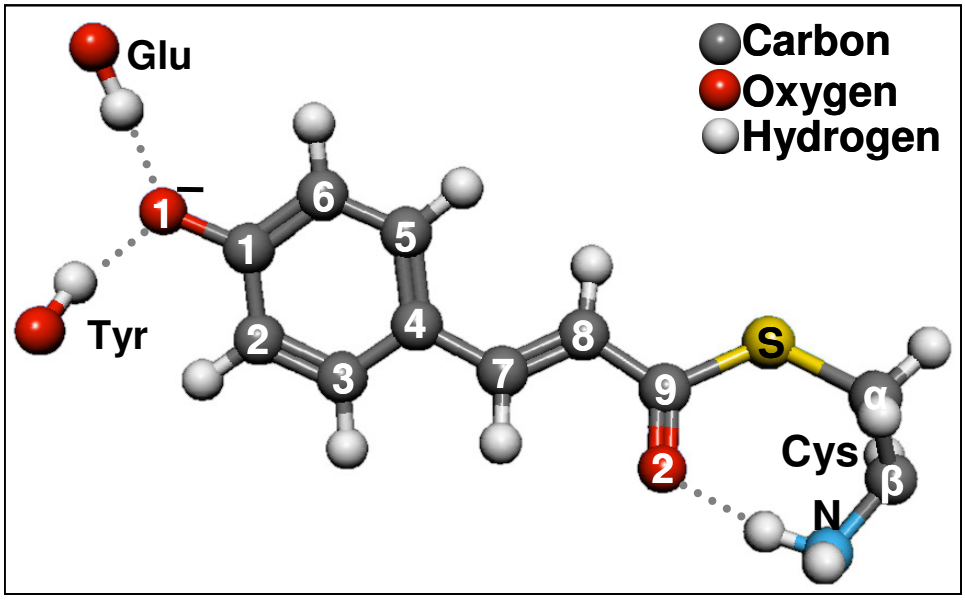

Figure II.2. Skeletal structure of pCA in receiver state, shown with H-bond network connecting it to protein molecule

The photocycle of PYP is initiated by the absorption of a blue photon (absorption peak at 446 nm) whose energy thereafter thermalizes through a chain of conformational states for both the chromophore and the protein, as seen in Figure II.3.[22, 26] Upon excitation, the chromophore photo-isomerizes to cis configuration about vinyl C7=C8 bond. Several studies, including those by Groenhof *et al.* [32-36] and Sergi *et al.*,[37] have computationally studied the isomerization process. Groenhof and coworkers introduced the idea of force field for the chromophore in its photo-states.[32] They also established the role that the positive charge on Arg52 plays in the stabilization of protein chromophore as well as in the photo-excitation and subsequent isomerization of PYP, with electrostatic stabilization of the chromophore's excited state by the guanidinium group of Arg52.[33] Sergi, on the other hand, studied the excitation of chromophore and calculated the activation energy barrier for process of isomerization.[37]

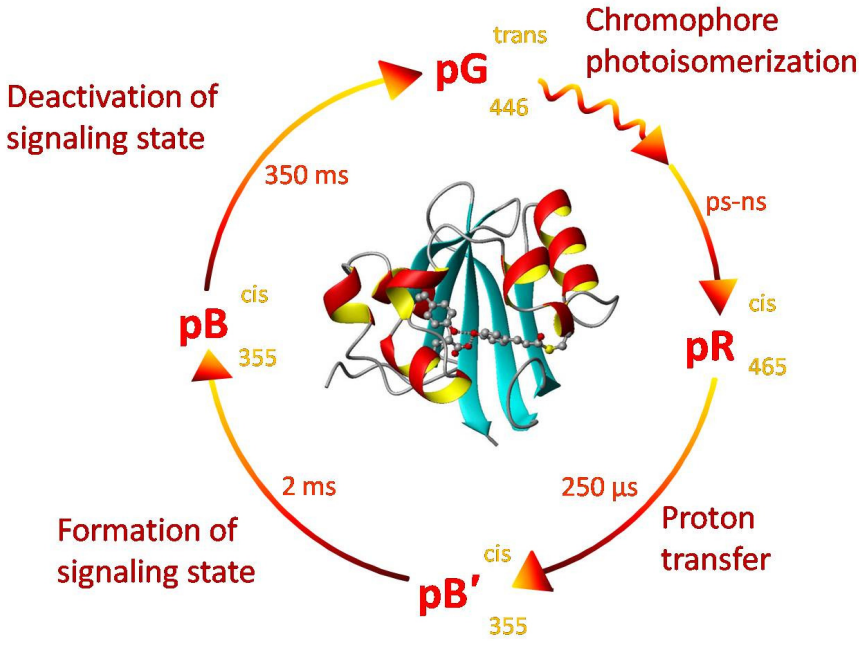

Figure II.3. Model for the photocycle of PYP. (Courtesy: Aihua Xie)

Associated with the photo-isomerization, flip of the thiolester carbonyl group by 180° and breaking of H-bond with the amide group of Cys69 [33] result in the red-shifted intermediate (**pR**) state (Figure II.4), which has an absorption peak at 465 nm.[23, 30, 38] Studies by Xie *et al.* [23, 30] suggested that the proton transfer from neutral Glu46 (resulting in $Glu46^{-}$) to phenolic O^{-} leads to the blue-shifted **pB'** state (Figure II.5). However, an independent study by Borucki *et al.* has suggested that the pCA acquires the proton from solvent water molecules.[39] The "protein-quake model" by Xie *et al.* suggests that this proton transfer is a crucial step in the photocycle as the resultant unstable buried charge of $Glu46^{-}$ drives the unfolding of the protein.[6, 23, 40, 41]

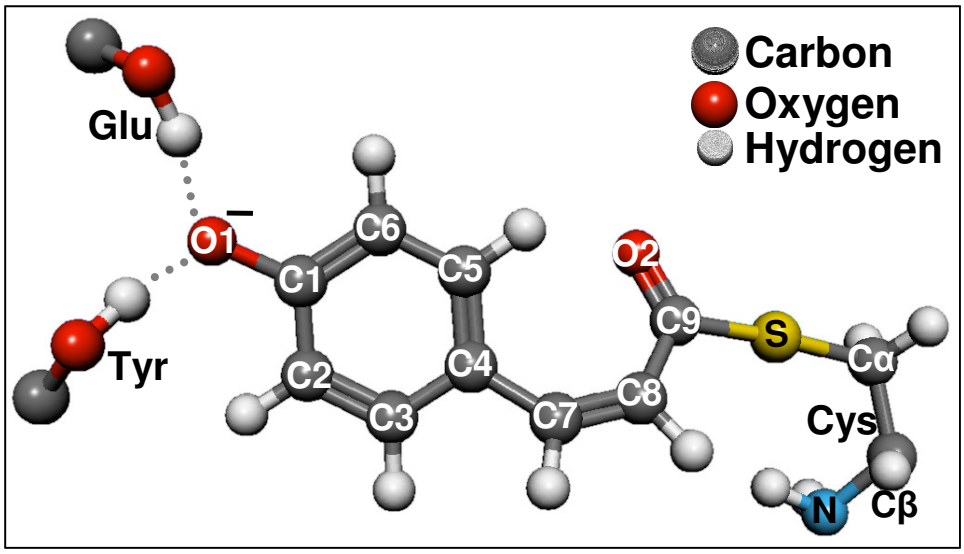

Figure II.4. Skeletal structure of PYP chromophore in red-shifted intermediate (pR) state after photoisomerization and breaking of H-bond.

The unfolding of the α-helix of the chromophore-binding pocket [40] is accompanied by re-establishment of H-bond between pCA carbonyl O and amide group of Cys69,[38] and breaking of H-bonds of phenolic O with Glu46 and Tyr42.[6] These changes result in exposure of the chromophore and Glu46 to the solvent,[42] and lead to

the formation of signaling (**pB**) state (Figure II.6). The signaling state is the most stable state in the photocycle with an absorbance maximum at 355 nm.

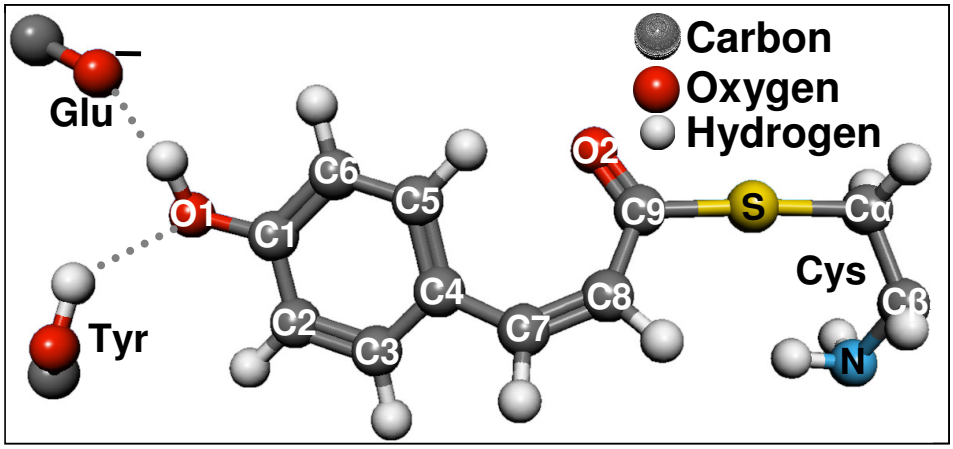

Figure II.5. Skeletal structure of PYP chromophore in blue-shifted (pB') state after protonation of phenolic oxygen.

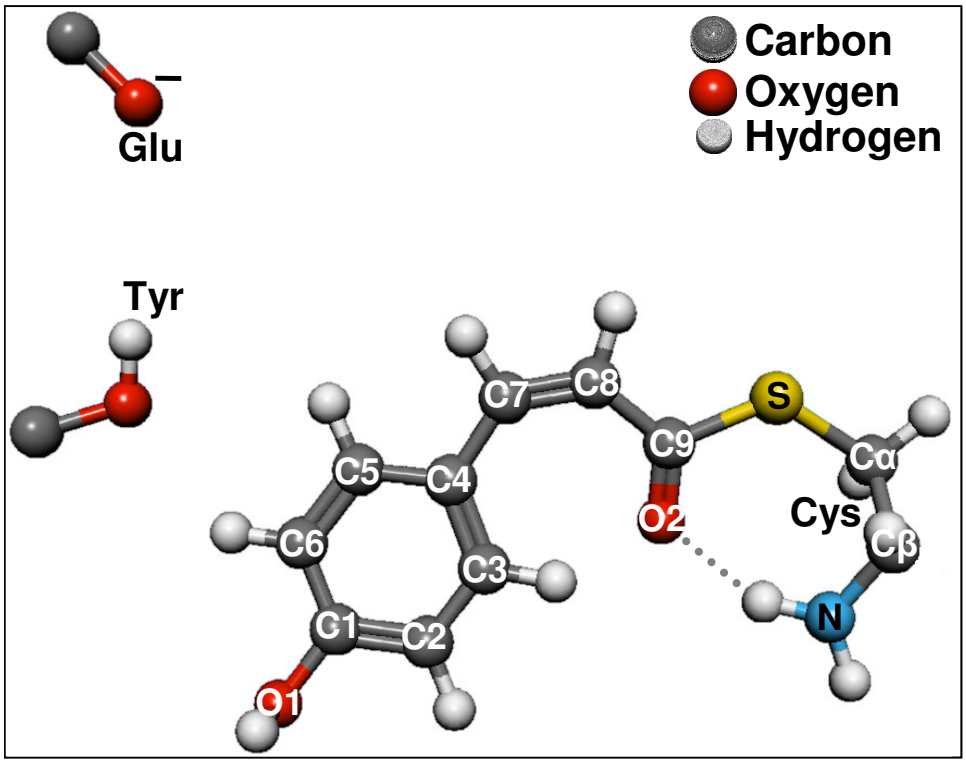

Figure II.6. Skeletal structure of PYP chromophore in blue-shifted signaling (pB) state showing unfolding of protein molecule and re-establishment of H-bond between O2 and Cys69.

These conformational changes in the protein structure provide a biological signal transduction that lasts for 350 ms before PYP recovers to its pG state to complete the photocycle.[22, 26] This recovery reaction or thermal decay to the folded pG state of PYP involves the following steps: (i) deprotonation of the *p*-CA chromophore, (ii) refolding of the protein, and (iii) the rate-limiting step of chromophore re-isomerization from the cis to the trans configuration.[2, 22, 26, 43, 44] Hellingwerf and coworkers have proposed that the formation of α-helix in the chromophore-binding pocket by the amino-acid residues at 43-52 is critical and forms a kinetic-barrier in the recovery of PYP.[43] They argue that the H-bonds between chromophore, Tyr42 and Glu46 are stabilized by this folding of the amino-acid residues to shape the chromophore-binding pocket for re-entry of solvent-exposed chromophore to the protein interior. They have also, in a recent study,[45] proposed the existence of an additional photocycle intermediate after pB state. This intermediate has a deprotonated chromophore, which is expected to facilitate the chromophore re-isomerization during the recovery reaction.

Several groups have employed computational methods like DFT (density functional theory) and ab-initio VSCF (vibrational self-consistent field) to calculate and assign the peak positions to various modes of vibration in the pCA chromophore.[29, 38, 46-49] Mathies and coworkers [48, 49] employed VSCF calculations and time-resolved resonance Raman spectroscopy to examine the role of anharmonic effects in the vibrational spectroscopy of the chromophore intermediates of the photoactive yellow protein (PYP) photocycle. Unno *et al.* [38, 46, 47] assigned Raman bands on the basis of normal mode calculations using DFT and isotope shifts observed in the chromophore labeled with ^{13}C at the carbonyl carbon atom or at the ring carbon atoms.

Table I shows the primary markers that are indicative of the transition of PYP molecule from one conformation to another. This table has been formulated on the basis of information available from the work of these two groups, whose comprehensive Raman assignments laid the framework for further investigation. Also, based on the discussions with Dr. A. Xie and Zhouyang Kang, we identified νC8—C9 and τCC (asymmetric) vibrational modes as the two most credible modes to determine structural transitions in single-molecule SERS. These two modes, unlike other transition markers in bulk-Raman of PYP, don't exhibit an inordinately high amount of fluctuations with the change in internal protein environment, i.e. H-bond network.[50]

Table I. Transition markers for the photocycle of PYP: observed Raman peaks.[29, 38, 46-50]

Isomerization	**Trans**	**Cis**
νC8—C9	1054	1002
H-Bond at O2	**H-Bond**	**No H-Bond**
νC9=O2	1633	1666
Protonation of O1	**Deprotonated**	**Protonated**
δCH	1163	1174
νC7=C8	1557/1534	1576/1599
τCC (Asym.)	1495	1515

ν: stretching, τ: ring breathing and torsion, δ: rocking

The aforementioned analytical studies on PYP have been conducted using NMR, X-ray crystallography, infrared spectroscopy, Raman scattering, fluorescence spectroscopy, and time resolved Raman scattering.[6, 30, 31, 51-54] However, there are no reports of SERS studies on PYP. Raman spectroscopy is a valuable technique to study the conformational dynamics of molecules in solution through vibrational modes, and unlike Infrared spectroscopy, it can be conducted in H_2O-based solutions. Also,

compared to other single molecule techniques like fluorescence spectroscopy, atomic force microscopy (AFM) and FRET, Raman spectrum of a molecule contains a high degree of structural information about it. However, extremely small cross sections of the effect preclude its use at single molecule level, and limit its employment to probing analytes at high concentrations (~1×10^{-4} M). On the other hand, the key advantage of SERS is the dramatic gains in Raman signal intensity as high as 10^{14}-10^{15}, allowing the detection of Raman spectra from single molecules using data collection times of less than 1 s.[55] The following section explores the studies that helped in learning of nuances of SERS for employment in the present study.

II.2 Single-Molecule Surface-Enhanced Raman Scattering

SERS was first reported in 1974 by Fleischmann [56] when he observed a strong Raman scattering signal from pyridine adsorbed on roughened silver electrodes. Fleischmann observed enhancements as high as 10^6, and attributed them to increase in surface area for adsorption on nanoparticles.[56] However, independent investigations by Jeanmarie and Van Duyne [57] and Albrecht and Creighton [58] disagreed with his explanation. Instead, they attributed these high Raman scattering enhancements to electromagnetic effect - localization of electromagnetic fields in the vicinity of nanoparticles as a result of resonant coupling between coherent electron oscillations (plasmons) and the photons (i.e., plasmon polaritons).[21, 55, 59, 60] Localized surface plasmons are the collective oscillations of free conduction electrons in a confined region that is significantly smaller (>20 times) than excitation wavelength. They are induced as a result of interaction with the applied electric field of incident light. This localized surface plasmon resonance (LSPR) leads to an enhancement in the local field as

experienced by the adsorbed analyte molecules. This electromagnetic effect produces a higher enhancement for the adsorbed molecules with polarization axis normal to the surface than those adsorbed with axis parallel, and decays exponentially with distance from the surface.

The electromagnetic enhancement can also be explained through a simple electrostatic model. The dipole induced in the nanoparticle by incident radiation creates an electric field E along the dipole axis, such that:

$$E \propto \frac{1}{d^3}$$

where, d = distance from center of the dipole. The intensity of the local radiation around the nanoparticle is directly proportional to the square of the electric field:

$$I_{Local} \propto E_{Local}{}^2 \propto \frac{1}{d^6}$$

On the other hand, the enhancement is for both incident radiation as well as scattered radiation.[61] Therefore:

$$I_{SERS} \propto E_i{}^2 . E_s^2 \propto \frac{1}{d^{12}}$$

where, E_i = Electric field of incident light, E_s = Electric field of scattered radiation. This simple model explains the localization of incident and scattered fields in the vicinity of the nanoparticles and thus, enhancements in Raman scattering on silver nanoparticles.

Additionally, Albrecht and Creighton also suggested the possibility of charge-transfer effect (chemical enhancement) being responsible for such high gains.[58] A small number of research groups, especially those led by Otto,[62-65] have thence maintained a

strong stance on the contribution of chemical enhancement and analyzed its dependence on atomic scale roughness. The adsorption of molecules on surface leads to formation of new electronic states through transfer of electron or charge from surface metal atoms to adsorbed molecule.[63] This interaction between adsorbed molecule and surface metal atoms leads to increase in molecular polarizability, thus resulting in chemical enhancement.

While the debate on the mechanism of enhancement responsible for SERS continues, SERS has been established as a successful trace-level detection technique.[66-70] Moreover, in 1997, Nie *et al.* [55, 71] demonstrated surface-enhanced Raman scattering (SERS) from single Rhodamine 6G molecule. This discovery implicated the possibility of resolving protein structure-activity relationships at the single molecule (SM) level using SERS. Nie *et al.* also established the concept of "hot-spots" - the high SERS-enhancement yielding regions on surface that provide single-molecule sensitivity. Following their work, several research groups independently claimed single-molecule enhancement factors on the order of 10^{13}-10^{15}.[59, 72-77] According to calculations by Xu *et al.,*[59, 75, 76] the maximum electromagnetic enhancement can be on the order of 10^{11}, thus the maximum chemical enhancement is on the order of 10^{3}-10^{4}. However, in a recent study, Moerner *et al.* suggested that the value for chemical enhancement factor can be as high as 10^{7}.[78] Such gains are sufficient to increase the Raman cross-section area of analyte molecules from ~10^{-30} cm^2 to ~10^{-16} cm^2, which is within the requisite single-molecule sensitivity.

Despite the significant promise of single-molecule SERS, literature reports only one study that has employed SERS to probe the structural dynamics of single protein

molecule.[79] In this study, Habuchi *et al.* (2003) monitored dynamic conversion of single GFP molecule between protonated and deprotonated forms.[80] It is likely that the lack of SM-SERS studies on protein structural dynamics is due to the irreproducibility and inefficiency encountered in available SERS methodologies. The SERS studies traditionally employ a lengthy citrate reduction procedure to prepare colloidal AgNPs. [55-59, 71-77] Three of the major disadvantages of this procedure, besides the amount of time involved, are:

- The need to immobilize the nanoparticles on a substrate.
- Noise from residual surfactants on nanoparticles. [75]
- Needs to be repeated for different analytes.[21]

Rothberg and coworkers (2003) successfully detected single polymer chains on roughened silver films deposited on glass slides.[81] They identified that the substrates with self-similar fractal topology exhibit "giant" SERS enhancements sites or hot-spots that were found to be sensitive to incident wavelength and polarization. They were able to minimize the noise due to residual surfactants and also the substrates did not require functional groups for adsorption of analyte molecules. Among the different substrate-preparation methods Rothberg *et al.* employed, Tollen's reaction was found to produce the single-molecule SERS substrates with most efficient fractal character. However, it requires overnight drying, thus making it relatively less time-efficient.

However, Kalkan *et al.* [21, 82] developed high throughput "nanometal-on-semiconductor" single-molecule SERS substrates, on which multiple analytes can be spotted and immediately analyzed. These substrates were prepared by immersion of glass-slides coated with silicon columnar films in silver nitrate solution, leading to

reduction of Ag^+ ions to silver nanoparticles on silicon film. These substrates exploited a unique effect accounting for single-molecule sensitivity – laser-induced electrochemical Ostwald ripening. This phenomenon involves the growing of metal nanoparticles in water and under laser exposure at the expense of smaller ones. The process is thermodynamically driven and continues as Ag^+ ions migrate from smaller to larger particles. However, electron transport is also required for charge balance, which is enabled through the underlying semiconductor film as it turns photoconductive under laser-excitation.

CHAPTER III. EXPERIMENTAL DETAILS

III.1 Outline

This chapter presents the details on the methodology employed to develop reproducible substrates that exhibit a high SERS enhancement for single molecule detection. The chapter also discusses the measurement conditions and protocols employed to detect single PYP molecules.

"Nanometal-on-semiconductor" structures, prepared by reduction of metal ions to metal nanoparticles on thin semiconductor films, were used. The semiconductor films were prepared by physical vapor deposition (PVD) process on Corning 1737 code glass slides using a Cressington 208 High Vacuum Turbo Carbon Coater. The films were then immersed in $AgNO_3$ for semiconductor to reduce Ag^+ to Ag nanoparticles on the film surface, thus producing SERS-active substrates.

For spectral acquisition, a Renishaw RM 1000 system (with a CCD detector) was employed. SERS was excited with a Spectra-Physics 160-series 514 nm Ar^+ ion laser. A grating of 1800 l/mm was used and centered at 1350 cm^{-1}. Aliquots of diluted PYP were spotted on the substrates and SERS was subsequently conducted by collecting the back-scattered radiation from the solution-nanoparticle interface with a 20× objective lens (with numerical aperture of 0.4).

III.2 Film Deposition

Corning 1737 code glass slides were treated in 50% IPA (in DI water) solution and scrubbed clean with a soft brush to remove organic residues and macroscopic particles. The slides were then ultrasonicated in the 50% IPA solution at a temperature of 70 ºC to remove the adsorbed impurities. They were then washed with DI water and subsequently ultrasonicated at 70 ºC in DI water. After blow-drying with nitrogen, the rinsed slides were put on a hot-plate for 10 minutes at 150 ºC to remove the moisture.

Figure III.1 shows the schematic of the PVD process employed to deposit thin semiconductor film on the prepared glass slides. As shown in the figure, the glass slides were placed on the platform under the shutter, and pellets of germanium/silicon were loaded in the tungsten-wire basket. A turbo pump backed-up by a mechanical pump was employed to vacuum the deposition chamber to a base pressure of 4×10^{-5} mBar. Having set the values of density of the material and tooling factor, crystal thickness monitor was reset to zero before the deposition started (i.e. shutter was opened).

Electric current was passed through the tungsten basket to heat (Joulean heating) it and consequently melt the deposition precursor. The current was gradually increased as the deposition material melted and wetted the tungsten-wire. After setting the rate of deposition to pre-decided value (1.0-3.0 Å/s) by adjusting the current through the basket, the shutter was removed to deposit a thin (4.0-10.0 nm) film of semiconductor on the glass slide. After the deposition, the shutter was closed and the chamber was allowed to cool down under vacuum before it was vented; and then the deposited film was replaced. Thin (<10 nm thickness) germanium films were thus prepared to subsequently produce SERS substrates (Appendix A).

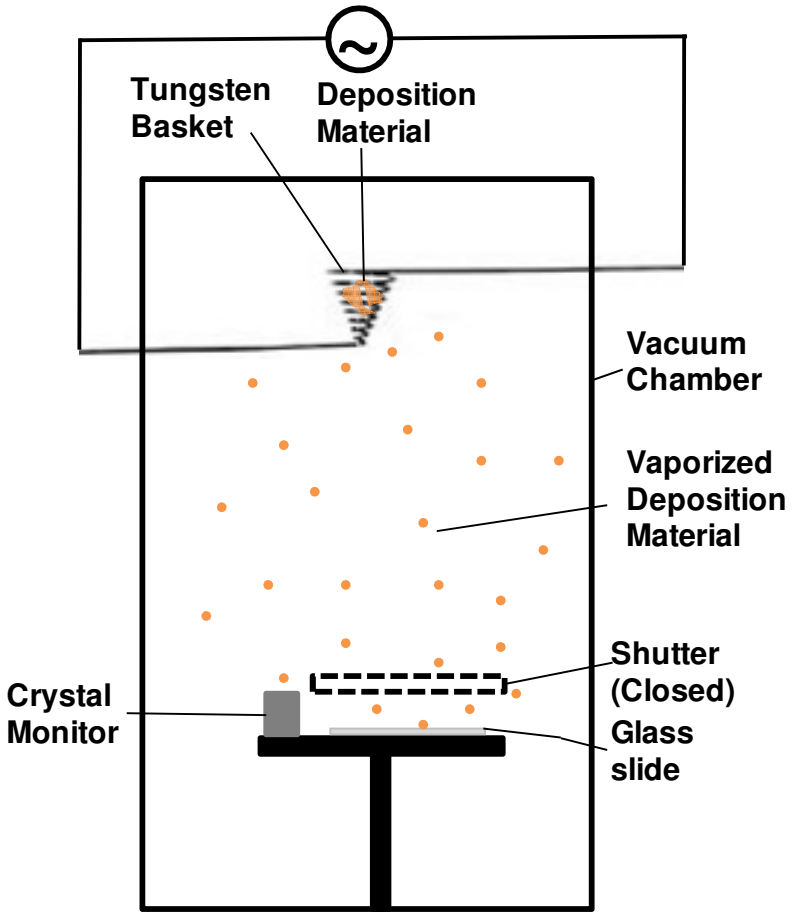

Figure III.1. Sketch of Physical Vapor Deposition process employed to deposit thin semiconductor film on glass-substrate.

III.3 SERS Substrate Development

Figure III.2 shows the reduction process in preparation of SERS-active nanometal-on-semiconductor substrates. The "semiconductor-on-glass" films were immersed in a metal salt solution. In this case, we used 0.002 M silver nitrate ($AgNO_3$). In case of silicon films, the substrates were first etched in 5% HF (hydrofluoric acid) solution before being immersed in 0.002 M $AgNO_3$ + 0.1% HF solution. Germanium films, however, were directly immersed in 0.002 M $AgNO_3$ after deposition. The semiconductor material reduced Ag^+ ions to form Ag nanoparticles on the surface, thus

producing SERS-active substrates. The salient features of this technique are: no surfactants are used; no capping agent are used; and better size control.[21]

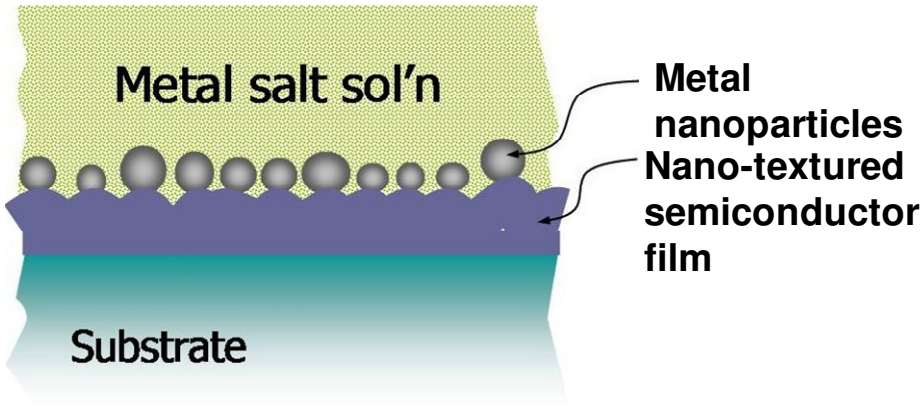

Figure III.2. Graphic demonstration of the reduction process in preparation of SERS-active substrates (Courtesy: Dr. Kaan Kalkan).

III.3 Surface-Enhanced Raman Spectroscopy Measurement

Figure III.3 shows the general schematic for excitation of analyte (in this study, PYP) on SERS substrate. The original analyte sample (1×10^{-5} M of *halo*-PYP with Histidine-tag) was provided by Dr. Aihua Xie (Professor, Department of Physics, Oklahoma State University), and was further diluted for the present study.

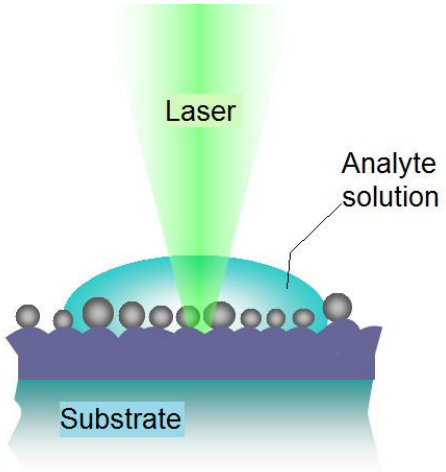

Figure III.3. Graphic demonstration of laser exposure of analyte and SERS measurement (Courtesy: Dr. Kaan Kalkan).

For ensemble-averaged SERS scans, 1 µL aliquots of 1×10^{-8} M PYP were spotted on the substrate and the 20× lens was focused at the aliquot/substrate interface (Appendix C). The substrate was excited with an Ar^+ ion laser at an incident power of ~8.3mW. To avoid photobleaching, and thus degradation of Raman signal, the laser probe was digitally defocused by 20% (using Wire 2.0 interface software) to diffuse the laser intensity over a larger area (i.e. 20 µm diameter).

For single molecule SERS scans with low background signal and high signal-to-noise ratio, aliquots of 1×10^{-9} M PYP were spotted on the substrate and excited with the laser at an incident power of 0.83 mW and further reduced to 25–50% using a graduated neutral density filter; thus effectively employing an incident power of 0.21-0.42 mW. The laser probe was defocused by 2-5% (using Wire 2.0 interface software), and time series spectra were collected over a region of 4–5 µm diameter with integration time of 0.25 s, shorter than PYP's photocycle. Employing a Renishaw RM 1000 Raman spectrometer, each 0.25 s scan was followed by a shutter/read-out time of 1 s that only permitted us to monitor the photocycle intermittently (Appendix D).

CHAPTER IV. RESULTS AND DISCUSSION

IV.1 Outline

Our “nanometal-on-semiconductor” SERS substrates were found to exhibit small (~30nm) nanoparticles arranged in various surface structures like nanochains. This feature is believed to create the plasmon hybridization for high surface-enhancement sites (“hot-spots”) on the substrate, which result in sudden appearance of discernable sharp and narrow (through elimination of spectral broadening) Raman peaks with spectral fluctuations and shifts. This observation is indicative of single PYP molecules undergoing weak chemisorption at high-enhancement-factor SERS sites. The single molecule spectra of PYP captured photo-isomerization, breaking of H-bond, and protonation that are the instrumental steps in the photocycle of PYP. Average of 385 of such individual single molecule spectra revealed a higher statistical broadening than that observed in ensemble-averaged SERS data. We attribute this remarkable spectral diffusion to strong chemical and electromagnetic enhancement, as discussed later in the chapter. Although multiple peaks (markers) identify a certain PYP state, not all appear in the same SM-SERS spectrum; some vibrational modes were observed to be mutually exclusive. Additionally, we observed the appearance of new SERS-active peaks that were not originally observed in Raman scattering. Also, nearly 5% single molecule SERS spectra captured only one dominant mode of vibration while other modes were suppressed.

IV.2 Substrates for single molecule detection

Figure IV.1 shows the comparative optical extinction spectra and AFM images of silver nanoparticles (AgNP) synthesized on thin (<10 nm) Ge and 20 nm thick hydrogenated amorphous Si films (deposited by plasma-enhanced chemical vapor deposition at The Pennsylvania State University), respectively.

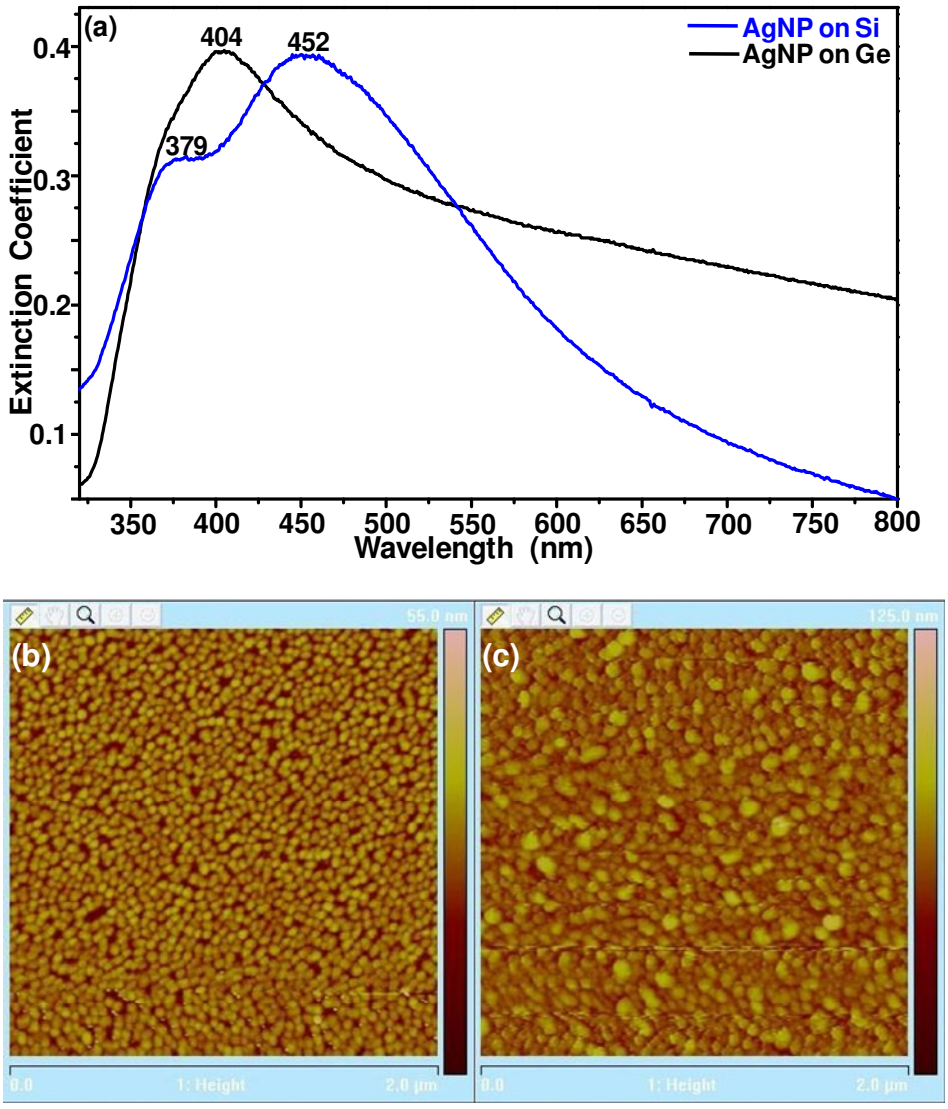

Figure IV.1. (a) Optical extinction spectrum showing quadrupole and dipole plasmon bands for silver nanoparticles on silicon film and a strong plasmon hybridization (through a long tail) in silver nanoparticles on germanium film, **(b)** AFM topography of AgNP-on-Ge substrate, **(c)** AFM topography of AgNP-on-Si substrate. The images show small nanoparticles in (b), while big nanoparticles in (c).

For the optical extinction spectrum of AgNPs synthesized on Si, bands at 379 nm and 452 nm are attributed to quadrupole and dipole plasmon modes respectively, indicative of nanoparticles larger than ~50 nm.[83] Whereas, the 404 nm band for AgNP reduced on Ge is characteristic of an average size smaller than ~30 nm.[83] These inferences were found to be in agreement with the AFM topography data. Extensive broadening for both spectra towards red is attributed to plasmon hybridization due to electromagnetic interaction of the closely spaced (spacing < diameter)[83] nanoparticles. The absence of a well-resolved hybrid plasmon peak was believed to result from distribution of inter-particle spacings. In other words, the hybrid plasmon energy (wavelength) is a function of inter-particle spacing whose distribution leads to a distribution of hybrid plasmon energies. The broader extinction tail of AgNPs on Ge film suggests a stronger hybridization.

Figure IV.2 shows AFM topography of silver nanoparticles synthesized on a thin (<10 nm) germanium film. The average size of nanoparticles was deduced to be 30 nm. An isolated 30 nm silver nanoparticle can account for a maximum enhancement of ~10^6.[59] In single molecule SERS literature, the typical nanostructural elements yielding single-molecule sensitivity are reported to be nanoparticle dimers, where the particle diameter is 90 nm or more.[59] On the other hand, the particle size of 30 nm in the present study is much smaller than this value. Therefore, the nanostructural element responsible for single-molecule sensitivity in the current study must be of a different form.

Upon careful examination of the AFM images, we observed exhibition of nanoparticle chains by the substrates, as highlighted in the Figure IV.2 by circles. It is

likely that these chains are responsible for the plasmon hybridization/localization that produces the electromagnetic enhancement enabling single-molecule detection. In a recent report, de Waele *et al.* [84] established the idea of localization of light by NSOM for nanoparticle chains at their either ends. In their study, the propagation of light was along the array axis; while in the present study, the propagation vector is normal to the chain-axis. However, Knight *et al.* (2007) [85] demonstrated that incident light can be coupled to nanowire plasmons in normal direction to the light by means of a nanoparticle antennae interacting with the nanowire. Therefore, similar coupling can take place for a nanoparticle chain on our substrates aligned perpendicular to the propagation of light.

Alternatively, the observed enhancement can also result from simple plasmon hybridization between the particles giving rise to a higher degree of light concentration than that observed in dimers. Future research should elucidate the near-field distribution around the nanochains of the present work.

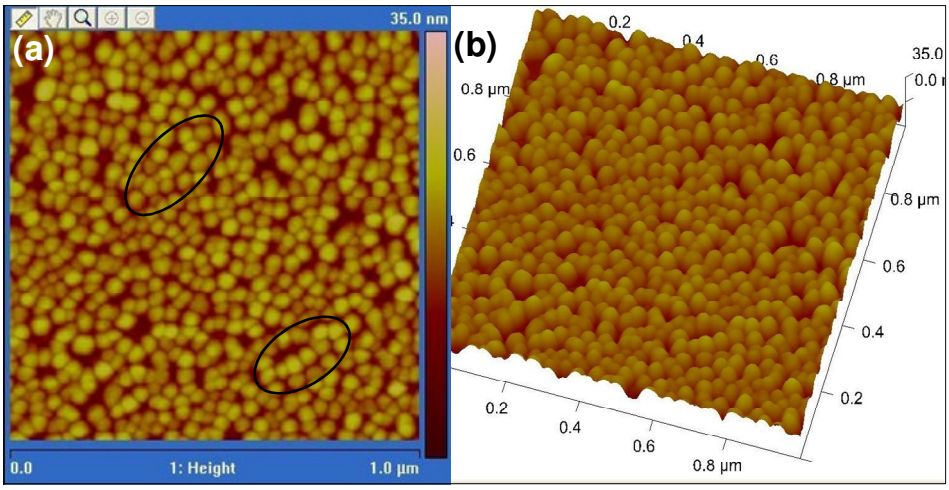

Figure IV.2. (a) AFM image of AgNPs synthesized on thin germanium film. The circled area shows nanoparticle chains, believed to generate hot-spots for single-molecule detection. **(b)** 3-D view of the substrate demonstrating non-uniform distribution of nanoparticles.

IV.3 Raman Spectroscopy

Figure IV.3 shows the spectra obtained by Raman scattering from 7×10^{-3} M halo-PYP and1×10^{-4} M p-Coumaric Acid (pCA) in 7.2 pH Sodium Hydrophosphate ($NaHPO_4$) buffer.

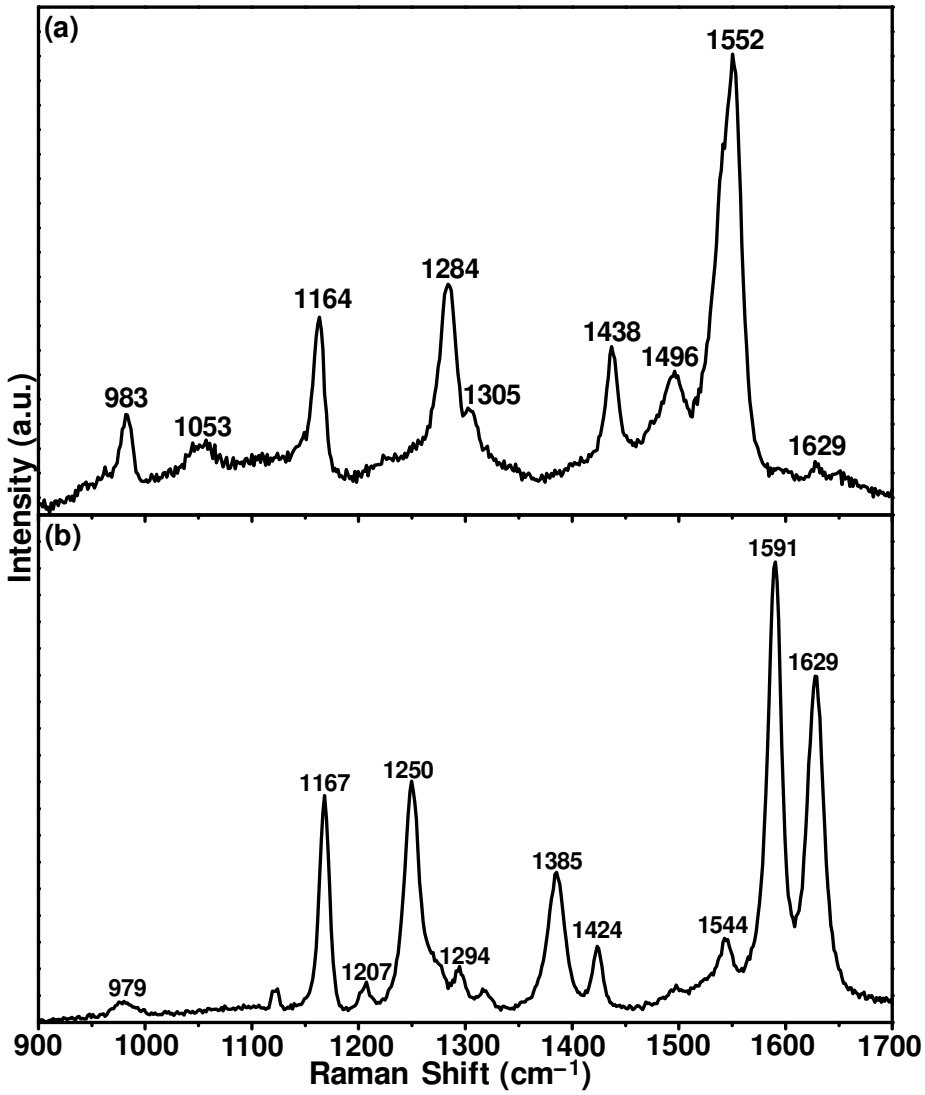

Figure IV.3. (a) Raman spectrum obtained from 7×10^{-3} M PYP, demonstrating the peaks attributed to receiver state. **(b)** Raman scattering data obtained from 4 mM solution of pCA.

Raman scattering data of pCA exhibits strong peaks at 1250, 1385, and 1591 cm^{-1}, which aren't observed in the Raman scattering data of halo-PYP. We attribute the

differences in the spectra primarily to the differences, listed below, in the structure of PYP chromophore and an individual pCA molecule (Figure IV.4):[2]

- Free pCA is neutral, while protein chromophore is anionic.
- Free pCA is carboxylic acid bound, while chromophore is covalently bonded to Cys69 through a thiolester bond. Thus, the symmetric νC9=O2 vibration mode becomes asymmetric because of covalent and H-bonds with Cys69.

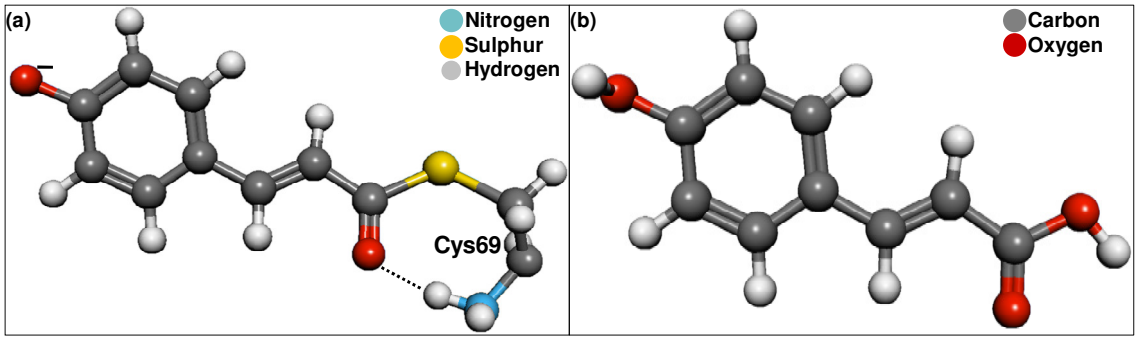

Figure IV.4. Comparison between the structures of **(a)** pCA chromophore covalently bonded with Cys69 in PYP, and **(b)** individual pCA molecule.

IV.4 Surface-Enhanced Raman Scattering

IV.4.1 Ensemble-Averaged Data

Figure IV.5 and Figure IV.6 show the ensemble-averaged SERS spectra of PYP and neutral pCA. Unlike the respective Raman spectra, the two SERS spectra were interestingly found to be very similar. These almost identical ensemble-averaged SERS spectra of neutral pCA and PYP suggest that the SERS signal of PYP solely originates from its chromophore.

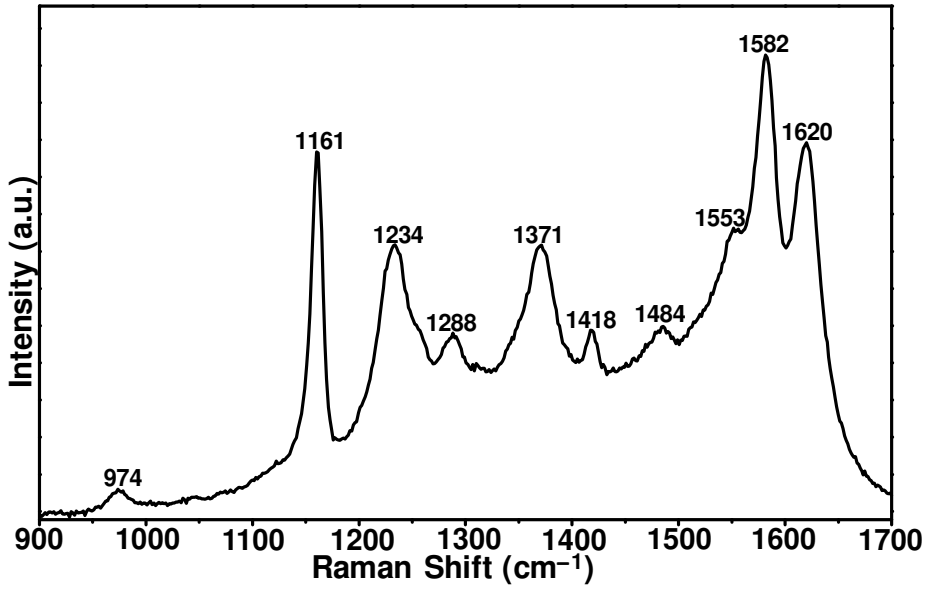

Figure IV.5. Ensemble-averaged spectrum of 1×10^{-8} M PYP acquired from AgNP-on-Ge substrate.

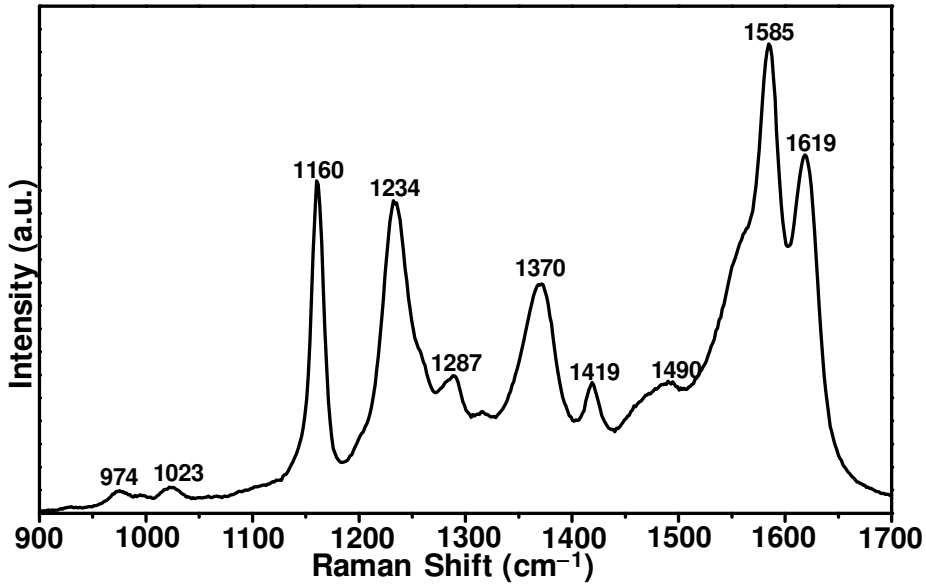

Figure IV.6. Ensemble-averaged spectrum of 1×10^{-6} M pCA acquired from AgNP-on-Ge substrate.

The ensemble average SERS spectrum of PYP is not, however, identical to the resonance Raman spectrum published of the pG state.[47, 49] However, the peaks at 1161, 1288 and 1552 cm^{-1} are inferred to correspond to the peaks observed in the Raman spectrum of the pG state at 1163, 1283 and 1555 cm^{-1} respectively.[47] Similarly, the peak at 1582 cm^{-1} appears to correspond to the reported signaling state Raman

peak at 1576 cm^{-1}.[46] Strong peaks in the PYP SERS spectrum at 1418 and 1620 cm^{-1} were not observed in the Raman spectrum, but were observed in infrared absorption spectrum.[50] The peak at 1624 cm^{-1} is attributed to τCC (symmetric ring stretching) vibration in the infrared absorption spectrum of pB state.[50] The peaks at 1234, 1345, 1370 and 1484 cm^{-1} have only been computationally predicted but not observed in Raman spectrum.[47, 49] This observation is suggestive of altered selection rules playing a significant role in determining the SERS spectrum of PYP. In other words, vibrational modes that are not found in the Raman spectrum but normally appear only in the infrared spectrum of the free molecule can also appear in the SERS spectrum.[16, 86, 87]

Appearance of strong peaks at 1582 and 1623 cm^{-1} characterizes protonated state in pCA as well as in PYP chromophore, while those at 1161, 1234, 1288 and 1553 cm^{-1} suggest existence of the chromophore in anionic state.[29, 46, 47, 49] This phenomenon is indicative of conformational changes, especially protonation/deprotonation, being captured by SERS.

Figure IV.7 shows time-series PYP ensemble-averaged SERS spectrum in the form of a waterfall plot. The SERS signal did not show any effect of photobleaching of PYP over 40 s of collection, thus indicative of stability of the molecule under high intensity laser conditions, as detailed in Chapter III.

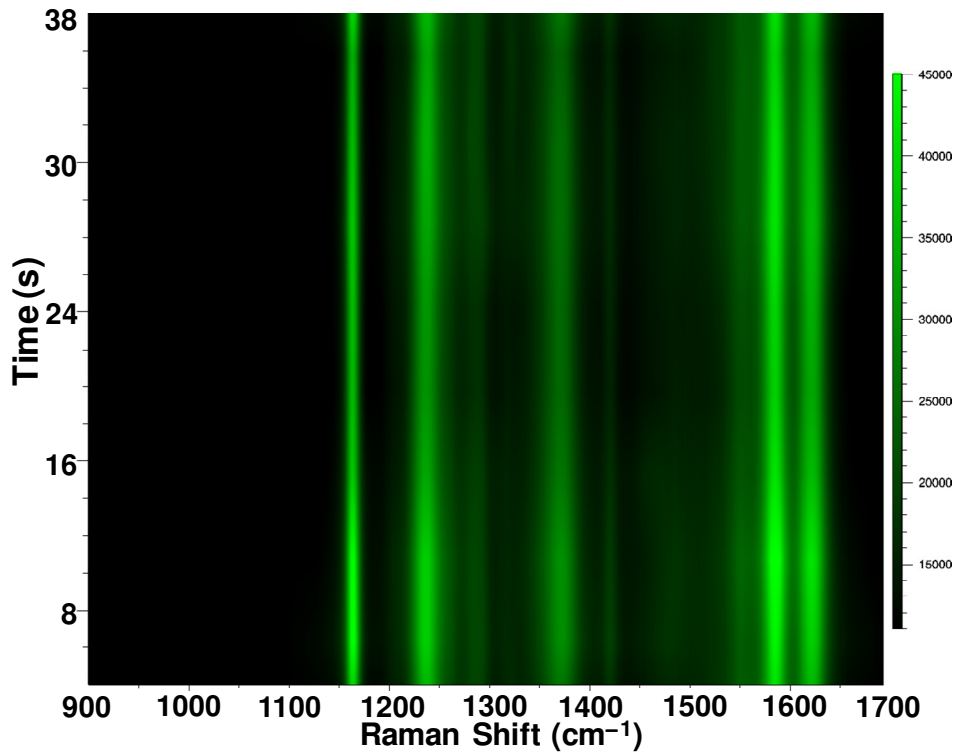

Figure IV.7. Time series ensemble-averaged SERS data from PYP solution in the form of a waterfall plot, showing stability of the molecule under high intensity laser.

IV.4.2 Single Molecule Detection

When the PYP concentration was lowered to 10^{-9} M, temporal fluctuations in the form of sudden appearances of sharp discernable Raman peaks were observed. On the average, these spectral jumps occur every few seconds and sustained less than one second, as depicted by Figure IV.8. Accordingly, we associate them with single PYP molecules diffusing in and out of ultra-high SERS enhancement sites on the substrate.[21] Figure IV.9 shows three time-series spectra, acquired from different sets of experiments, presented in the form of waterfall plots with bright green spots (on a dark background) illustrating single molecule jumps.

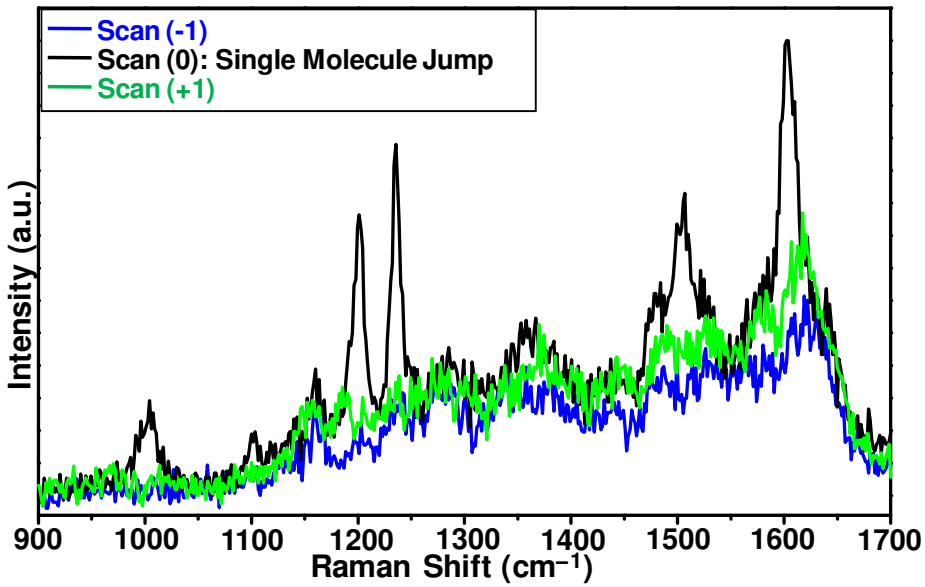

Figure IV.8. 3 consecutive SERS spectra demonstrating single-molecule jump in 0th scan. Every scan was captured over an integration time of 0.25 s, with a shutter time of 1 s.

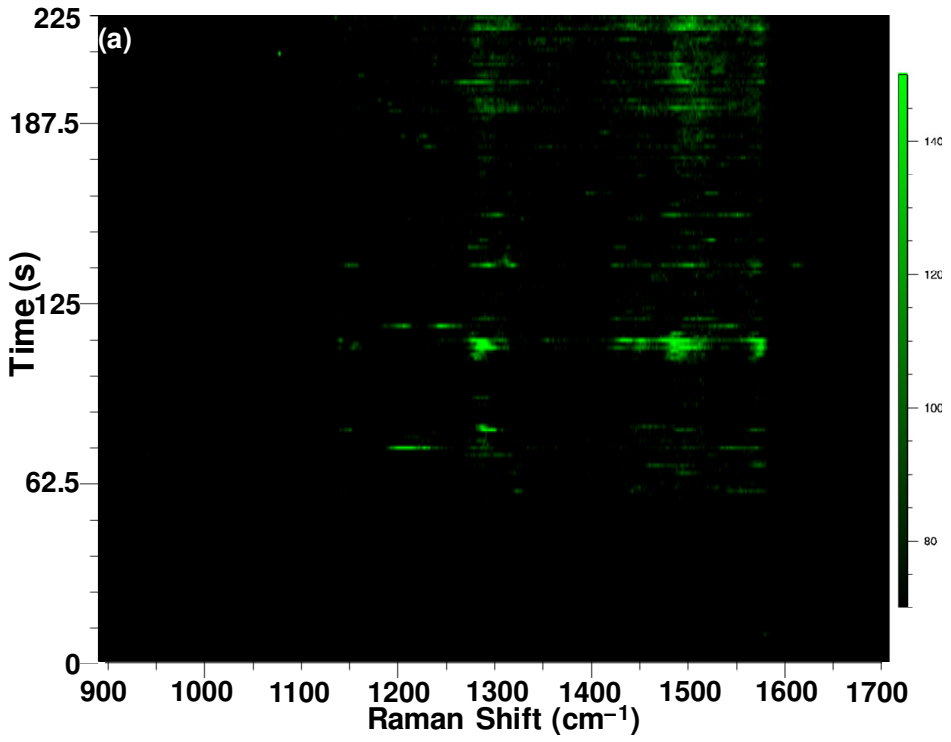

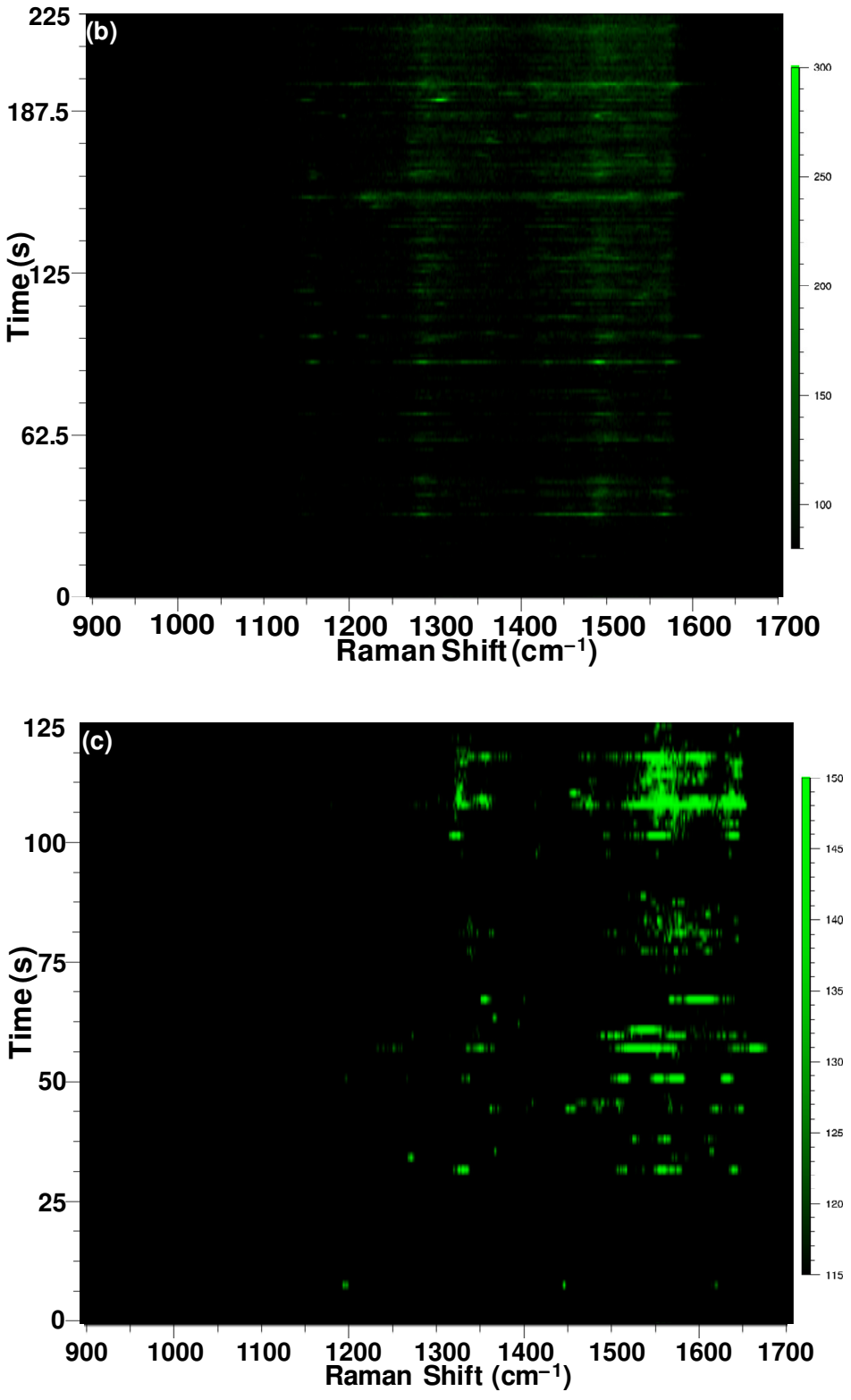

Figure IV.9. Waterfall plots illustrating single molecule detection, through bright spots indicating dominant peaks against a dark background.

A single molecule spectrum integrated for 0.25 s serves like the “molecule’s logbook” and records the conformational changes experienced by the molecule during that time-period. Figure IV.10 shows 2 of such “logbooks” recorded over 0.25 s in different measurements. Figure IV.10a shows a SM-SERS spectrum of PYP, which conforms to the pG state, while Figure IV.10b shows another SM-SERS spectrum of PYP that conforms to the pB state. When compared with EA-SERS spectrum, SM-SERS is distinguishable from narrower peaks, i.e. lack of heterogeneous spectral broadening.[55] In the absence of statistical averaging, a specific chemisorption configuration, orientation (with respect to polarization of local radiation) and environment of the chromophore results in well-resolved, sharp SM-SERS peaks. Likewise, changes in chemisorption configuration, orientation and environment also lead to fluctuations in energy and relative intensities of SM-SERS vibration modes.

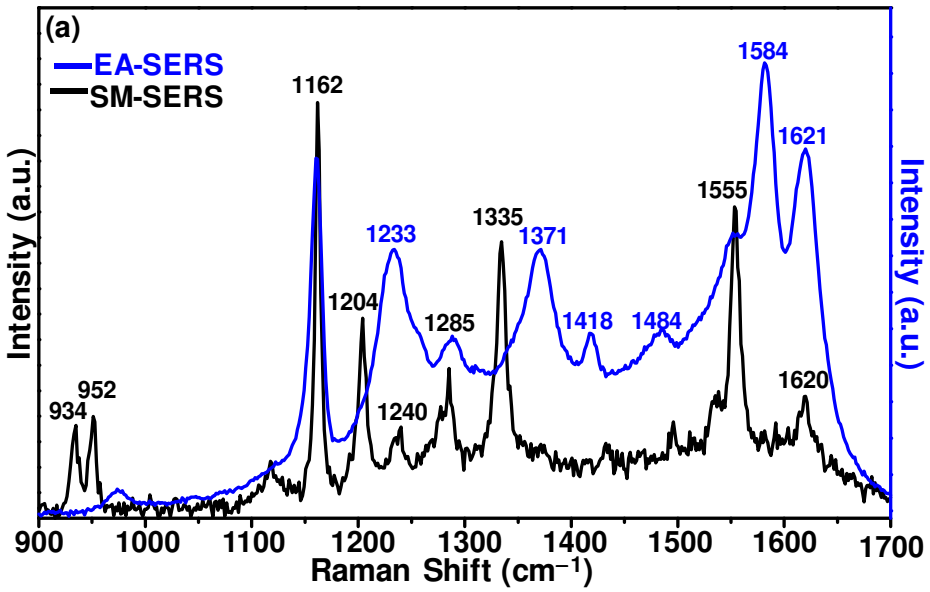

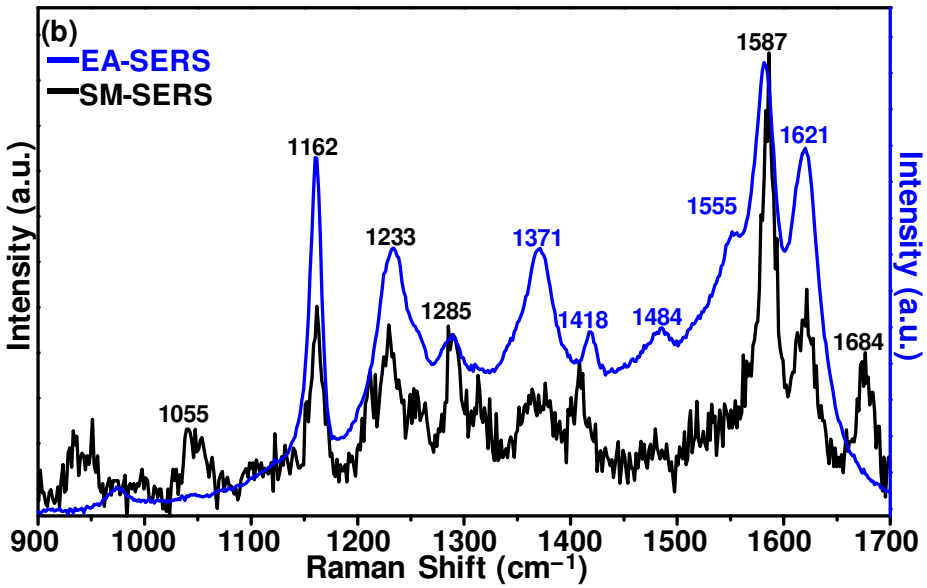

Figure IV.10. Graphs demonstrating comparison between ensemble-averaged SERS data and single-molecule SERS data, thus illustrating elimination of spectral broadening. The captured molecule is exhibiting Raman peaks primarily from: **(a)** receiver (pG) state, **(b)** signaling (pB) state.

In a significant number of SM-SERS spectra, peaks that are characteristic of the pB state were detected. Since these spectra were recorded in the dark and using a 514 nm laser line for the Raman scattering, the accumulation of the pB photo-intermediate was not expected. These results, thus, suggest that the 514 nm radiation is able to initiate the conformational changes in PYP at enhanced light intensities that the PYP molecule experiences in the hot spots of the SERS substrate. The data also indicates that structural transitions of a single PYP molecule can be monitored once it enters a hot site, although the molecules typically reside in the hot site for less than 1 s.

IV.4.3 Single Molecule Enhancement Factor

SERS enhancement factor was calculated for detected single PYP molecules ($E_{SM\text{-}SERS}$) as the ratio of SERS intensity to Raman scattering intensity per PYP molecule per incident laser intensity. In particular, the νC7=C8 mode (1555 cm^{-1}) was adopted for the calculation. The enhancement factor is given by:

$$E_{SMSERS} = \frac{\frac{I_{SMSERS}}{P_{SMSERS}/A_{SMSERS}}}{\frac{I_{Raman}/N_{Raman}}{P_{Raman}/A_{Raman}}}$$

where I = signal counts per second, P = laser power, A = effective laser probe cross-section area on the SERS substrate, and N = number of molecules probed. The subscripts denote these values are associated either with SM-SERS or Raman scattering. As mentioned in the manuscript, single-molecule SERS was conducted using 1×10^{-9} M PYP and 0.25 s integration time, while Raman scattering spectrum was obtained for 7×10^{-3} M PYP at an accumulation of 100 s.

In the case of Raman scattering, the signal was collected from a diffraction limited probe volume (0% defocus). Following Renishaw, this probe volume (V) is calculated as:

$$V = 3.21 \times \frac{\lambda^3}{(NA)^4} = 0.017\ \text{pL}$$

where, λ = wavelength of the incident laser = 514 nm, NA = numerical aperture of the 20× objective lens used = 0.40.

In addition, for Raman acquisition, the diffraction limited laser focus spot size (D_L) is given by:

$$d_l = \frac{1.22 \times \lambda}{NA \times n}$$

and estimated at 0.82 µm. d_l is determined by twice the Rayleigh criterion of the adjacent distance required to spatially resolve the presence of identical size spots. Here, n is the refractive index of the medium, which is 1.33 for water.

On the other hand, the laser focus spot size (d) for SM-SERS acquisition was 5 µm (2% defocus on the SERS substrate) and was not diffraction limited. Also, in this case, the probe volume is not needed since the signal is obtained from a single molecule. Accordingly, the parameters were determined as follows:

$I_{SM\text{-}SERS}$ = 900 counts per 0.25 s = 3600 counts/s

I_{Raman} = 180000 counts per 100 s = 1800 counts/s

$N_{Raman} = C \times V \times N_A = 7.2 \times 10^7$; where C = concentration of solution = 7×10^{-3} M, V = probe volume = 0.017 pL; and N_A = Avogadro number = 6.023×10^{23}

$P_{SM\text{-}SERS}$ = 0.38 mW

P_{Raman} = 6.00 mW

$$A_{SMSERS}/A_{Raman} = (d/d_l)^2 = (5/0.82)^2 = 37.2$$

Thus, substituting these parameter-values in the aforementioned formula, the single-molecule SERS enhancement factor has been calculated to be 1.1×10^{11}. When applied on PYP Raman cross-section area of 10^{-30} – 10^{-29} cm^2, this enhancement factor increases the cross-section to as high as 10^{-19} - 10^{-18} cm^2. This cross-section area, though 100-1000 times smaller than the cross-section area for single-molecule detection as reported in literature,[55] was found to exhibit sufficient single-molecule sensitivity on our SERS substrates.

IV.5 Photocycle of PYP

Figure IV.11 and Figure IV.12 show various SM-SERS PYP spectra that capture different structural changes in PYP. Well-established Raman markers identifying

different conformational states of PYP (Table I) were used to structurally interpret these single-molecule spectra. Those markers are: protonation markers (δCH, τCC, νC7=C8), trans/cis isomerization marker (νC8–C9) and H-bonding marker (νC9=O2).[29, 38, 46, 47]

In Figure IV.11a, the SERS spectrum shows an ensemble of peaks attributed to receiver (pG) state of PYP, and thus, possibly captures the molecule in its ground state. Figure IV.11b captures the shift of νC8-C9 (stretching) mode from ~1064 (1054) to ~992 (998) cm^{-1}, which is indicative of the chromophore undergoing photo-isomerization to cis about C7=C8 bond.[38, 47, 49] This step is followed by a 180º carbonyl (C9=O2) flip,[23, 30, 38] illustrated in Figure IV.11c, that is associated with breaking of H-bond between O2 and amide group of Cys69.[23, 38] This step is identified from shifting of νC9=O2 (stretching) mode from ~1633 to ~1666 cm^{-1}. In view of PYP Raman literature, these two frequency shifts suggest the transition of molecule from its receiver (pG) state to the red-shifted intermediate (pR) state. Therefore, Figure IV.11b and Figure IV.11c collectively suggest the transition of a single PYP molecule from pG to pR. Figure IV.11d shows both the modes that completely mark the isomerization followed by the carbonyl flip for a single PYP molecule.

Conversion to pR triggers a proton transfer from Glu46 to phenolic $O1^{-}$, leading to protonation of the chromophore.[23, 30] As captured for a single PYP molecule in Figure IV.11e and Figure IV.11f, this step of protonation was observed through at least 3 different markers[29, 30, 46, 47, 49]: (i) shift in νC7=C8 (stretching) peak from ~1534/1557 to ~1584/1600 cm^{-1}, (ii) shift in δCH (rocking) peak from ~1163 to ~1174 cm^{-1}, and (iii) shift in τCC (ring vibration) peak from ~1495 to ~1515 cm^{-1}. Figure IV.11g displays a single-molecule SERS spectrum, which captured a group of peaks that conform to pB

state of PYP. Figure IV.11h shows another SM-SERS spectrum of a PYP molecule with an ensemble of peaks that are characteristic of both pG and pB states. Therefore, this spectrum possibly captured a PYP molecule during its photocycle.

These spectra suggest that the observed structural changes conform to the steps that are instrumental in the photocycle of PYP and, thus, the PYP molecules were most likely captured in SERS hot-spots while undergoing structural transitions.

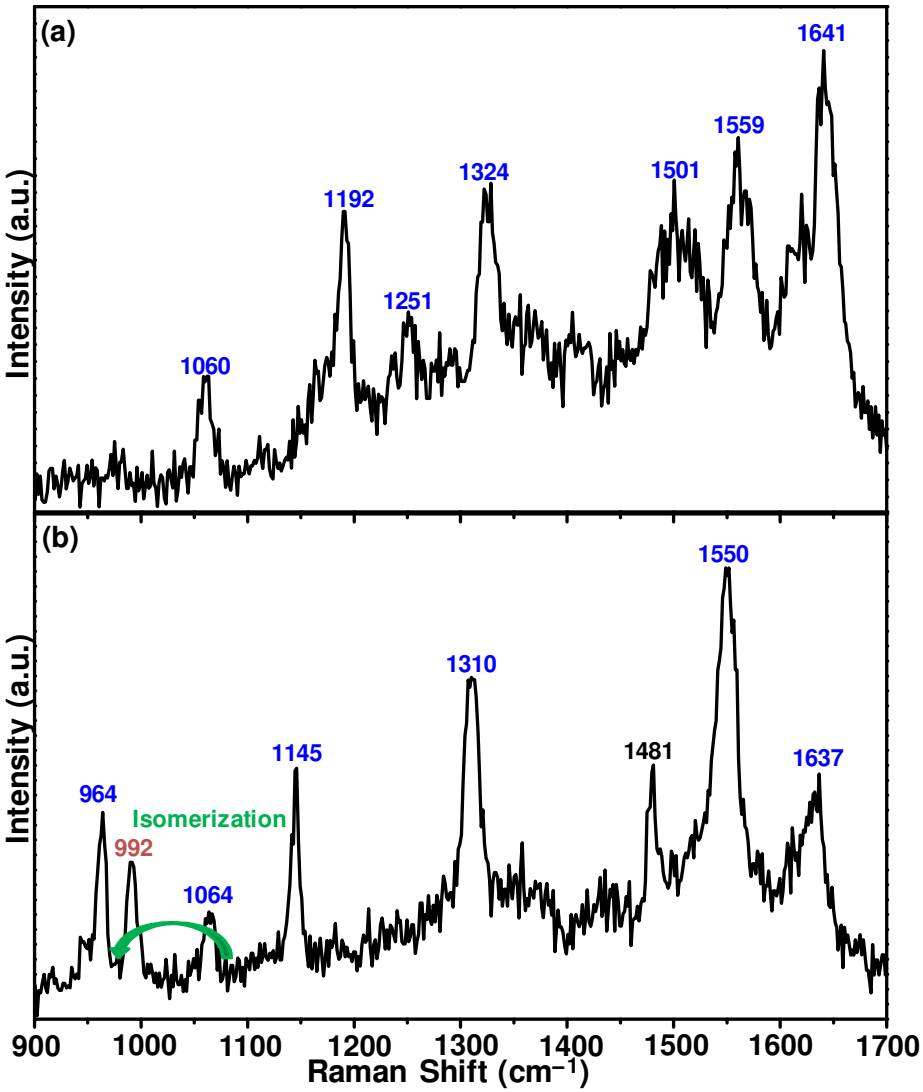

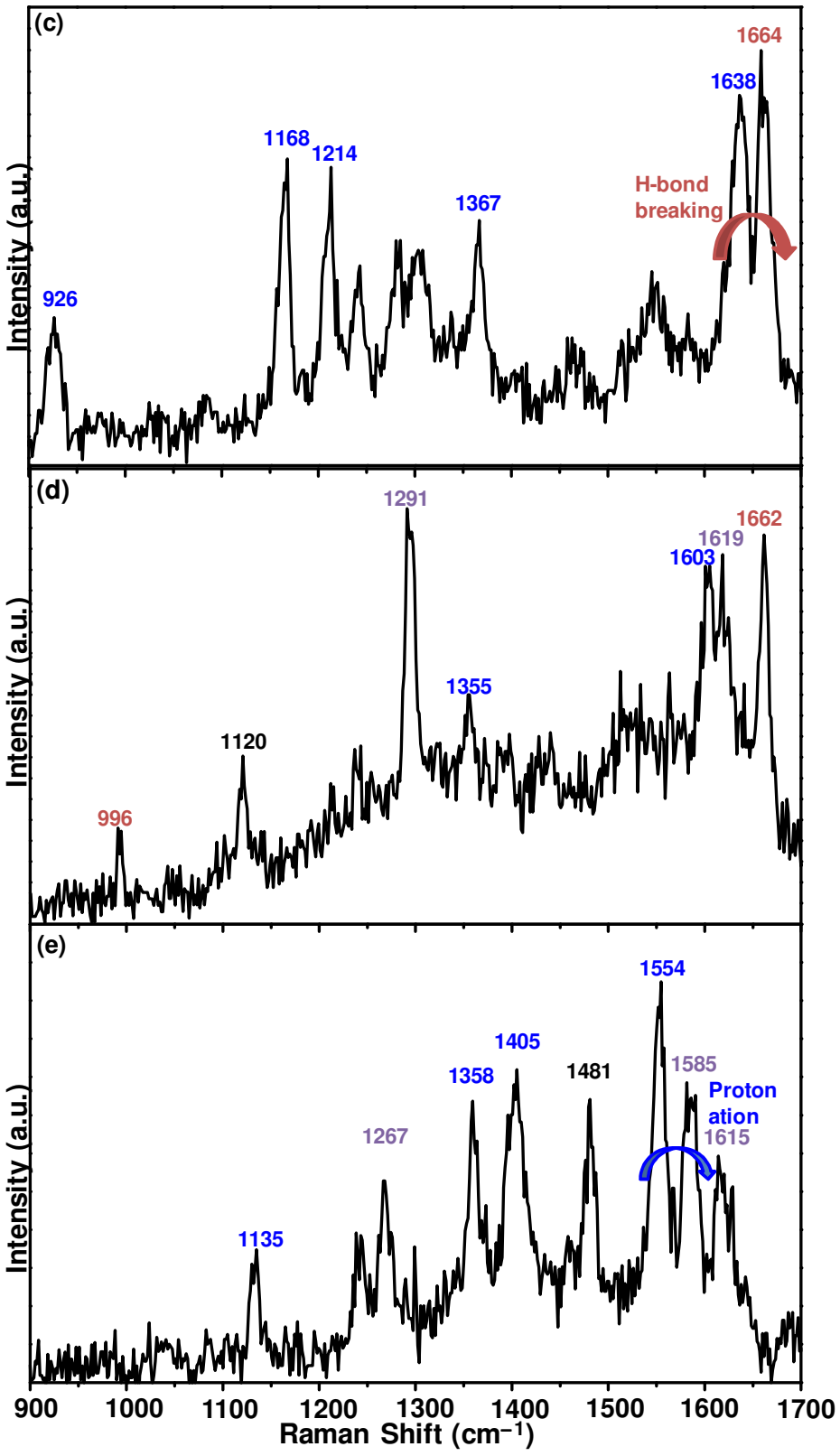
(c)
1664
1638
1168
1214
1367
H-bond
breaking
926
Intensity (a.u.)
(d)
1291
1662
1619
1603
1355
1120
996
Intensity (a.u.)
(e)
1554
1405
1585
1358
1481
Proton
ation
1615
1267
1135
Intensity (a.u.)
900
1000
1100
1200
1300
1400
1500
1600
1700
Raman Shift (cm⁻¹)

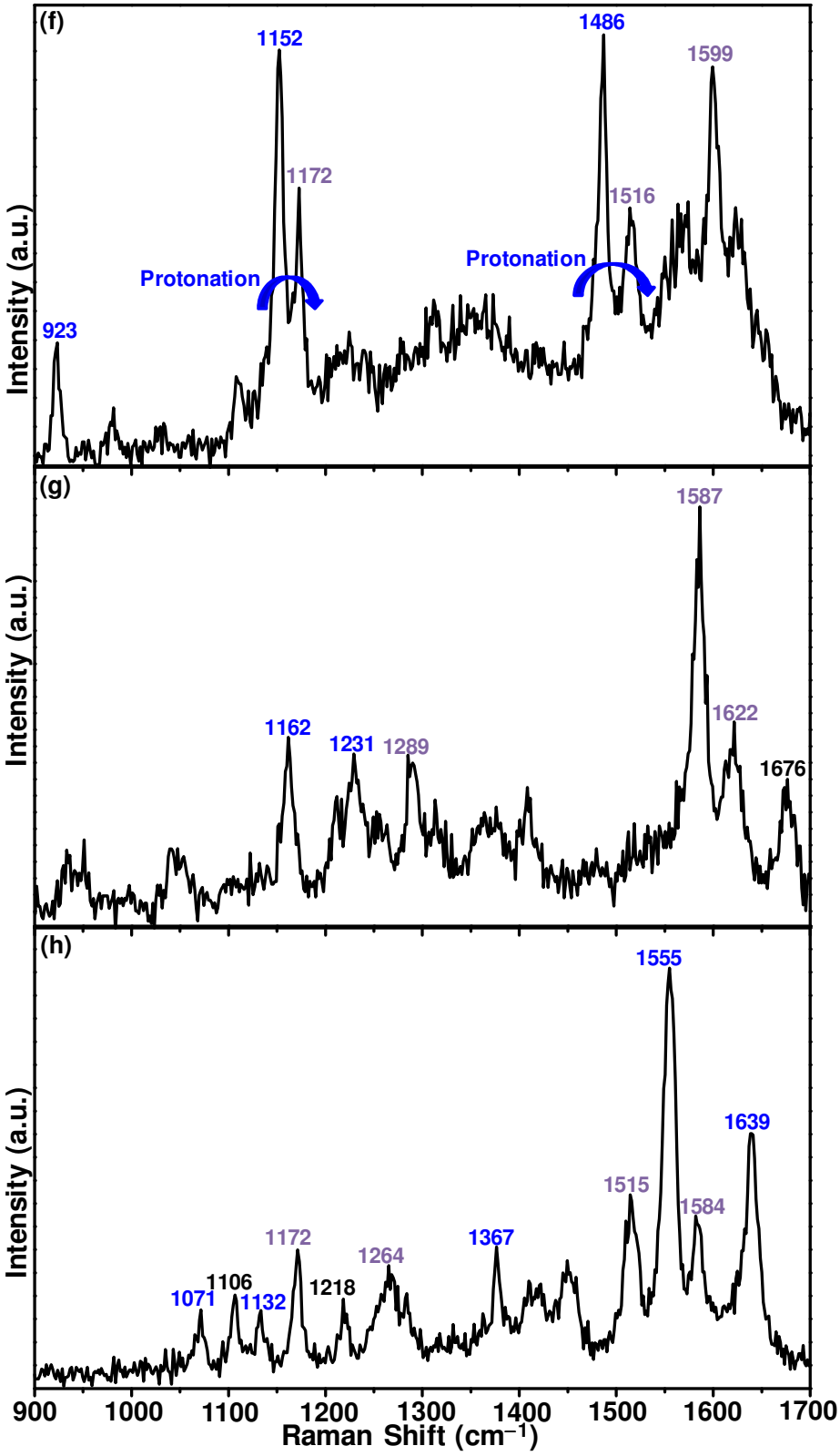

Figure IV.11. Single-molecule SERS spectra demonstrating: **(a)** PYP molecule captured in receiver state, **(b)** photo-isomerization to cis through shift in νC8-C9 from 1064 to 992 cm^{-1}, **(c)** Carbonyl flip with breaking of H-bond, observed through shift in νC9=O2 peak from 1638 to 1664 cm^{-1}, **(d)** 2 marker peaks

at 996 and 1662 cm^{-1} of the short-lived intermediate (pR) state, **(e)** Protonation through shift in νC7=C8 peak from 1554 to 1585 cm^{-1}, **(f)** 2 markers of Protonation: shift in δCH peak from 1152 (1163) to 1172 (1174) cm^{-1}, shift in τCC peak from 1488 (1495) to 1516 cm^{-1}, **(g)** 3 characteristic peaks of signaling (pB) state at 1289, 1587, and 1622 cm^{-1}, **(h)** PYP molecule captured in transition, with the appearance of peaks from pG (1132, 1555, 1639 cm^{-1}) and pB (1172, 1376, 1515, 1584 cm^{-1}) states. In the spectra, peaks from different states have been labeled in different colors: pG, pR and pB. Peaks that have not been reported in literature have been labeled in black.

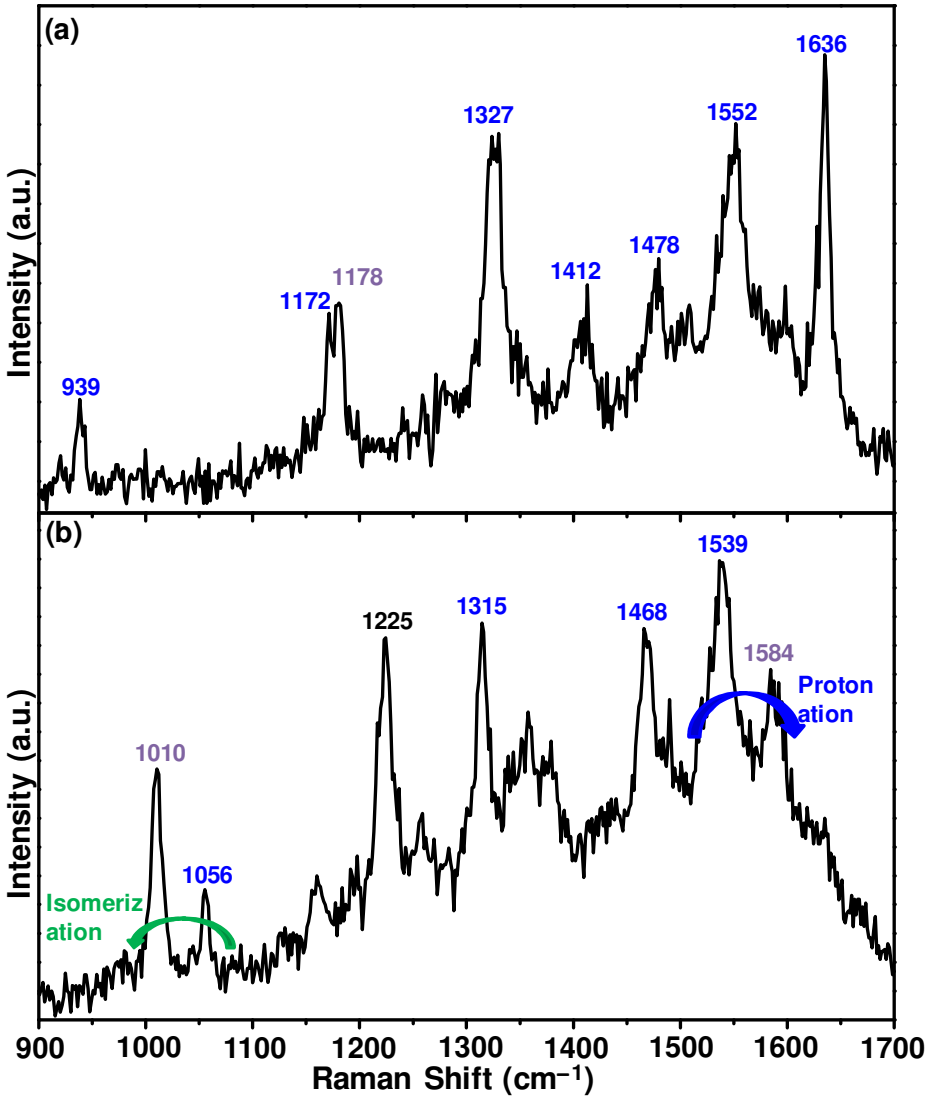

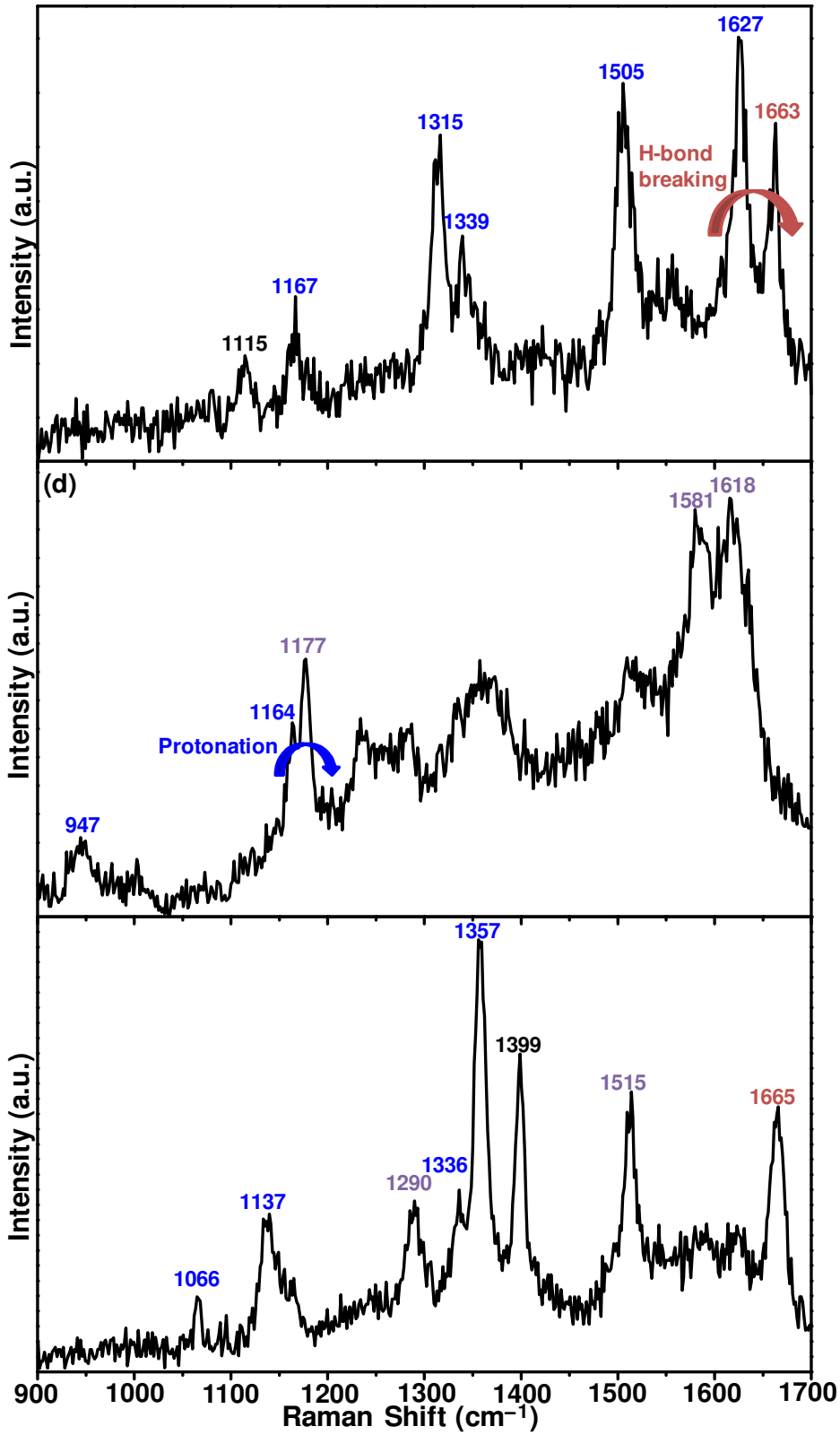

Figure IV.12. Single-molecule SERS spectra demonstrating: **(a)** PYP molecule captured in receiver (pG) state, **(b)** 2 steps of photocycle: photoisomerization to cis through shift in νC8-C9 from 1056 to 1010

(1000) cm^{-1}; Protonation: Shift in νC7=C8 peak from 1539 to 1584 cm^{-1}., **(c)** Carbonyl flip with breaking of H-bond, observed through shift in νC9=O2 peak from 1627 (1633) to 1663 cm^{-1}, **(d)** Protonation: shift in δCH peak from 1164 to 1177 (1174) cm^{-1}, **(e)** PYP molecule captured in transition, with the appearance of peaks from pG (1066, 1137, 1336, 1357 cm^{-1}), pR (1665 cm^{-1}) and pB (1290, 1515 cm^{-1}) states. In the spectra, peaks from different states have been labeled in different colors: pG, pR and pB. Peaks which have not been reported in literature have been labeled in black.

IV.6 Single-Molecule Data Average

Figure IV.13 compares the average of 385 SM-SERS spectra with the EA-SERS spectrum. The high level of spectral diffusion in averaged SM-SERS spectrum cannot be explained by statistical averaging because it is remarkably higher than that observed in EA-SERS. Therefore, this anomalous spectral diffusion can only originate from a mechanism that accounts for SERS-enhancement required for single-molecule detection. Accordingly, we attribute the observed spectral diffusion to pCA-Ag charge/electron transfer, i.e. chemical enhancement (up to 10^4), which together with the high electromagnetic enhancement (up to 10^9) provides the requisite SM sensitivity.[55, 76] Variations in PYP's chemisorption configuration on Ag are expected to lead to variations in pCA-Ag electron-transfer (wave function mixing) and variations in bond force constants resulting in heterogeneous peak broadening.[75, 78, 88] The electron transfer also allows new modes to be Raman-active,[78, 88] making the averaged SM-SERS spectrum more difficult to resolve. EA-SERS signal, on the other hand, is averaged dominantly from relatively lower enhancement sites, where electron transfer effects are missing or limited, hence the spectral diffusion is to a lesser degree.[55, 75]

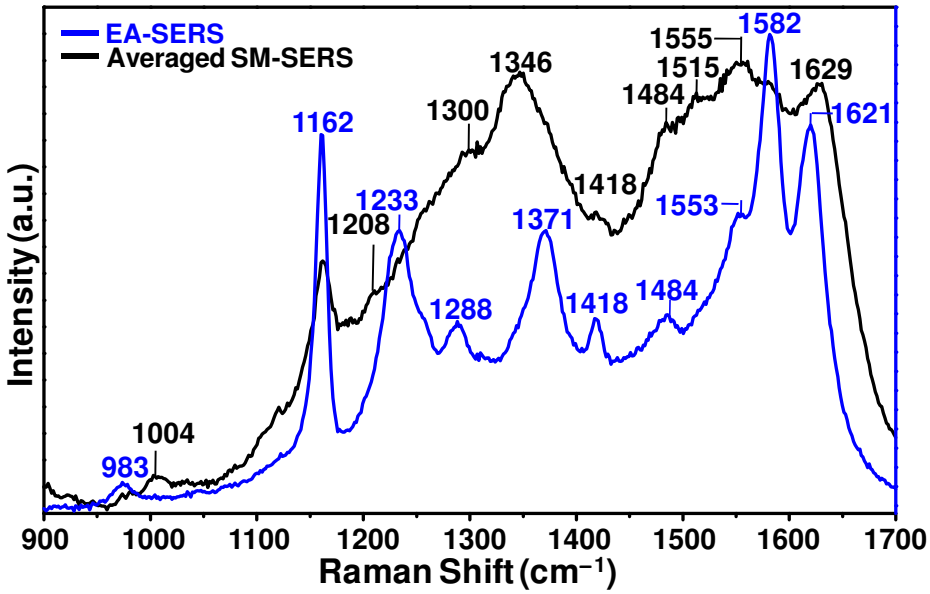

Figure IV.13. Comparison of averaged single-molecule SERS spectrum with ensemble-averaged SERS spectrum, revealing high spectral fluctuations in single molecule data, in contrast to the well-resolved ensemble-averaged spectrum.

The averaged SM-SERS spectrum exhibits strong bands at 1162, 1299, 1484, 1515, 1555, 1583 and 1629 (with a strong shoulder at 1620) cm^{-1} that are in agreement with the corresponding vibrational mode energies in PYP Raman literature [29, 46, 47, 49] and EA-SERS spectrum of PYP.[86] The bands at 1004 and 1200 cm^{-1} are discernable but not strong, consistent with the fact that these vibrational modes appear relatively less frequently in single-molecule spectra. The width of the bands in the averaged SM-SERS spectrum is a measure of spectral shifts/fluctuations observed in the corresponding vibrational modes.

From the analysis of this spectrum and more than 1000 SM-SERS spectra, Table II was prepared to list the spectral ranges of the vibrational modes observed in averaged SM-SERS spectrum. This table does not take into account the spectral shifts that result from the changes in chromophore environment, like breaking/re-establishment of H-bonds, in respective states. These shifts are generally more discrete

and well-resolved than those observed due to variations in chemisorption configuration. Thus, these changes result in discrete shifts that may not necessarily lead to broadening of vibrational bands in averaged SM-SERS spectrum; instead, they create new vibrational bands. For e.g., the νC9=O2 vibration peak at 1633 cm^{-1} shifts to 1672 cm^{-1} when the breaking of H-bond between carbonyl oxygen and amide group of Cys69 results in a discrete peak-shift of ~40 cm^{-1}. Also, such changes in H-bond environment of chromophore are perceived to result in different structural states rather than just spectral fluctuations in respective states.

Table II. Spectral fluctuations observed in single-molecule SERS spectra due to variations in chemisorption configuration. Assignments here are based on common Raman literature of PYP.

Vibration mode	Observed Raman shift (cm^{-1}) [29, 46-49]	Observed peak in averaged single-molecule SERS (cm^{-1}) [This work]	Estimated spectral range of Raman shift in single-molecule SERS (cm^{-1})
νC8—C9 (cis)	998/1002	1004	992 – 1020
δCH (pG)	1163	1162	1140 – 1170
δCH (pB)	1174	1174	1170 – 1179
νC4—C7 (pG)	1200*	1208	1192 – 1212
νC1—O1 (pG)	1345	1346	1335 – 1360
τCC (Asym.) (pG)	1495	1496	1488 – 1503
τCC (Asym.) (pB)	1515	1515	1504 – 1518
νC7=C8 (pG)	1537/1557	1555	1528 – 1566
νC7=C8 (pB)	1576/1599	1583	1568 – 1603
τCC (sym.) (pB)	1624#	1619	1612 – 1626
νC9=O2 (pG)	1633	1629	1627 – 1642

*: Theoretically computed value, not observed by Raman Scattering
#: Not observed in Raman scattering, but infrared absorption spectrum

Following deductions summarize the main features of the table:

1. The isomerization of PYP chromophore from trans to cis configuration is indicated by the shift in νC8—C9 vibrational mode from a peak at 1054 to 998/1002 cm^{-1}.[46, 47, 49, 89-93] The averaged SM-SERS spectrum exhibits a broad

though weak band at 1004 cm^{-1}, but no discernable band at 1054 cm^{-1}. We attribute this observation to better alignment of νC8—C9 vibration (after isomerization) with the enhanced field, which is normal to the surface. The spectral shifts/fluctuations in this mode in cis configuration of the chromophore were observed in the range from 992 to 1020 cm^{-1}.

2. Low spectral broadening in the δCH vibrational mode at 1163 cm^{-1} suggests a higher spectral consistency in appearance of this mode.[29, 47, 49] Indeed, analysis of this band along with its peak positions in single molecule spectra indicates that while spectral fluctuations lie in the range between 1140 and 1169 cm^{-1}, most appearances were recorded closer to the observed Raman scattering peak, i.e. 1163 cm^{-1}. We also observed a small shoulder at 1174 cm^{-1}. In literature, this band is attributed to δCH vibrational mode in the protonated configuration of the PYP chromophore.[30, 31, 38, 46, 48, 94] The single-molecule spectra did not record this mode frequently, but the analysis of few pertinent SM-SERS spectra shows fluctuations in peak ranging from 1170 to 1179 cm^{-1}.
3. The τCC (asymmetric) vibration mode in the protonated form of PYP chromophore at 1515 cm^{-1} appears as a band with high spectral fluctuations, exhibiting spectra with peaks ranging from 1505 to 1520 cm^{-1}. The corresponding mode in the receiver state of PYP chromophore [47] was observed at 1496 cm^{-1} and found to peak between 1487 and 1504 cm^{-1}.
4. The second strongest band in the averaged SM-SERS spectrum was observed at 1555 cm^{-1}. In the PYP Raman literature, this peak is attributed to νC7=C8 (stretching) vibration mode in the receiver state.[29, 47-49] The analysis of SM-SERS

spectra reveals spectral fluctuations in this mode with peaks ranging from 1528 to 1566 cm^{-1}.

The averaged SM-SERS spectrum in Figure IV.13 shows another strong band at 1582 cm^{-1} that is attributed to νC7=C8 (stretching) vibration in the signaling state.[29, 47, 49] Analysis of single-molecule spectra suggests that the discernable spectral fluctuations in the mode range from 1567 to 1605 cm^{-1}.

The band at 1582 cm^{-1} is observed to be stronger than the band at 1555 cm^{-1} in EA-SERS spectrum. However, in averaged SM-SERS spectrum the band at 1555 cm^{-1} appears stronger than that at 1582 cm^{-1}. At the same time, we observed the dominance of peak at 1004 cm^{-1} which is attributed to cis configuration in PYP. This "anomaly" can be explained by the model involving thermal energy produced at the "hot-spots" to overcome the kinetic barriers in the recovery reaction of PYP, and comparison of scan-integration time with duration of PYP recovery to folded receiver state.

As suggested by Hellingwerf and coworkers,[43] the formation of α-helix by amino acid residues forms a kinetic barrier for the recovery reaction. We propose that the unfolded PYP molecule in signaling state receives the requisite thermal energy at the high-intensity hot-spots to overcome the kinetic barrier that leads to folding of amino-acid residues at 43-52. This folding is followed by the formation of an intermediate with deprotonated chromophore in cis configuration about C7=C8 bond, which facilitates the isomerization from cis to trans.[45] This complete reaction takes 350 ms. However, we propose that the SERS captures, at best, the events occurring in only the first 250 ms of the recovery reaction. Thus, with

its formation facilitated by the high intensity hot-spots, the character of deprotonated chromophore in cis configuration is found most dominantly in the averaged SM-SERS spectrum.

5. In the literature, the νC9=O2 (stretching) vibration mode has been reported to be at 1633 cm^{-1} in the receiver state,[47, 49] but it was observed as a band at 1629 cm^{-1} in the averaged SM-SERS spectrum. It is likely that the shift is due to convolution of this peak with nearby lower energy peaks such as the peak at 1619 cm^{-1}. Based on the analysis of SM-SERS spectra, the spectral fluctuations in νC9=O2 (stretching) vibration mode are estimated to result in peaks in the range of 1627 to 1642 cm^{-1}.
6. We also observed a strong shoulder at 1619 cm^{-1} in the averaged SM-SERS spectrum, most likely attributed to τCC (symmetric ring stretching) vibration mode. This mode was not observed in Raman scattering, however infrared absorption spectrum of PYP's pB state shows a well-resolved peak at 1624 cm^{-1}.[50] From the analysis of SM-SERS spectra, it is inferred that this mode peaks in the range of 1612 to 1626 cm^{-1}.

IV.7 New Vibrational Modes and Peaks

In the majority of single-molecule spectra, we observed vibrational modes that were theoretically computed but not detected by Raman scattering. Figure IV.14 shows three spectra demonstrating at least 2 of such unreported vibrational modes. Possibly, these Raman-inactive modes become SERS-active by modified selection rules due to chemisorption-induced symmetry lowering and mixing of vibronic states between pCA and Ag.[16, 55, 78, 88] Upon adsorption to the Ag surface, the molecules can lose their center

of symmetry that originally dictated the mode selection; as a result, the requirements of mutual exclusion rule, which governs the Raman and infrared activation of modes, are eliminated leading to modification in selection rules and, thus, differences in mode selection.[16] The orientation of adsorption of molecule on the surface governs the modification in the symmetry and thus the selection rules. Also, since scattering is a result of molecular polarizability caused by normal electrical dipole component, the orientation of adsorption of molecule also affects the efficiency of scattering. Adsorption of molecule with its dipolar axis perpendicular to the Ag surface (i.e., parallel to the enhanced fields) leads to more efficient scattering while parallel-axis adsorption attenuates the same.

SM spectra in Figure IV.14a and Figure IV.14b show a well-resolved peak at ~1200 cm^{-1}. This peak was not observed in the time-resolved Raman scattering studies in the literature; though predicted by theoretical calculations as the νC4–C7 mode in pG state.[47] The shoulder attributed to this mode was observed at 1208 cm^{-1} in the averaged SM-SERS spectrum (Figure IV.13). The analysis of SM-SERS spectra revealed that the spectral shifts and fluctuations in the mode ranged from peaks at 1192 to 1212 cm^{-1} (Figure IV.10a, Figure IV.11a, Figure IV.14a and Figure IV.14b).

Another new mode was observed in SM-SERS spectrum at 1345 cm^{-1} and is attributed to νC1–O1 vibration in the receiver state.[47] This mode appeared very strongly and frequently in PYP SM-SERS spectra, but was not observed in Raman scattering.[47] Figure IV.14a and Figure IV.14c demonstrate two SM-SERS spectra with sharp peaks at 1345 cm^{-1}. Analysis of SM-SERS spectra suggests that this mode is highly sensitive to variations in chemisorption configuration; as a result, it exhibits spectral fluctuations

and peaks in the range of 1335 to 1360 cm^{-1} (Figure IV.10a, Figure IV.11d, Figure IV.11e, Figure IV.12c and Figure IV.12e).

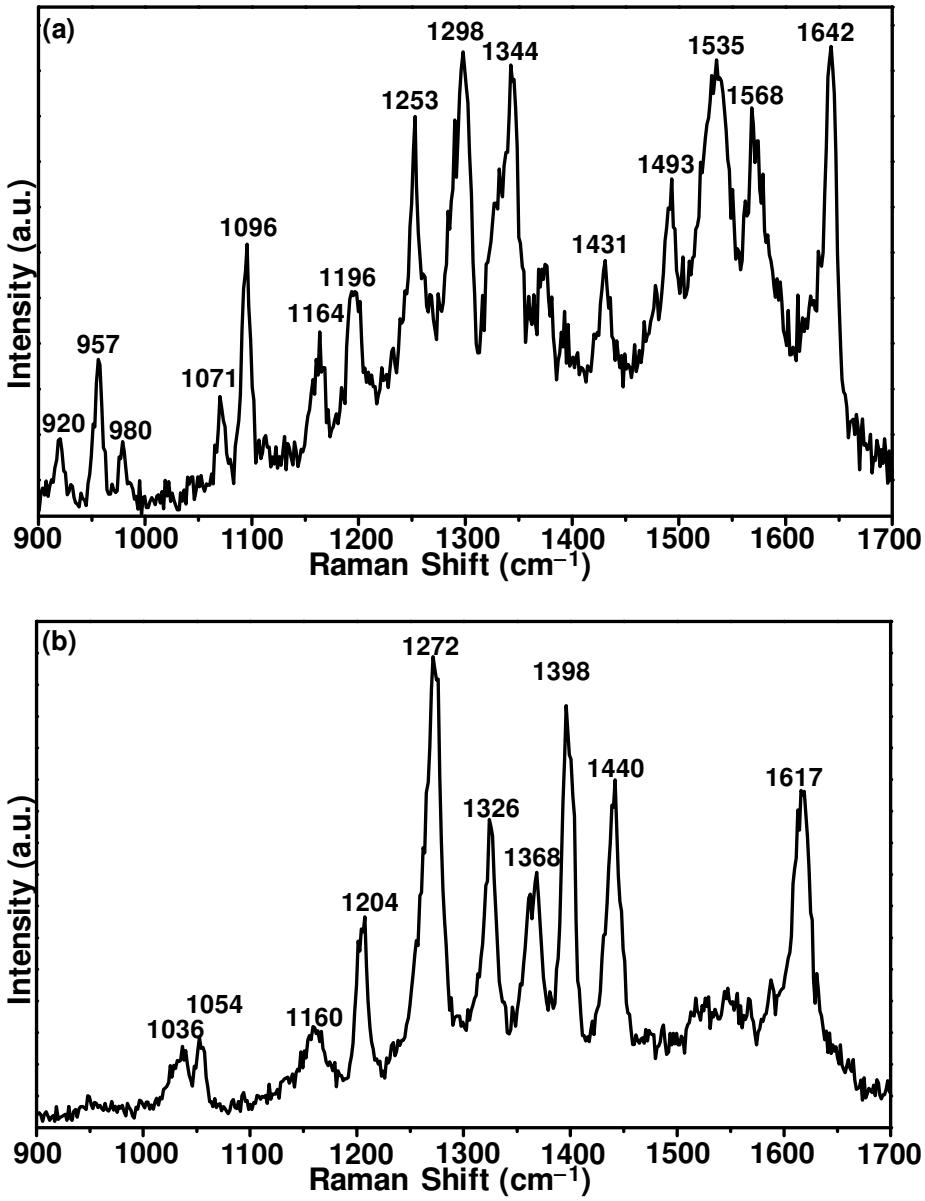

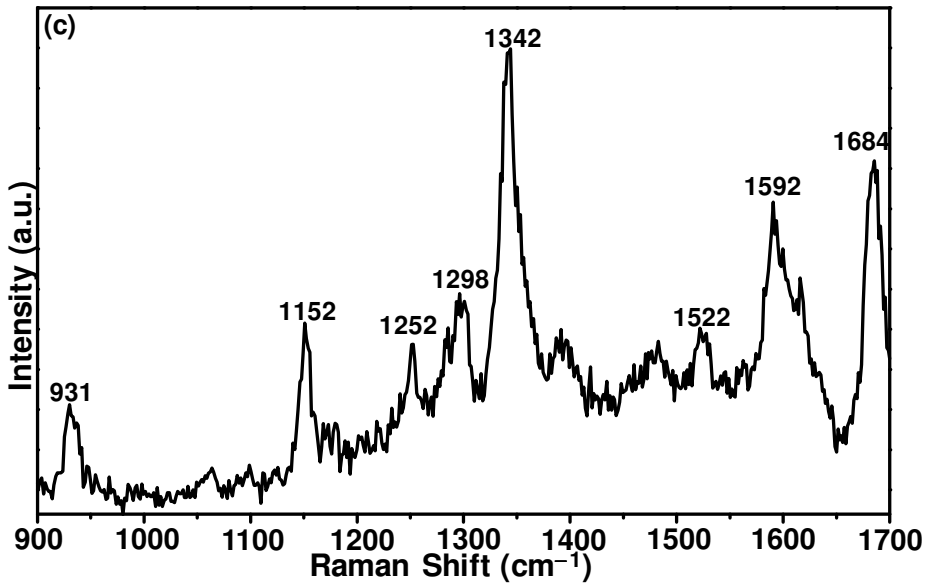

Figure IV.14. Single-molecule SERS spectra exhibiting the appearance of some vibrational modes not observed in Raman scattering of PYP: **(a)** peaks at 920, 957 (961), 1071, 1096 (1091), 1196 (1200), 1344, 1535 cm^{-1}, **(b)** peaks at 1036, 1204 (1200), 1326, 1368, 1398, 1617 cm^{-1}, **(c)** peaks at 931, 1252, 1342, 1684 cm^{-1}.

IV.8 Correlations between Vibrational Modes

IV.8.1 νC4–C7 versus νC9=O2

The analysis of more than one thousand SM-SERS spectra of PYP reveals the existence of an inverse correlation between the νC4–C7 (Raman peak at 1208 cm^{-1}) and νC9=O2 (observed Raman peak at 1633 cm^{-1}) vibrational modes in receiver state, i.e. the strength of one mode decreases as that of the other increases. Figure IV.15 demonstrates this inverse correlation by formulating a histogram over ratio of peak-intensities of modes at 1200 and 1633 cm^{-1}. The "ratio" is defined as: smaller peak intensity divided by larger intensity which lies between 0 and 1. The histogram was formulated over 100 spectra that captured at least one of the two modes. The bin size employed is 0.1. The graph shows a 69% probability for the ratio of peak-intensities to lie between 0 and 0.1, indicating that the two modes are generally mutually exclusive.

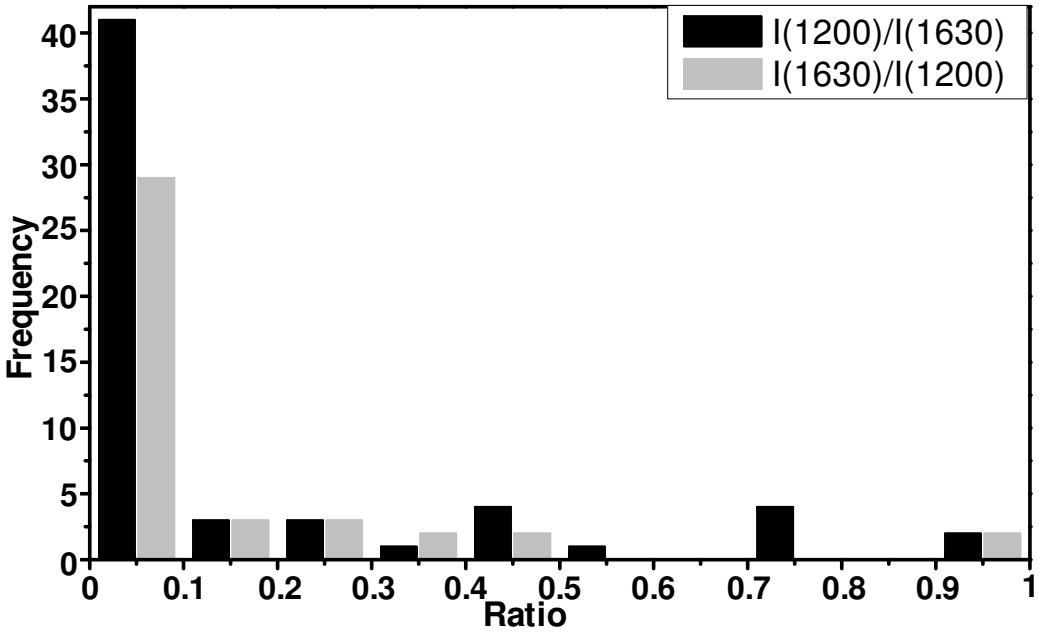

Figure IV.15. Histogram depicting the ratio between intensities of peaks at 1630 and 1200 cm^{-1} in 100 SM-SERS spectra. The bin size is 0.1, and ranges from 0 to 1.

Figure IV.16 shows three consecutive SM-SERS spectra that illustrate the disappearance of the νC4–C7 mode at 1200 cm^{-1} with the appearance and strengthening of the νC9=O2 mode at 1633 cm^{-1}. This mutual exclusion suggests that the transition moments of these two modes are orthogonal.[16] In other words, PYP must have two typical adsorption configurations on Ag. For each configuration, only one of the transition moments must align with the electric field at the hot spot (which is dominantly normal to the Ag surface),[78, 88] hence the enhanced field on the nanoparticle surface aligns with only one of these two transition moments at a time. Thus, at any point of time, one of the modes would be enhanced while the other would be attenuated. As a result, the modes of vibration are observed to be mutually exclusive of each other.

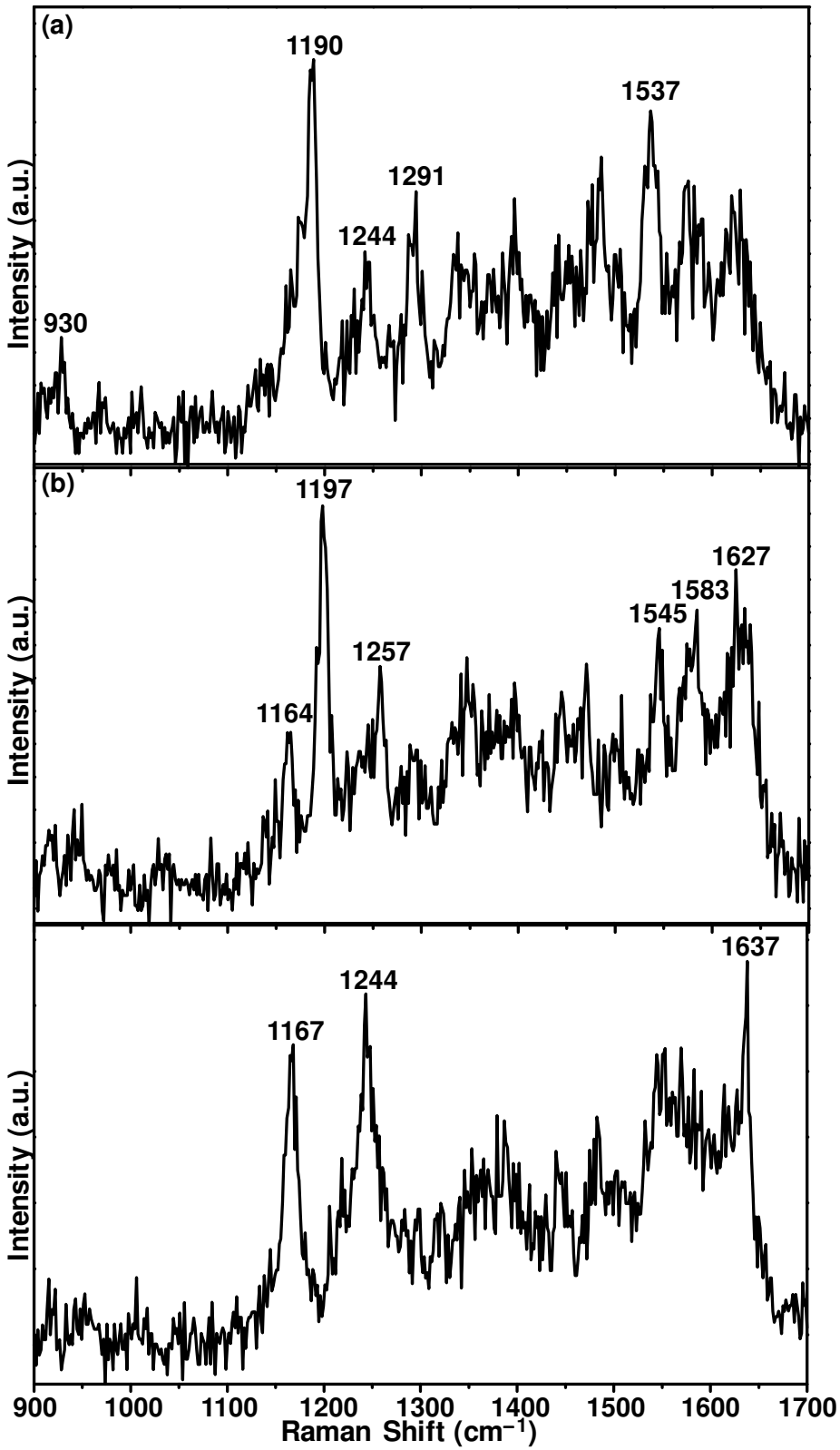

Figure IV.16. Consecutive single-molecule SERS spectra demonstrating the gain in strength of νC9=O2 vibrational mode (1633 cm^{-1}) and concurrent loss in the strength of νC4–C7 mode (at 1200 cm^{-1}).

Figure IV.17 shows the isolated PYP chromophore structure illustrating the angle between the C4–C7 and C9=O2 bonds. Although the angle between the bonds is about 120º, this is not the angle between the transition moments of νC4–C7 and νC9=O2 modes. These modes are dominated by the stretching motion of C4–C7 and C9=O2 bonds, but they also involve the motion of all other atoms in the molecule. It is, thus, likely that when the whole molecule vibrates, the net dipolar axes of the two vibrational modes are normal to each other. Future theoretical work should determine the exact angle between the transition moments of these two modes. In some rare spectra where the two modes did appear together, we observed that one peak was distinctly stronger and better-resolved than the other. However, if the electric field bisects the two vibration axes, both the modes can appear simultaneously with diminished intensities. In this case, the molecule's adsorption configuration is different, and favors both modes. Otherwise, it is also possible that the molecule switches from one adsorption configuration to another, each of which select one mode only.

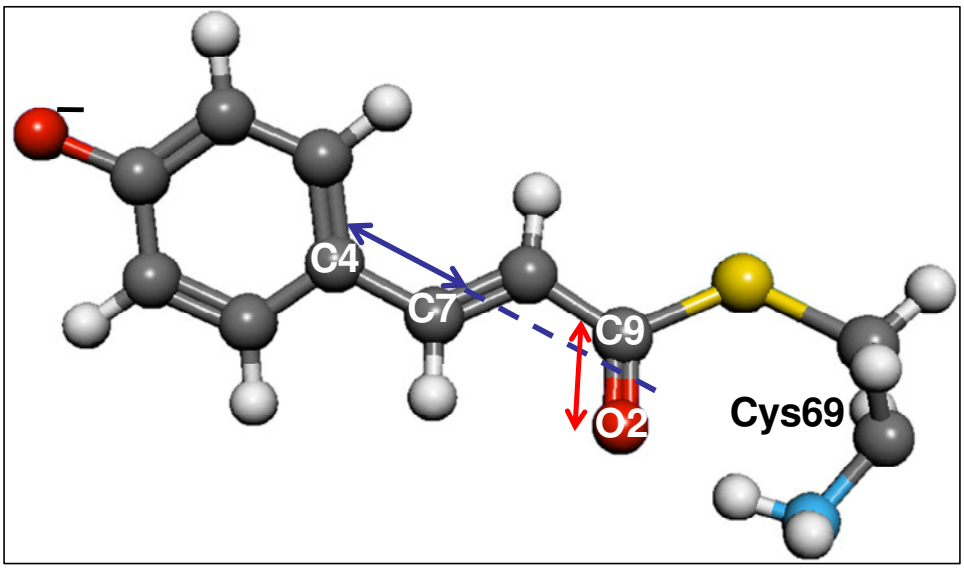

Figure IV.17. Structure of PYP chromophore demonstrating apparent angle between the axes of C4–C7 and C9=O2 bonds.

IV.8.2 δCH in pG and pB states versus peak at 1240 cm^{-1}

Figure IV.18 shows three consecutive SM-SERS spectra demonstrating the negative correlation between the vibrational bands at 1176 and 1240 cm^{-1}, and the positive correlation between the bands at 1163 and 1240 cm^{-1}. From Figure IV.18a to Figure IV.18b, the appearance of the peak at ~1240 cm^{-1} coincides with the disappearance of the peak at 1176 cm^{-1} and strengthening of peak at 1163 cm^{-1}. The next spectrum in Figure IV.18c shows the peaks at ~1163 and ~1240 cm^{-1} staying unaffected by other modes of vibration. Figure IV.19a displays a SM-SERS spectra that shows the mutually exclusive properties of two bands at 1176 and 1240 cm^{-1}, while the spectrum in Figure IV.19a shows that appearance of the band at 1240 cm^{-1} makes the appearance of peak at 1163 cm^{-1} more likely.

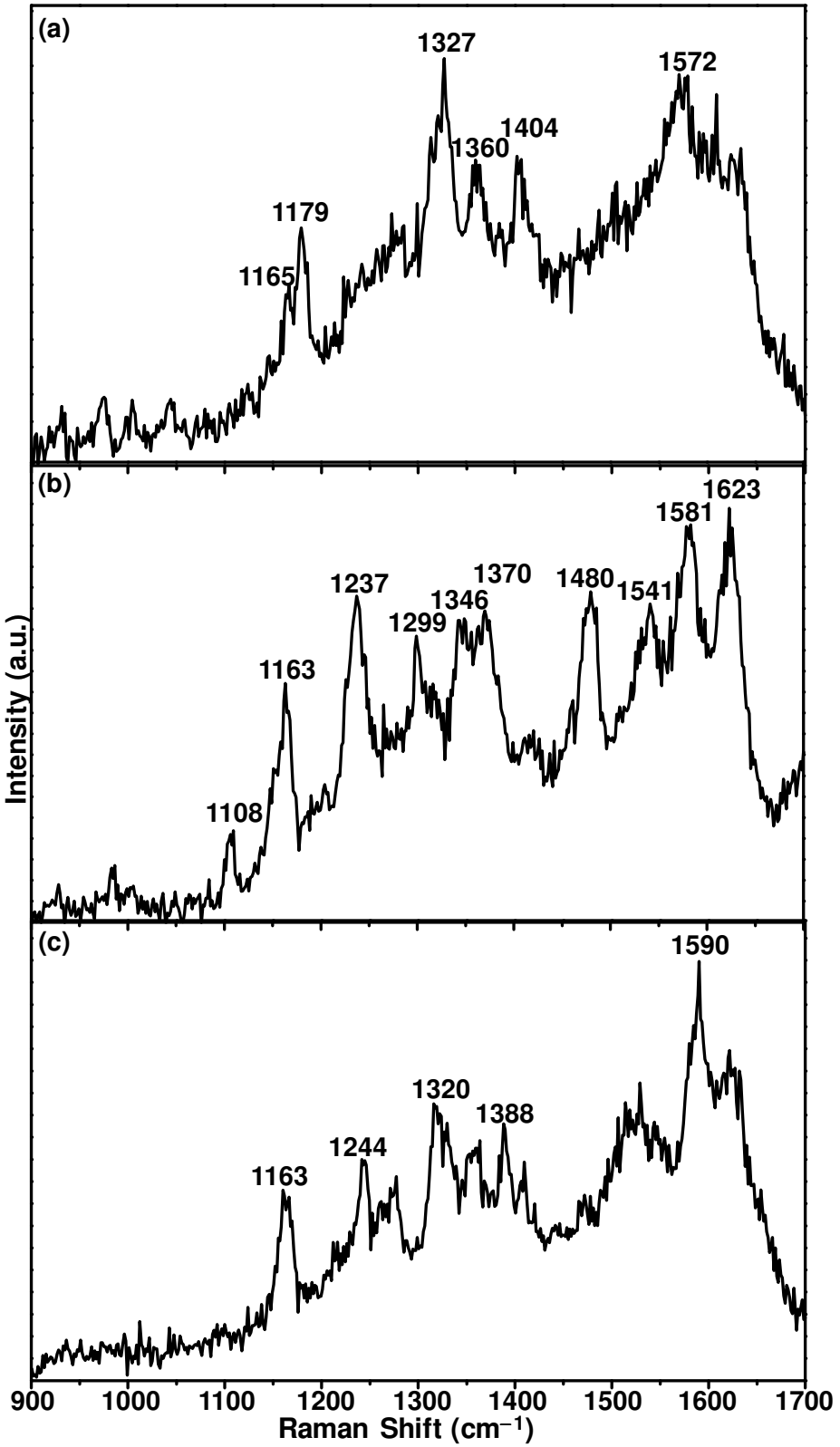

Figure IV.18. Consecutive spectra demonstrating negative correlation between vibrational bands at 1176 and 1240 cm^{-1}, while a positive correlation between those at 1163 and 1240 cm^{-1}.

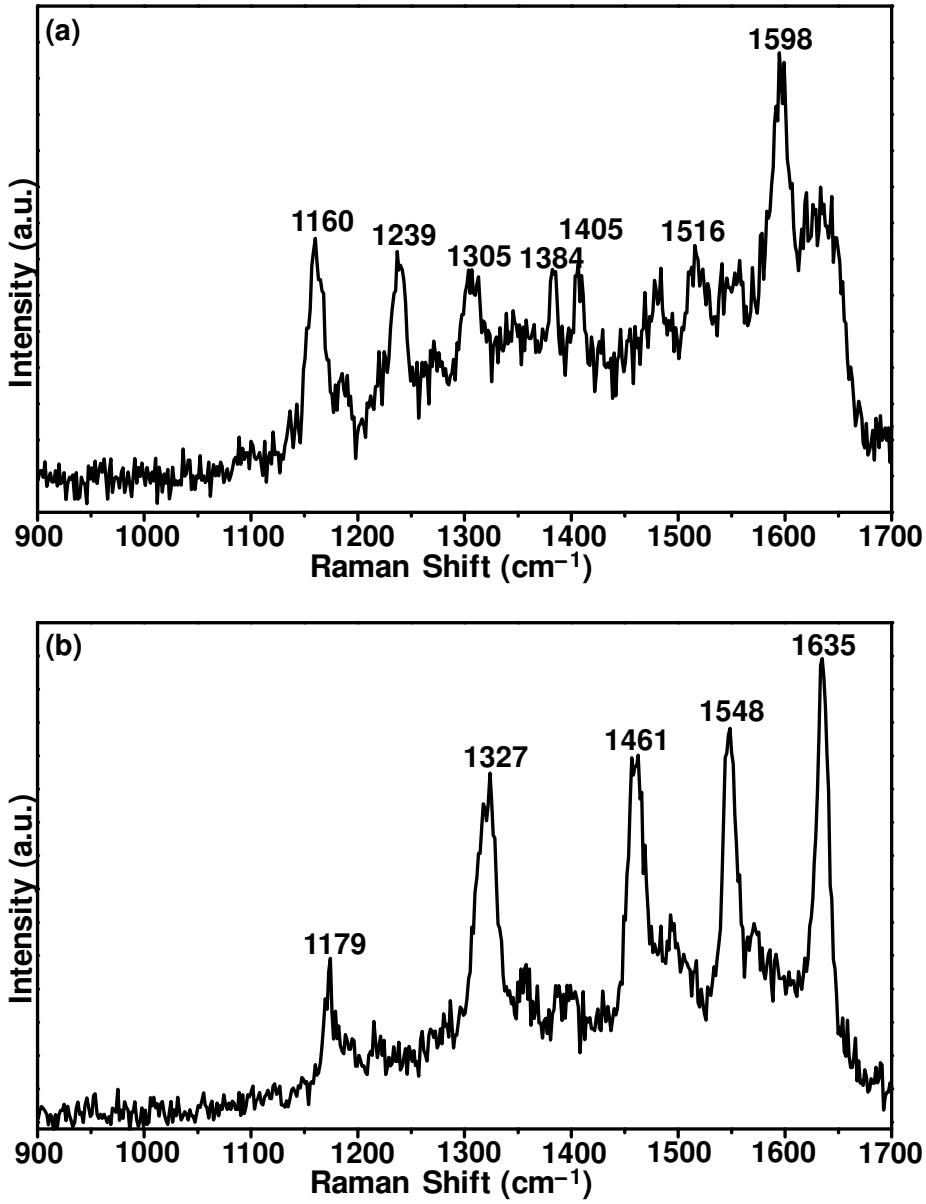

Figure IV.19. Single molecule SERS spectra demonstrating: **(a)** Concurrent appearance of bands at 1160 and 1240 cm^{-1}; **(b)** Appearance of band at 1176 cm^{-1} indicating its mutual exclusiveness with the band at 1240 cm^{-1}.

Although the 1240 cm^{-1} peak shows up strongly at 1234 cm^{-1} in EA-SERS spectrum of PYP (Figure IV.5) and pCA (Figure IV.6), it has not been reported in Raman literature. In the comparison of Raman scattering spectra of anionic and neutral configurations of pCA, we observed the appearance of a peak at 1248 cm^{-1} in the former configuration (Figure IV.20). The peak at 1240 cm^{-1} bears a negative correlation

with the protonation marker at 1176 cm^{-1}, and hence is likely a deprotonation marker. This observation is further compounded by the likelihood of the peak at 1248 cm^{-1} in deprotonated pCA Raman scattering belonging to the same mode as 1240 cm^{-1} in PYP SM-SERS.

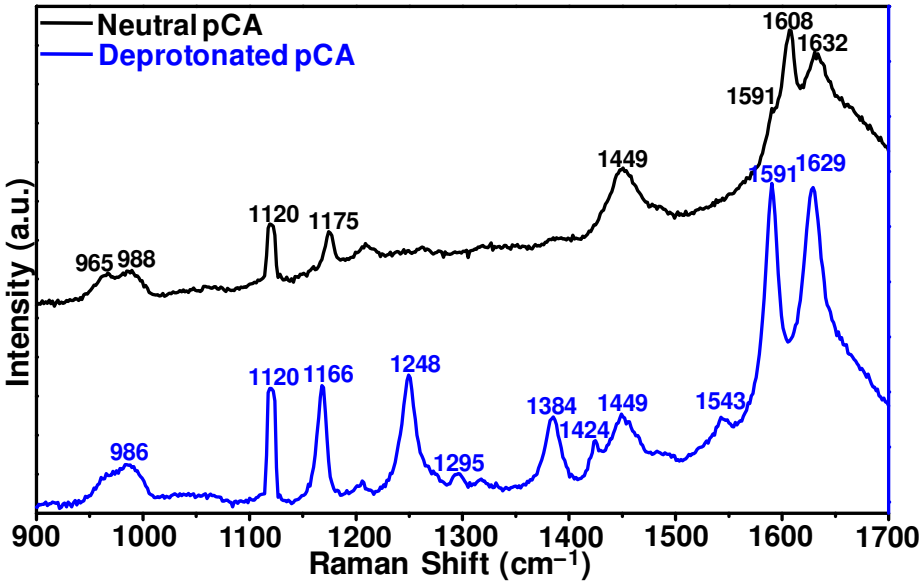

Figure IV.20. Comparison between Raman scattering data of p-Coumaric Acid in neutral and basic solutions, thus neutral and deprotonated molecules respectively. Peak at 1120 cm^{-1} results from the ambient fluorescent light.

IV.9 Single Peak Jumps

We observed that about 1 in every 25 SM-SERS spectra recorded only 1 dominant mode of vibration; the other modes were observed to be either relatively subdued or completely absent. Figure IV.21 shows 7 of such spectra with respective single dominant modes of vibration. We did not observe any definite pattern in the frequency or in the peak-intensity of singularly enhanced modes in such spectra. As evident from the SM-SERS spectra in Figure IV.21, we didn't observe dominance of any

specific mode(s) of vibration in frequency of spectra, i.e. we observed different modes of vibration appear in different spectra.

This phenomenon can be attributed to chemisorption of PYP molecules on AgNPs that results in modifications in selection rules for SERS, with the introduction of new and more restrictive selection rules. These new selection rules likely lead to suppression of other modes of vibrations while resulting in enhancement of individual modes of vibration. Combined with these new selection rules, the already existing selection rules favoring individual modes of vibration that are in alignment with the enhanced field lead to such singular enhancements.[88] Since chemisorption of molecules on nanoparticles plays an important role in these single-peak enhancements, this effect is unique to SERS.

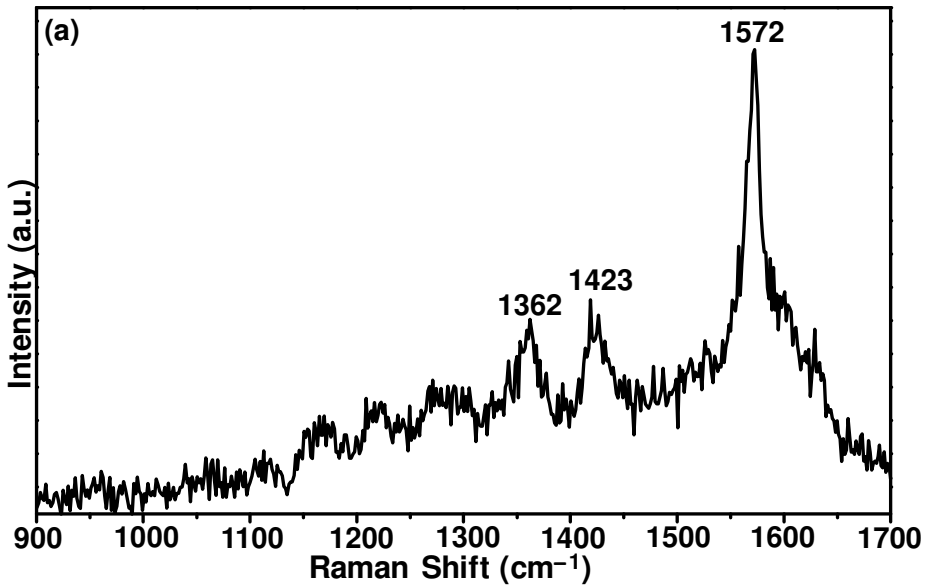

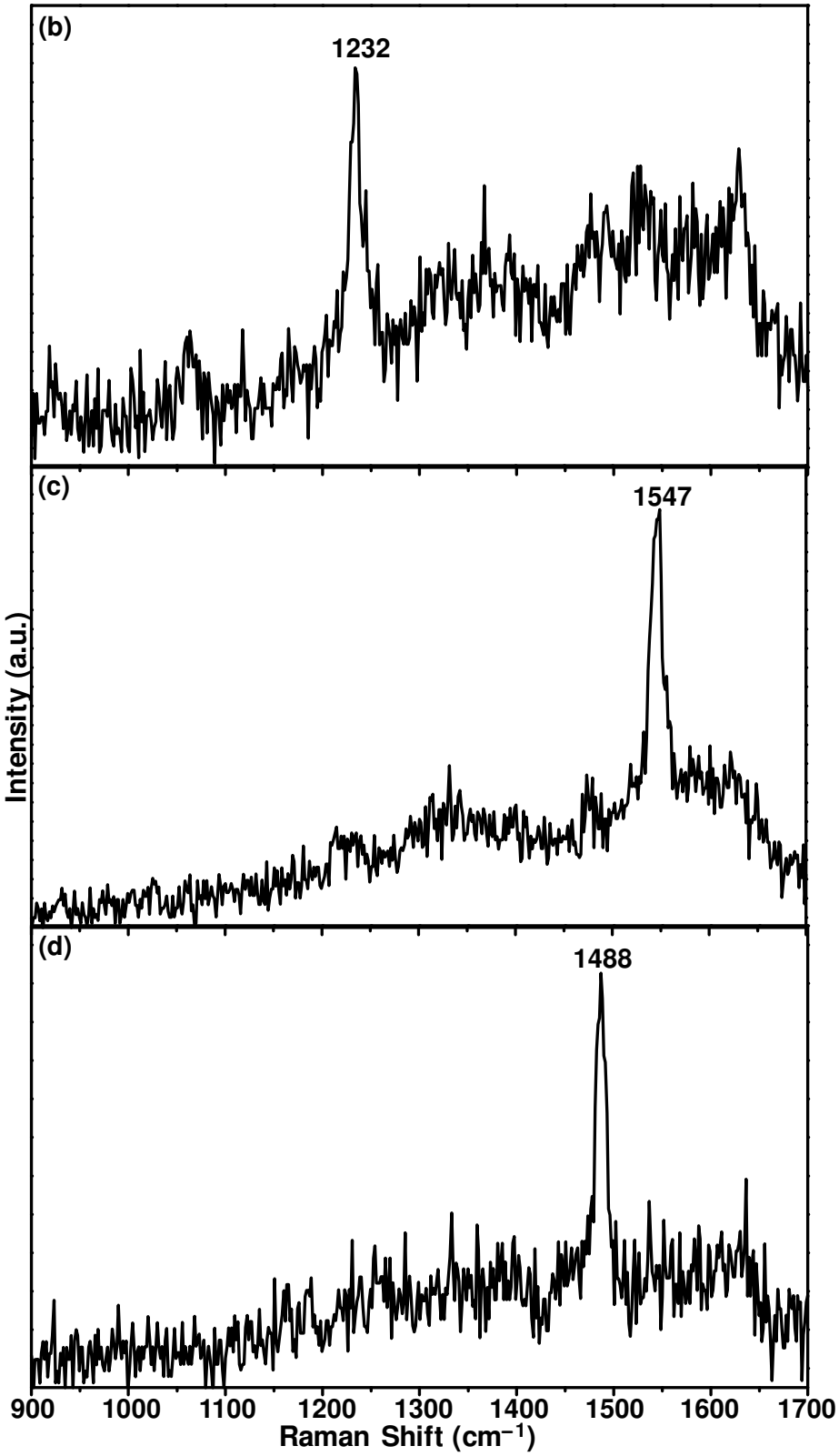
(b)
1232
(c)
1547
(d)
1488
Intensity (a.u.)
900
1000
1100
1200
1300
1400
1500
1600
1700
Raman Shift (cm^{-1})

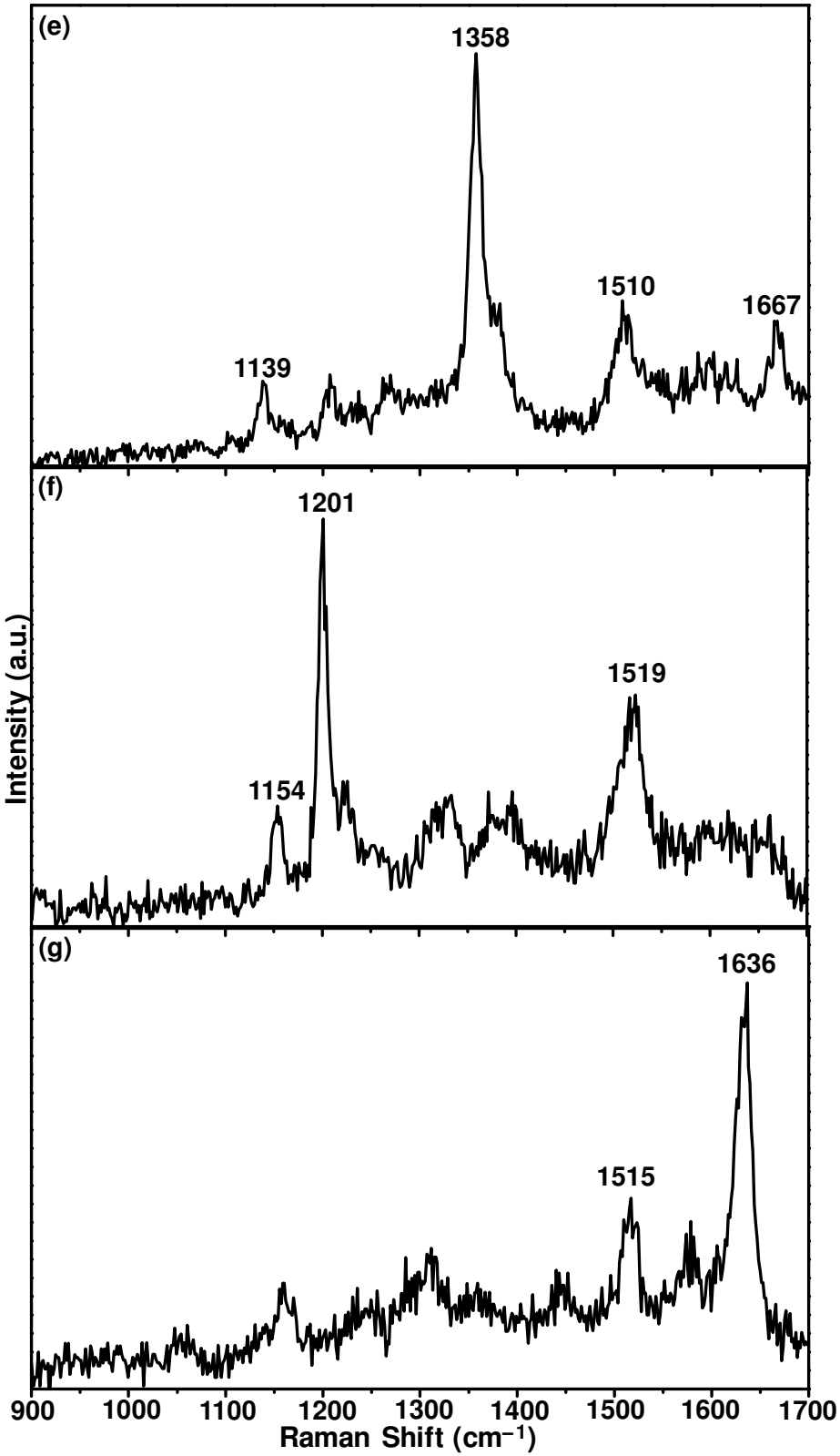

Figure IV.21. Single-molecule SERS spectra exhibiting exclusive enhancement for single modes of vibration.

CHAPTER V. CONCLUSION

V.1 Conclusions

Single-molecule SERS of PYP was demonstrated on “nanometal-on-semiconductor” SERS substrates that were prepared by reducing Ag nanoparticles on Ge films. Temporal appearance of sharp discernable SERS peaks of PYP with significant spectral shifts in consecutive spectra are associated with single PYP molecules chemisorbing on the high enhancement sites (“hot spots”) on our SERS substrates. These SERS-enhancement sites are found to be associated with plasmon hybridization that possibly results from “metal nanochains” or other complex metal nanostructures on the substrates.

The single-molecule spectra of PYP in this study reveal various structural conformations and transitions of the PYP chromophore that are homologous to different conformational steps of single PYP molecules during photocycle. The analysis of these spectra thus suggests that the PYP molecules undergo structural transitions while they are captured in hot-spots. Thus, it is fair to state that PYP is a tolerant protein in the sense that its chemisorption at high SERS enhancement sites does not prevent it from exhibiting its typical conformational transitions. The ensemble-averaged SERS of PYP and isolated pCA show almost identical spectra, indicating that the Raman signal primarily results from the chromophore of PYP.

When compared with EA-SERS spectrum, the SM-SERS spectra are distinguishable from narrower, sharper and better-resolved peaks, i.e. lack of heterogeneous spectral broadening.[55] We also observed fluctuations in energy and relative intensities of SM-SERS vibration modes due to changes in chemisorption configuration, orientation (with respect to polarization of local radiation) and environment of the chromophore. These fluctuations also indicate capturing SM-SERS spectra. Based on the vibration mode at 1555 cm^{-1} in these SM-SERS spectra and Raman scattering spectrum, we calculated SM-SERS enhancement factor on the substrates at 1.1×10^{11}.

In the majority of SM-SERS spectra, we observed sharp and well-resolved peaks belonging to vibrational modes that were theoretically computed but not reported in PYP Raman literature. Possibly, these Raman-inactive modes become SERS-active by modified selection rules due to chemisorption-induced symmetry lowering and mixing of vibronic states between pCA and Ag.[16, 78, 88] This observation hints at the significance of single molecule SERS studies in allowing us to observe and analyze modes that are otherwise hidden, and thus get a better understanding of the PYP photocycle.

To get a better understanding of the SM-SERS spectra of PYP, we averaged 385 single-molecule spectra and observed an inordinately high level of spectral diffusion in the averaged SM-SERS spectrum. Accordingly, we attribute this spectral diffusion to variations in PYP's chemisorption configuration on Ag leading to variations in pCA-Ag electron-transfer (wave function mixing) and variations in bond force constants. These factors along with the appearance of new modes result in heterogeneous peak broadening, making the averaged SM-SERS spectrum more difficult to resolve.[75, 78, 88]

We also observed that though multiple peaks (markers) identify a certain PYP state, not all appear in the same SM-SERS spectrum. For example, it was observed that when the 1200 cm^{-1} peak (νC4-C7, pG) is strong, the 1630 cm^{-1} peak (νC9=O2, pG) is weak and vice versa. This phenomenon suggests that given the signal is from a single molecule, the transition moments of such exclusive modes are orthogonal;[16] and only one of those transition moments must align with the electric field at the hot spot (which is dominantly normal to the Ag surface).[78, 88] Such mutually exclusive peak pairs were identified in this study, which can help elucidate the molecular structure and configuration using the SERS selection rules. For example, based on such exclusive pairs we have been able to categorize the frequently appearing peak at ~1234 cm^{-1} (also observed in EA-SERS) as a deprotonation marker, possibly the same peak as observed in Raman scattering scan of deprotonated pCA at 1248 cm^{-1} (Figure IV.20).

About 5% of the SM-SERS spectra recorded only one dominant mode of vibration, the other modes were observed to be either relatively subdued or almost completely absent. We attribute this exclusive enhancement for different modes of vibration to the combination of introduction of new restrictive selection rules due to chemisorption of molecule and the incumbent selection rules that favor individual modes of vibration modes aligned with the enhanced fields.

These results, thus, provide a framework for future analysis of the photocycle in PYP using single-molecule SERS studies with high structural sensitivity, and scope for more insight into the biophysics of the molecule.

V.2 Limitations of the Study

With the mandatory 1 s shutter/read-out time in the Renishaw RM1000 system that was employed in this study, we lost the information on upward and downward progressions of single-molecule jumps as well as the order of events as they occurred during the photocycle. This affects the system's ability to resolve the events in the structural transition of the molecule. As a result, each spectrum intermittently collects information, like a "logbook", on every structural motion that occurs in the protein molecule during the scan-integration time. This integration time of 0.25 s is relatively short when compared to the integration times in other SM-SERS studies reported in literature. However, when compared with the duration of events in the PYP's photocycle, it is quite long. This makes the resolution of the events difficult, which also negatively affects the analysis of SM-SERS spectra.

V.3 Future Work

This study sets a platform for further studies to explore the biophysics, especially resolution of photocycle, of PYP. The newly employed WITec Raman system (in Kalkan group's lab) with no shutter/read-out time, along with low integration time (as low as 35 ms), can help better resolve the order of events in the structural transition of PYP. Better resolution of events of molecule's structural transitions would also be helpful in the study of variations of PYP's intermediate conformational states, with and without photo-excitation. The understanding gained from single-molecule SERS of PYP can be translated into engineering of PYP molecules as optical switches.

REFERENCES

1. Moerner, W.E., A dozen years of single-molecule spectroscopy in physics, chemistry, and biophysics. *Journal of Physical Chemistry B* **2002,** *106* (5), 910.

2. Meyer, T.E., Isolation and characterization of soluble cytochromes, ferredoxins and other chromophoric proteins from the halophilic phototrophic bacterium ectothiorhodospira-halophila. *Biochimica Et Biophysica Acta* **1985,** *806* (1), 175.

3. Meyer, T.E.; Cusanovich, M.A.; Tollin, G., A water-soluble, photoactive protein with kinetics similar to those of sensory rhodopsin. *Federation Proceedings* **1987,** *46* (6), 2114.

4. Kort, R.; Hoff, W.D.; VanWest, M.; Kroon, A.R.; Hoffer, S.M.; Vlieg, K.H.; Crielaard, W.; VanBeeumen, J.J.; Hellingwerf, K.J., The xanthopsins: A new family of eubacterial blue-light photoreceptors. *Embo Journal* **1996,** *15* (13), 3209.

5. Sprenger, W.W.; Hoff, W.D.; Armitage, J.P.; Hellingwerf, K.J., The eubacterium ectothiorhodospira-halophila is negatively phototactic, with a wavelength dependence that fits the absorption-spectrum of the photoactive yellow protein. *Journal of Bacteriology* **1993,** *175* (10), 3096.

6. Hellingwerf, K.J.; Hendriks, J.; Gensch, T., Photoactive yellow protein, a new type of photoreceptor protein: Will this "Yellow lab" Bring us where we want to go? *Journal of Physical Chemistry A* **2003,** *107* (8), 1082.

7. Stenkamp, R.E.; Teller, D.C.; Palczewski, K., Crystal structure of rhodopsin: A g-protein-coupled receptor. *Chembiochem* **2002,** *3* (10), 963.

8. Gensch, T.; Churio, M.S.; Braslavsky, S.E.; Schaffner, K., Primary quantum yield and volume change of phytochrome-a phototransformation determined by laser-induced optoacoustic spectroscopy. *Photochemistry and Photobiology* **1996,** *63* (6), 719.

9. Andel, F.; Murphy, J.T.; Haas, J.A.; McDowell, M.T.; van der Hoef, I.; Lugtenburg, J.; Lagarias, J.C.; Mathies, R.A., Probing the photoreaction mechanism of phytochrome through analysis of resonance raman vibrational spectra of recombinant analogues. *Biochemistry* **2000,** *39* (10), 2667.

10. Gordeliy, V.I.; Labahn, J.; Moukhametzianov, R.; Efremov, R.; Granzin, J.; Schlesinger, R.; Buldt, G.; Savopol, T.; Scheidig, A.J.; Klare, J.P.; Engelhard, M., Molecular basis of transmembrane signalling by sensory rhodopsin ii-transducer complex. *Nature* **2002,** *419* (6906), 484.

11. Spudich, J.L.; Luecke, H., Sensory rhodopsin ii: Functional insights from structure. *Curr. Opin. Struct. Biol.* **2002,** *12* (4), 540.

12. Wegener, A.A.; Klare, J.P.; Engelhard, M.; Steinhoff, H.J., Structural insights into the early steps of receptor-transducer signal transfer in archaeal phototaxis. *Embo Journal* **2001,** *20* (19), 5312.

13. Haupts, U.; Tittor, J.; Oesterhelt, D., Closing in on bacteriorhodopsin: Progress in understanding the molecule. *Annu. Rev. Biophys. Biomolec. Struct.* **1999,** *28*, 367.

14. Lanyi, J.K., Molecular mechanism of ion transport in bacteriorhodopsin: Insights from crystallographic, spectroscopic, kinetic, and mutational studies. *Journal of Physical Chemistry B* **2000,** *104* (48), 11441.

15. Chen, E.F.; Lapko, V.N.; Song, P.S.; Kliger, D.S., Dynamics of the n-terminal alpha-helix unfolding in the photoreversion reaction of phytochrome a. *Biochemistry* **1997,** *36* (16), 4903.

16. Smith, E.; Dent, G., *Modern raman spectroscopy: A practical approach*. John Wiley and Sons, Ltd: West Sussex, England, 2005; p 210.

17. Smekal, A., Zur quantentheorie der dispersion. *Naturwissenschaften* **1923,** *11* (43), 873.

18. Raman, C.V.; Krishnan, K.S., A new type of secondary radiation. *Nature* **1928,** *121* (3048), 501.

19. Http://carbon.Cudenver.Edu/public/chemistry/classes/chem4538/raman.Htm.

20. Gardiner, D.J.; Graves, P.R., *Practical raman spectroscopy*. Springer-Verlag: Berlin & New York, 1989; p 157.

21. Kalkan, A.K.; Fonash, S.J., Laser-activated surface-enhanced raman scattering substrates capable of single molecule detection. *Applied Physics Letters* **2006,** *89* (23).

22. Meyer, T.E.; Yakali, E.; Cusanovich, M.A.; Tollin, G., Properties of a water-soluble, yellow protein isolated from a halophilic phototrophic bacterium that has photochemical activity analogous to sensory rhodopsin. *Biochemistry* **1987,** *26* (2), 418.

23. Xie, A.H.; Kelemen, L.; Hendriks, J.; White, B.J.; Hellingwerf, K.J.; Hoff, W.D., Formation of a new buried charge drives a large-amplitude protein quake in photoreceptor activation. *Biochemistry* **2001,** *40* (6), 1510.

24. Hoff, W.D.; Dux, P.; Hard, K.; Devreese, B.; Nugterenroodzant, I.M.; Crielaard, W.; Boelens, R.; Kaptein, R.; Vanbeeumen, J.; Hellingwerf, K.J., Thiol ester-linked p-coumaric acid as a new photoactive prosthetic group in a protein with rhodopsin-like photochemistry. *Biochemistry* **1994,** *33* (47), 13959.

25. Baca, M.; Borgstahl, G.E.O.; Boissinot, M.; Burke, P.M.; Williams, D.R.; Slater, K.A.; Getzoff, E.D., Complete chemical-structure of photoactive yellow protein - novel

thioester-linked 4-hydroxycinnamyl chromophore and photocycle chemist. *Biochemistry* **1994,** *33* (48), 14369.

26. Hoff, W.D.; Vanstokkum, I.H.M.; Vanramesdonk, H.J.; Vanbrederode, M.E.; Brouwer, A.M.; Fitch, J.C.; Meyer, T.E.; Vangrondelle, R.; Hellingwerf, K.J., Measurement and global analysis of the absorbency changes in the photocycle of the photoactive yellow protein from ectothiorhodospira-halophila. *Biophysical Journal* **1994,** *67* (4), 1691.

27. Vanbeeumen, J.J.; Devreese, B.V.; Vanbun, S.M.; Hoff, W.D.; Hellingwerf, K.J.; Meyer, T.E.; McRee, D.E.; Cusanovich, M.A., Primary structure of a photoactive yellow protein from the phototrophic bacterium ectothiorhodospira-halophila, with evidence for the mass and the binding-site of the chromophore. *Protein Science* **1993,** *2* (7), 1114.

28. Borgstahl, G.E.O.; Williams, D.R.; Getzoff, E.D., 1.4 angstrom structure of photoactive yellow protein, a cytosolic photoreceptor - unusual fold, active-site, and chromophore. *Biochemistry* **1995,** *34* (19), 6278.

29. Kim, M.; Mathies, R.A.; Hoff, W.D.; Hellingwerf, K.J., Resonance raman evidence that the thioester-linked 4-hydroxycinnamyl chromophore of photoactive yellow protein is deprotonated. *Biochemistry* **1995,** *34* (39), 12669.

30. Xie, A.H.; Hoff, W.D.; Kroon, A.R.; Hellingwerf, K.J., Glu46 donates a proton to the 4-hydroxycinnamate anion chromophore during the photocycle of photoactive yellow protein. *Biochemistry* **1996,** *35* (47), 14671.

31. Genick, U.K.; Borgstahl, G.E.O.; Ng, K.; Ren, Z.; Pradervand, C.; Burke, P.M.; Srajer, V.; Teng, T.Y.; Schildkamp, W.; McRee, D.E.; Moffat, K.; Getzoff, E.D., Structure of a protein photocycle intermediate by millisecond time-resolved crystallography. *Science* **1997,** *275* (5305), 1471.

32. Groenhof, G.; Lensink, M.F.; Berendsen, H.J.C., Exploring the photoactive yellow protein photocycle by combining quantum mechanics and molecular dynamics. *Journal of Molecular Graphics & Modelling* **1998,** *16* (4-6), 277.

33. Groenhof, G.; Schafer, L.V.; Boggio-Pasqua, M.; Grubmuller, H.; Robb, M.A., Arginine52 controls the photoisomerization process in photoactive yellow protein. *Journal of the American Chemical Society* **2008,** *130* (11), 3250.

34. Groenhof, G.; Lensink, M.F.; Berendsen, H.J.C.; Snijders, J.G.; Mark, A.E., Signal transduction in the photoactive yellow protein. I. Photon absorption and the isomerization of the chromophore. *Proteins-Structure Function and Genetics* **2002,** *48* (2), 202.

35. Groenhof, G.; Lensink, M.F.; Berendsen, H.J.C.; Mark, A.E., Signal transduction in the photoactive yellow protein. Ii. Proton transfer initiates conformational changes. *Proteins-Structure Function and Genetics* **2002,** *48* (2), 212.

36. Groenhof, G.; Bouxin-Cademartory, M.; Hess, B.; De Visser, S.P.; Berendsen, H.J.C.; Olivucci, M.; Mark, A.E.; Robb, M.A., Photoactivation of the photoactive yellow protein: Why photon absorption triggers a trans-to-cis Isomerization of the chromophore in the protein. *Journal of the American Chemical Society* **2004,** *126* (13), 4228.

37. Sergi, A.; Gruning, M.; Ferrario, M.; Buda, F., Density functional study of the photoactive yellow protein's chromophore. *Journal of Physical Chemistry B* **2001,** *105* (19), 4386.

38. Unno, M.; Kumauchi, M.; Sasaki, J.; Tokunaga, F.; Yamauchi, S., Resonance raman spectroscopy and quantum chemical calculations reveal structural changes in the active site of photoactive yellow protein. *Biochemistry* **2002,** *41* (17), 5668.

39. Borucki, B.; Devanathan, S.; Otto, H.; Cusanovich, M.A.; Tollin, G.; Heyn, M.P., Kinetics of proton uptake and dye binding by photoactive yellow protein in wild type and in the e46q and e46a mutants. *Biochemistry* **2002,** *41* (31), 10026.

40. Lee, B.C.; Pandit, A.; Croonquist, P.A.; Hoff, W.D., Folding and signaling share the same pathway in a photoreceptor. *Proceedings of the National Academy of Sciences of the United States of America* **2001,** *98* (16), 9062.

41. Derix, N.M.; Wechselberger, R.W.; van der Horst, M.A.; Hellingwerf, K.J.; Boelens, R.; Kaptein, R.; van Nuland, N.A.J., Lack of negative charge in the e46q mutant of photoactive yellow protein prevents partial unfolding of the blue-shifted intermediate. *Biochemistry* **2003,** *42* (49), 14501.

42. Vreede, J.; Crielaard, W.; Hellingwerf, K.J.; Bolhuis, P.G., Predicting the signaling state of photoactive yellow protein. *Biophysical Journal* **2005,** *88* (5), 3525.

43. Vreede, J.; Hellingwerf, K.J.; Bolhuis, P.G., Helix formation is a dynamical bottleneck in the recovery reaction of photoactive yellow protein. *Proteins* **2008,** *72* (1), 136.

44. Hendriks, J.; van Stokkum, I.H.M.; Crielaard, W.; Hellingwerf, K.J., Kinetics of and intermediates in a photocycle branching reaction of the photoactive yellow protein from ectothiorhodospira halophila. *Febs Letters* **1999,** *458* (2), 252.

45. Hendriks, J.; Hellingwerf, K.J., Ph dependence of the photoactive yellow protein photocycle recovery reaction reveals a new late photocycle intermediate with a deprotonated chromophore. *J Biol Chem* **2009,** *284* (8), 5277.

46. Unno, M.; Kumauchi, M.; Sasaki, J.; Tokunaga, F.; Yamauchi, S., Assignment of resonance raman spectrum of photoactive yellow protein in its long-lived blue-shifted intermediate. *Journal of Physical Chemistry B* **2003,** *107* (12), 2837.

47. Unno, M.; Kumauchi, M.; Tokunaga, F.; Yamauchi, S., Vibrational assignment of the 4-hydroxycinnamyl chromophore in photoactive yellow protein. *Journal of Physical Chemistry B* **2007,** *111* (10), 2719.

48. Pan, D.H.; Philip, A.; Hoff, W.D.; Mathies, R.A., Time-resolved resonance raman structural studies of the pb ' intermediate in the photocycle of photoactive yellow protein. *Biophysical Journal* **2004,** *86* (4), 2374.

49. Adesokan, A.A.; Pan, D.H.; Fredj, E.; Mathies, R.A.; Gerber, R.B., Anharmonic vibrational calculations modeling the raman spectra of intermediates in the photoactive yellow protein (pyp) photocycle. *Journal of the American Chemical Society* **2007,** *129* (15), 4584.

50. Kang, Z.; Xie, A., Oklahoma State University: Stillwater, 2008.

51. Kort, R.; Vonk, H.; Xu, X.; Hoff, W.D.; Crielaard, W.; Hellingwerf, K.J., Evidence for trans-cis isomerization of the p-coumaric acid chromophore as the photochemical basis of the photocycle of photoactive yellow protein. *Febs Letters* **1996,** *382* (1-2), 73.

52. Cusanovich, M.A.; Meyer, T.E., Photoactive yellow protein: A prototypic pas domain sensory protein and development of a common signaling mechanism. *Biochemistry* **2003,** *42* (17), 4759.

53. Hoff, W.D.; Kwa, S.L.S.; Vangrondelle, R.; Hellingwerf, K.J., Low-temperature absorbency and fluorescence spectroscopy of the photoactive yellow protein from ectothiorhodospira-halophila. *Photochemistry and Photobiology* **1992,** *56* (4), 529.

54. Ng, K.; Getzoff, E.D.; Moffat, K., Optical studies of a bacterial photoreceptor protein, photoactive yellow protein, in single-crystals. *Biochemistry* **1995,** *34* (3), 879.

55. Nie, S.M.; Emory, S.R., Probing single molecules and single nanoparticles by surface-enhanced raman scattering. *Science* **1997,** *275* (5303), 1102.

56. Fleischmann, M.; Hendra, P.J.; McQuillan, A.J., Raman spectra of pyridine adsorbed at a silver electrode. *Chemical Physics Letters* **1974,** *26* (2), 163.

57. Jeanmaire, D.L.; Vanduyne, R.P., Surface raman spectroelectrochemistry .1. Heterocyclic, aromatic, and aliphatic-amines adsorbed on anodized silver electrode. *Journal of Electroanalytical Chemistry* **1977,** *84* (1), 1.

58. Albrecht, M.G.; Creighton, J.A., Anomalously intense raman spectra of pyridine at a silver electrode. *Journal of the American Chemical Society* **1977,** *99* (15), 5215.

59. Xu, H.X.; Bjerneld, E.J.; Kall, M.; Borjesson, L., Spectroscopy of single hemoglobin molecules by surface enhanced raman scattering. *Physical Review Letters* **1999,** *83* (21), 4357.

60. Talley, C.E.; Jackson, J.B.; Oubre, C.; Grady, N.K.; Hollars, C.W.; Lane, S.M.; Huser, T.R.; Nordlander, P.; Halas, N.J., Surface-enhanced raman scattering from individual au nanoparticles and nanoparticle dimer substrates. *Nano Letters* **2005,** *5* (8), 1569.

61. Kneipp, K.; Wang, Y.; Kneipp, H.; Perelman, L.T.; Itzkan, I.; Dasari, R.; Feld, M.S., Single molecule detection using surface-enhanced raman scattering (sers). *Physical Review Letters* **1997,** *78* (9), 1667.

62. Otto, A., On the contribution of charge-transfer excitations to sers. *Journal of Electron Spectroscopy and Related Phenomena* **1983,** *29* (JAN), 329.

63. Otto, A.; Mrozek, I.; Grabhorn, H.; Akemann, W., Surface-enhanced raman-scattering. *Journal of Physics-Condensed Matter* **1992,** *4* (5), 1143.

64. Sinther, M.; Pucci, A.; Otto, A.; Priebe, A.; Diez, S.; Fahsold, G., Enhanced infrared absorption of sers-active lines of ethylene on cu. *Physica Status Solidi a-Applied Research* **2001,** *188* (4), 1471.

65. Otto, A., What is observed in single molecule sers, and why? *Journal of Raman Spectroscopy* **2002,** *33* (8), 593.

66. Kneipp, K.; Kneipp, H., Surface enhanced raman scattering - a tool for ultrasensitive trace analysis. *Canadian Journal of Analytical Sciences and Spectroscopy* **2003,** *48* (2), 125.

67. Baker, G.A.; Moore, D.S., Progress in plasmonic engineering of surface-enhanced raman-scattering substrates toward ultra-trace analysis. *Analytical and Bioanalytical Chemistry* **2005,** *382* (8), 1751.

68. Angebranndt, M.J.; Winefordner, J.D., Surface enhanced raman-spectroscopy on copper hydrosols. *Talanta* **1992,** *39* (6), 569.

69. Laserna, J.J., Combining fingerprinting capability with trace analytical detection - surface-enhanced raman-spectrometry. *Analytica Chimica Acta* **1993,** *283* (1), 607.

70. Vodinh, T., Sers chemical sensors and biosensors - new tools for environmental and biological analysis. *Sensors and Actuators B-Chemical* **1995,** *29* (1-3), 183.

71. Nie, S.M.; Emory, S.R., Single-molecule detection and spectroscopy by surface-enhanced raman scattering. *Abstracts of Papers of the American Chemical Society* **1997,** *213*, 177.

72. Michaels, A.M.; Nirmal, M.; Brus, L.E., Surface enhanced raman spectroscopy of individual rhodamine 6g molecules on large ag nanocrystals. *Journal of the American Chemical Society* **1999,** *121* (43), 9932.

73. Michaels, A.M.; Jiang, J.; Brus, L., Ag nanocrystal junctions as the site for surface-enhanced raman scattering of single rhodamine 6g molecules. *Journal of Physical Chemistry B* **2000,** *104* (50), 11965.

74. Bosnick, K.A.; Jiang, J.; Brus, L.E., Fluctuations and local symmetry in single-molecule rhodamine 6g raman scattering on silver nanocrystal aggregates. *Journal of Physical Chemistry B* **2002,** *106* (33), 8096.

75. Bjerneld, E.J.; Johansson, P.; Käll, M., Single molecule vibrational fine-structure of tyrosine adsorbed on ag nano-crystals. *Single Molecules* **2000,** *3*, 10.

76. Xu, H.X.; Aizpurua, J.; Kall, M.; Apell, P., Electromagnetic contributions to single-molecule sensitivity in surface-enhanced raman scattering. *Physical Review E* **2000,** *62* (3), 4318.

77. Haslett, T.L.; Tay, L.; Moskovits, M., Can surface-enhanced raman scattering serve as a channel for strong optical pumping? *Journal of Chemical Physics* **2000,** *113* (4), 1641.

78. Fromm, D.P.; Sundaramurthy, A.; Kinkhabwala, A.; Schuck, P.J.; Kino, G.S.; Moerner, W.E., Exploring the chemical enhancement for surface-enhanced raman scattering with au bowtie nanoantennas. *Journal of Chemical Physics* **2006,** *124* (6), 061101.

79. Habuchi, S.; Dedecker, P.; Hotta, J.I.; Flors, C.; Ando, R.; Mizuno, H.; Miyawaki, A.; Hofkens, J., Photo-induced protonation/deprotonation in the gfp-like fluorescent protein dronpa: Mechanism responsible for the reversible photoswitching. *Photochemical & Photobiological Sciences* **2006,** *5* (6), 567.

80. Habuchi, S.; Cotlet, M.; Gronheid, R.; Dirix, G.; Michiels, J.; Vanderleyden, J.; Schryver, F.C.D.; Hofkens, J., Single-molecule surface enhanced resonance raman spectroscopy of the enhanced green fluorescent protein. *Journal of American Chemical Society* **2003,** *125*, 8446.

81. Wang, Z.J.; Pan, S.L.; Krauss, T.D.; Du, H.; Rothberg, L.J., The structural basis for giant enhancement enabling single-molecule raman scattering. *Proceedings of the National Academy of Sciences of the United States of America* **2003,** *100* (15), 8638.

82. Kalkan, A.K.; Fonash, S.J., Electroless synthesis of ag nanoparticles on deposited nanostructured si films. *Journal of Physical Chemistry B* **2005,** *109* (44), 20779.

83. Kreibig, U.; Vollmer, M., *Optical properties of metal clusters*. Springer-Verlag: Berlin, 1995; Vol. 25, p 532.

84. de Waele, R.; Koenderink, A.F.; Polman, A., Tunable nanoscale localization of energy on plasmon particle arrays. *Nano Letters* **2007,** *7* (7), 2004.

85. Knight, M.W.; Grady, N.K.; Bardhan, R.; Hao, F.; Nordlander, P.; Halas, N.J., Nanoparticle-mediated coupling of light into a nanowire. *Nano Letters* **2007,** *7* (8), 2346.

86. Singhal, K.; Bhatt, K.; Kang, Z.; Hoff, W.; Xie, A.; Kalkan, A.K.: Structural dynamics of a single photoreceptor protein molecule monitored with surface-enhanced raman scattering substrates, in *Functional Plasmonics and Nanophotonics*, edited by Maier, S.; Kawata, S. (Mater. Res. Soc. Symp. Proc. *Volume 1077E*, Warrendale, PA, **2008**), 1077.

87. Moskovits, M.; Suh, J.S., Surface selection-rules for surface-enhanced raman-spectroscopy - calculations and application to the surface-enhanced raman-spectrum of phthalazine on silver. *Journal of Physical Chemistry* **1984,** *88* (23), 5526.

88. Lombardi, J.R.; Birke, R.L., A unified approach to surface-enhanced raman spectroscopy. *Journal of Physical Chemistry C* **2008,** *112* (14), 5605.

89. Kort, R.; Crielaard, W.; Hellingwerf, K.J., Photosensing in eubacteria: Trans/cis isomerization of the chromophore of pyp. *Progress in Biophysics & Molecular Biology* **1996,** *65*, PA303.

90. Genick, U.K.; Soltis, S.M.; Kuhn, P.; Canestrelli, I.L.; Getzoff, E.D., Structure at 0.85 angstrom resolution of an early protein photocycle intermediate. *Nature* **1998,** *392* (6672), 206.

91. Xie, A.; Hoff, W.D.; Hellingwerr, K.J., Activation of photoactive yellow protein by photochemical chromophore double/single bond coisomerization. *Biophysical Journal* **1998,** *74* (2), A291.

92. Brudler, R.; Rammelsberg, R.; Woo, T.T.; Getzoff, E.D.; Gerwert, K., Structure of the i-1 early intermediate of photoactive yellow protein by ftir spectroscopy. *Nature Structural Biology* **2001,** *8* (3), 265.

93. Thompson, M.J.; Bashford, D.; Noodleman, L.; Getzoff, E.D., Photoisomerization and proton transfer in photoactive yellow protein. *Journal of the American Chemical Society* **2003,** *125* (27), 8186.

94. Unno, M.; Kumauchi, M.; Hamada, N.; Tokunaga, F.; Yamauchi, S., Resonance raman evidence for two conformations involved in the I intermediate of photoactive yellow protein. *Journal of Biological Chemistry* **2004,** *279* (23), 23855.

APPENDICES

A. Cressington 208 High Vacuum Turbo Carbon Coater

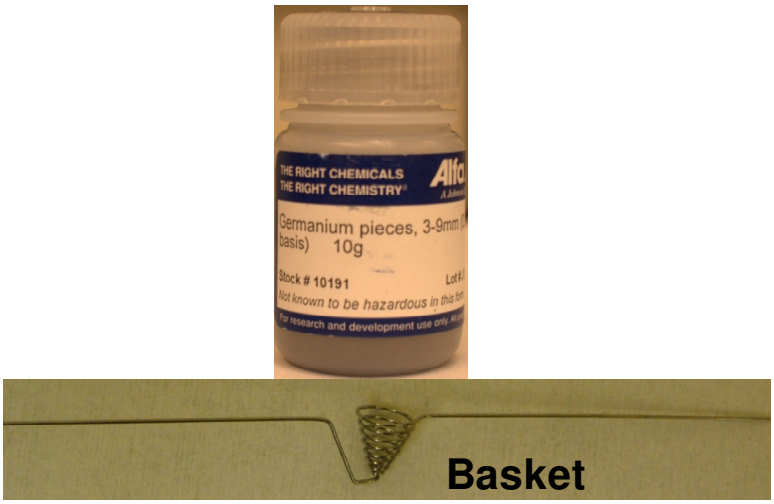

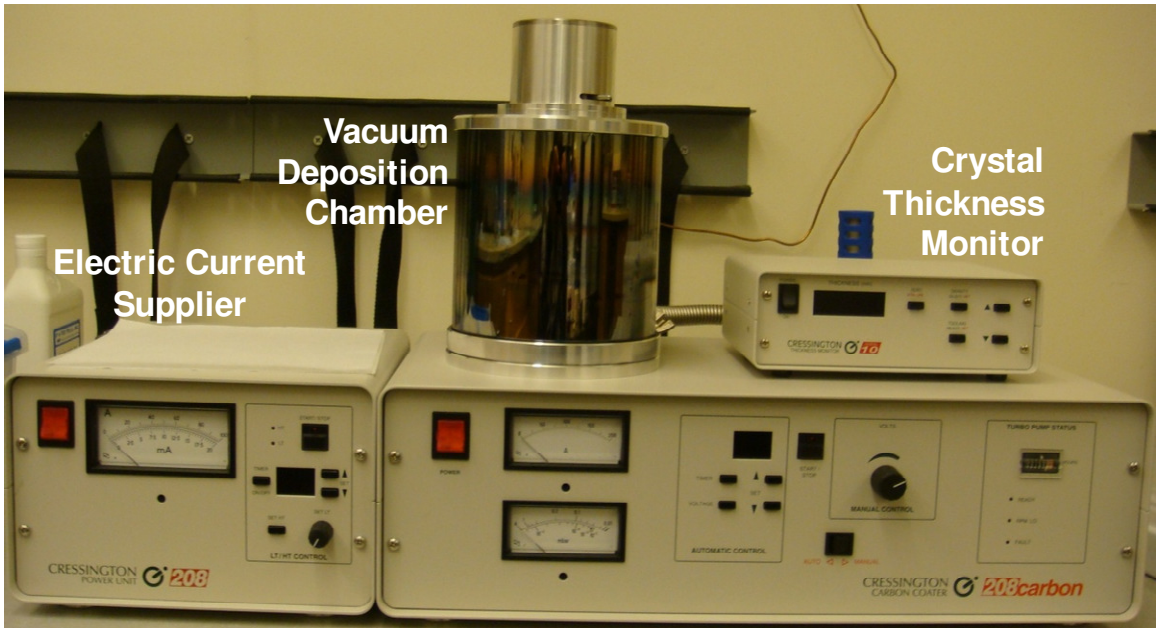

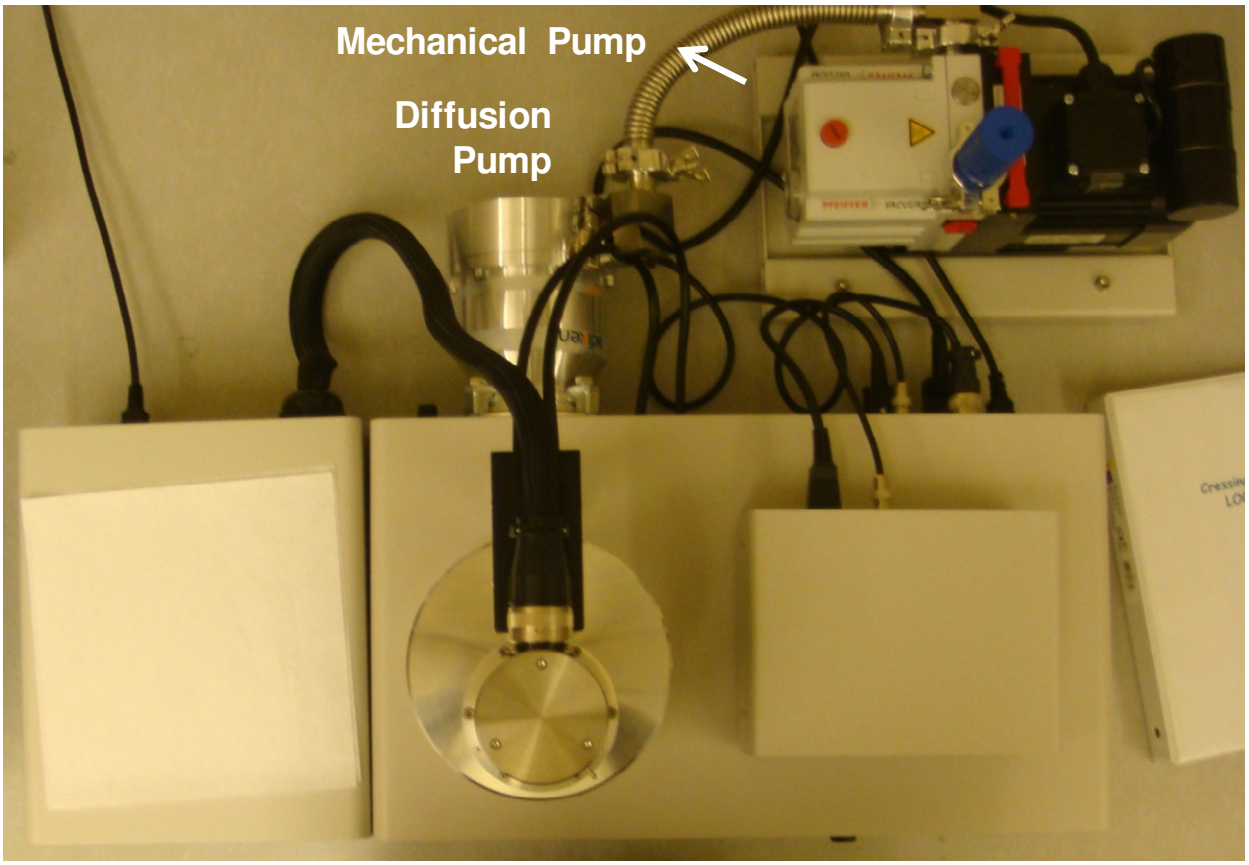
Mechanical Pump
Diffusion
Pump

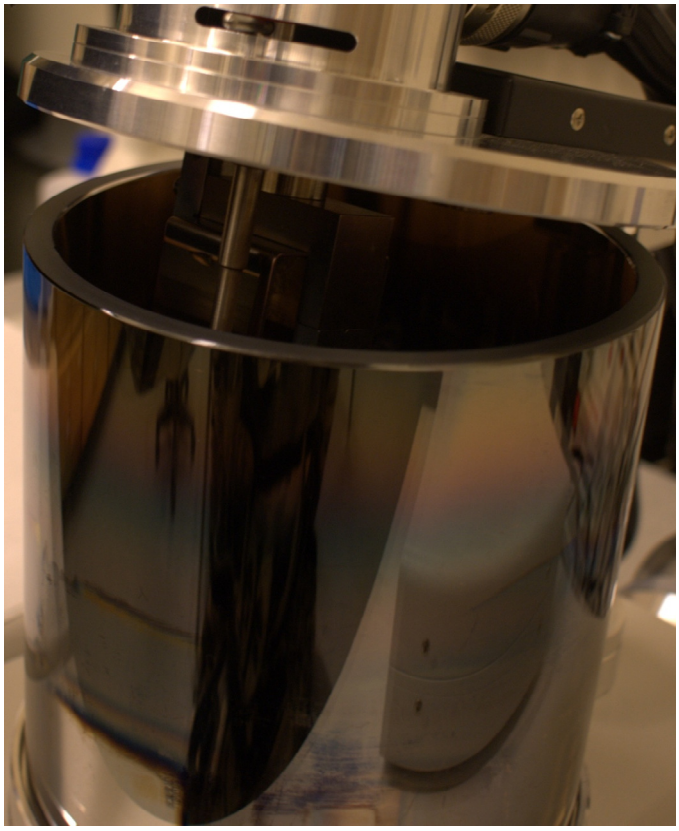

B. UV-Vis Spectroscopy

UV-Vis Spectrometer

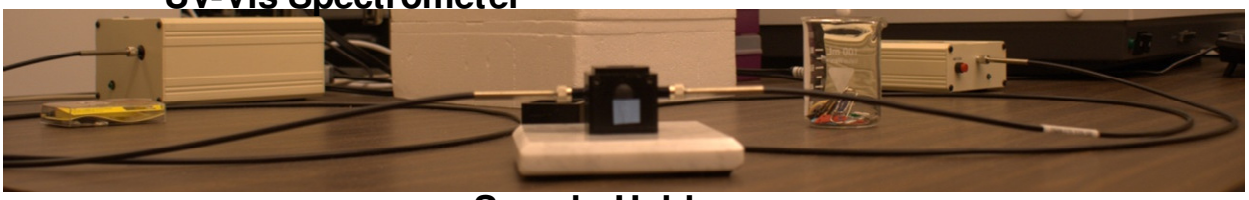

Sample Holder

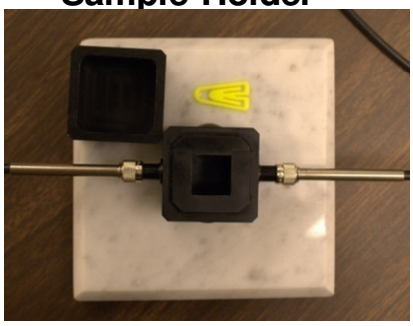

Sample in Vial

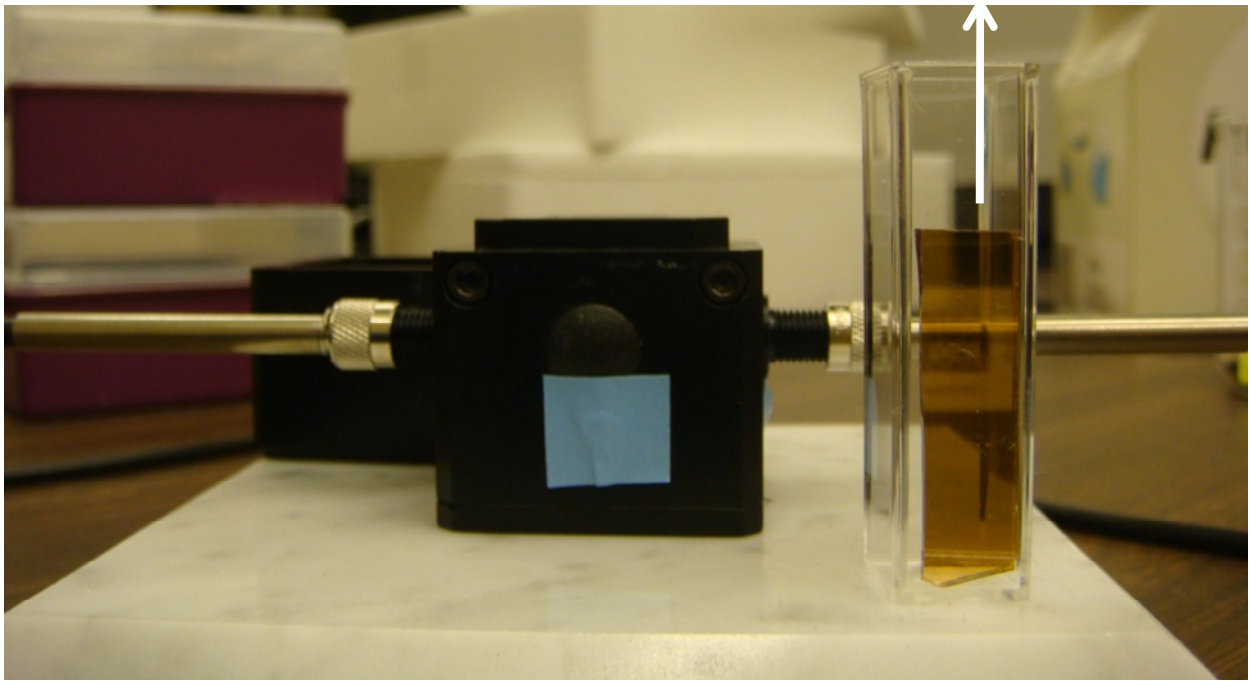

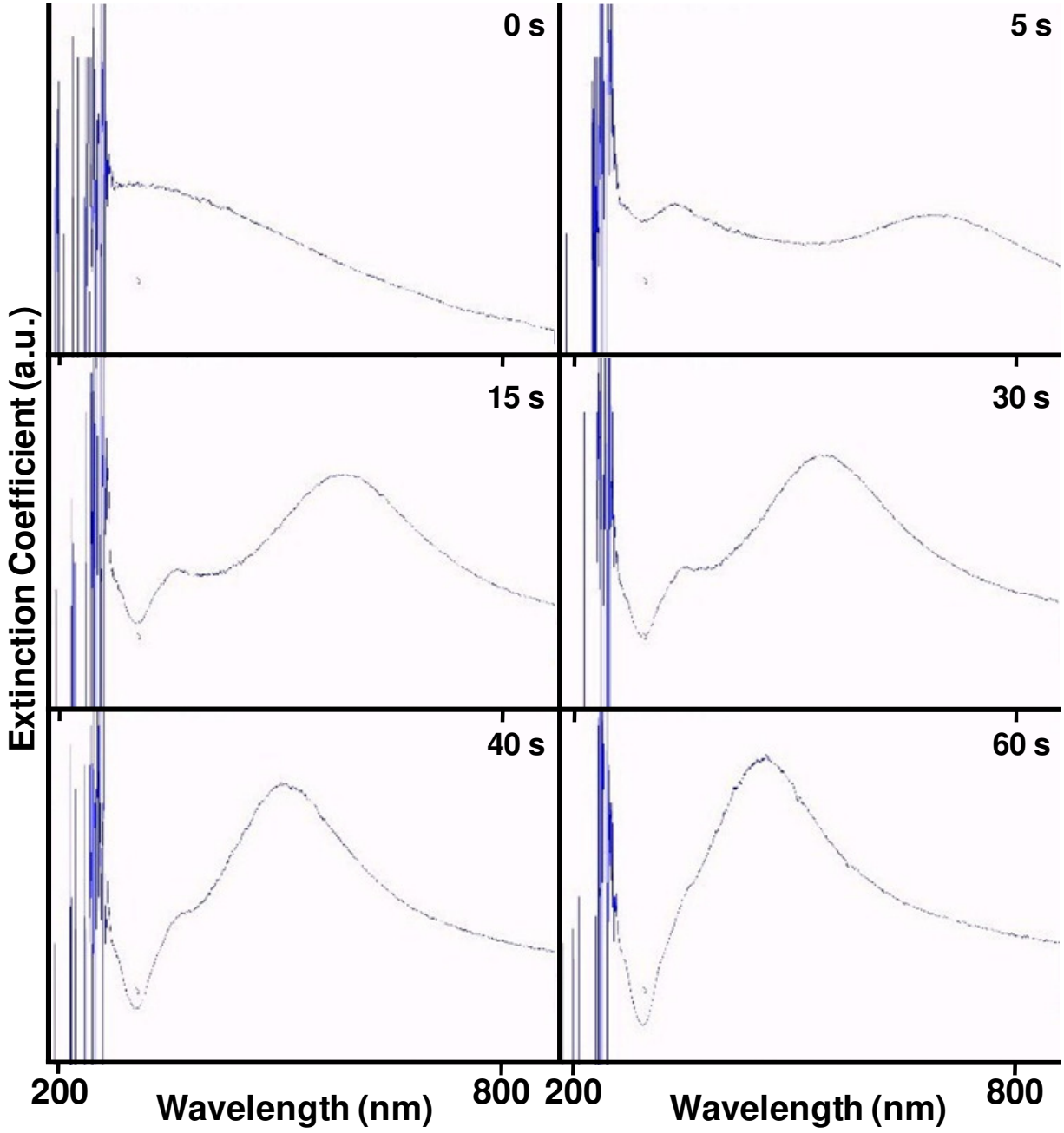

UV-Vis spectra of silver nanoparticle SERS substrates at different immersion times of thin (4-10 nm) germanium film in $AgNO_3$ solution. The progress of plasmon band shows the change in size and distribution of nanoparticles with immersion time.

C. Spotting the Analyte

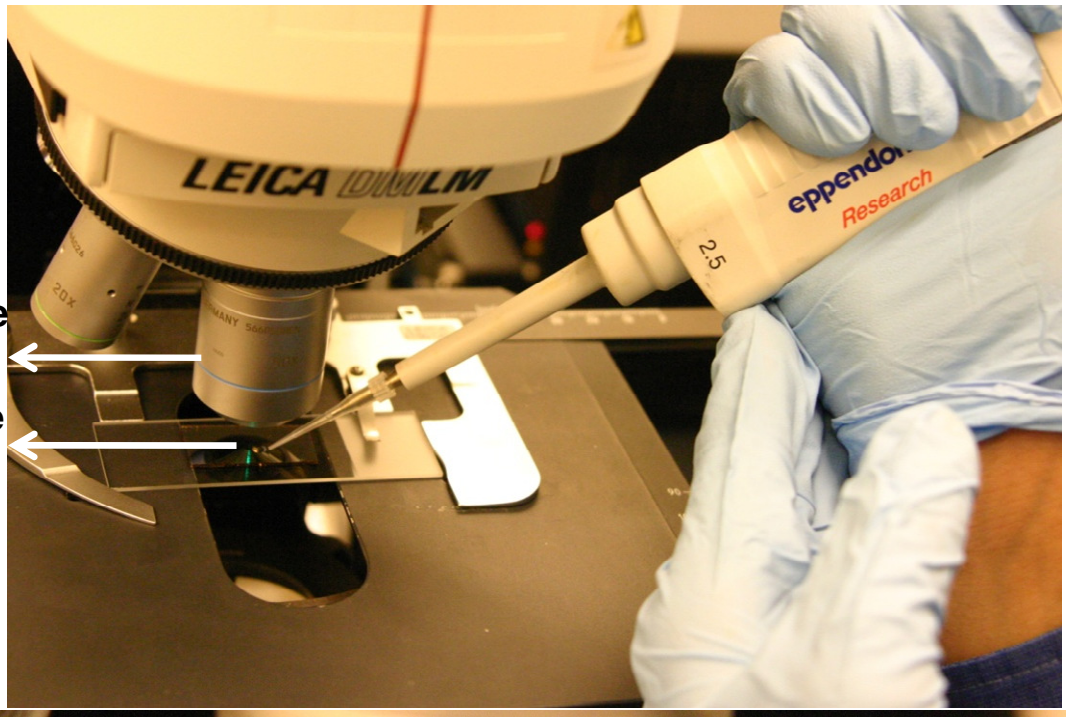

Objective lens

Analyte aliquot

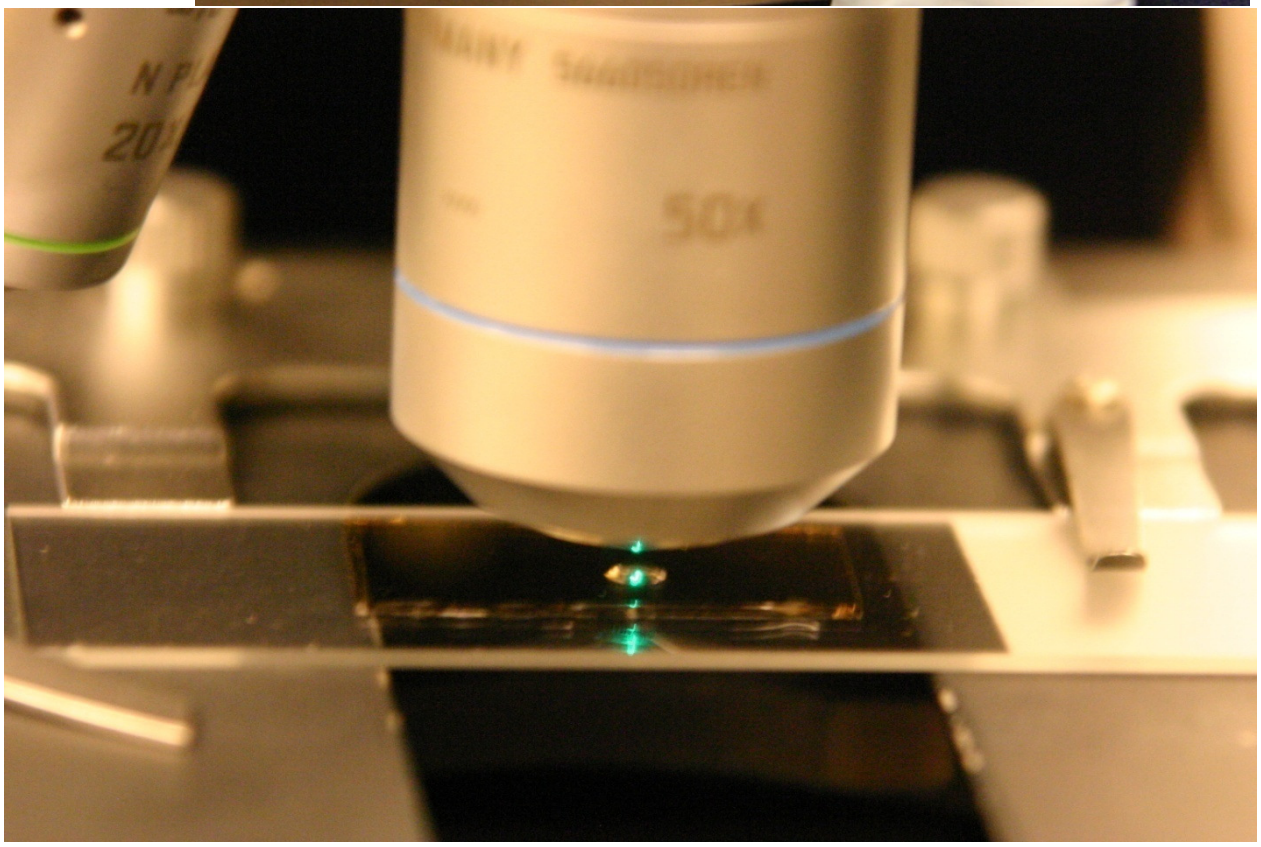

D. Renishaw RM 1000 system (with a CCD detector)

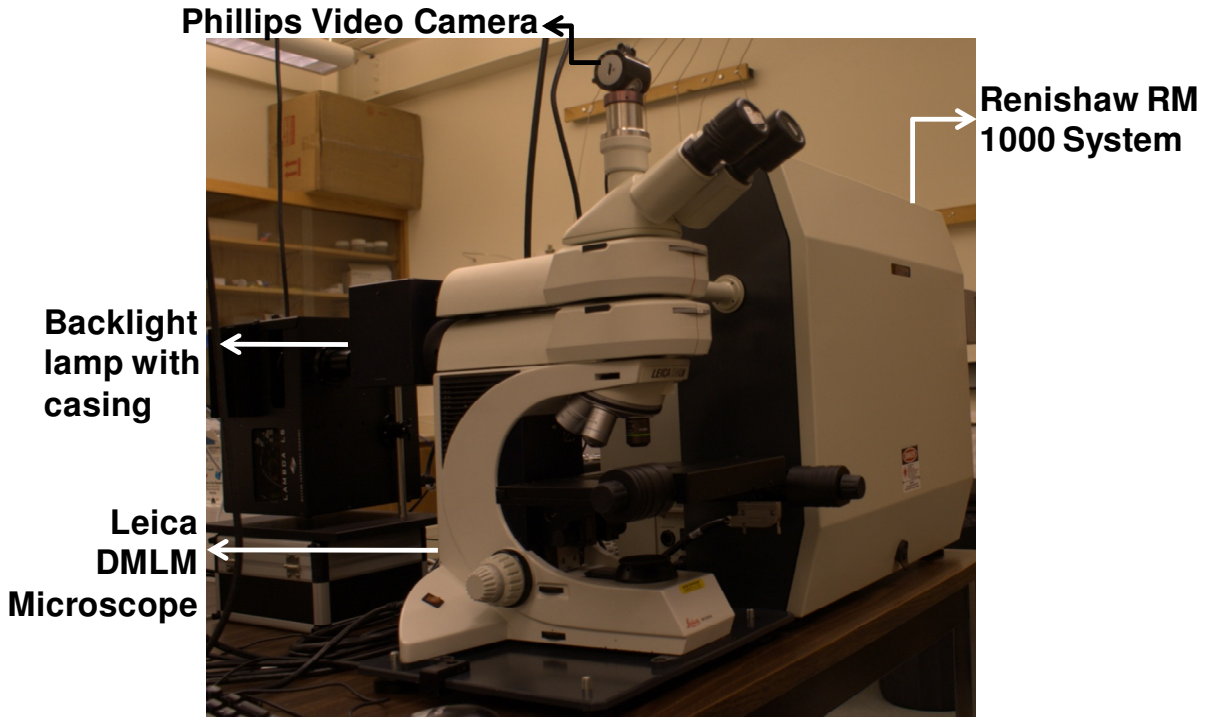

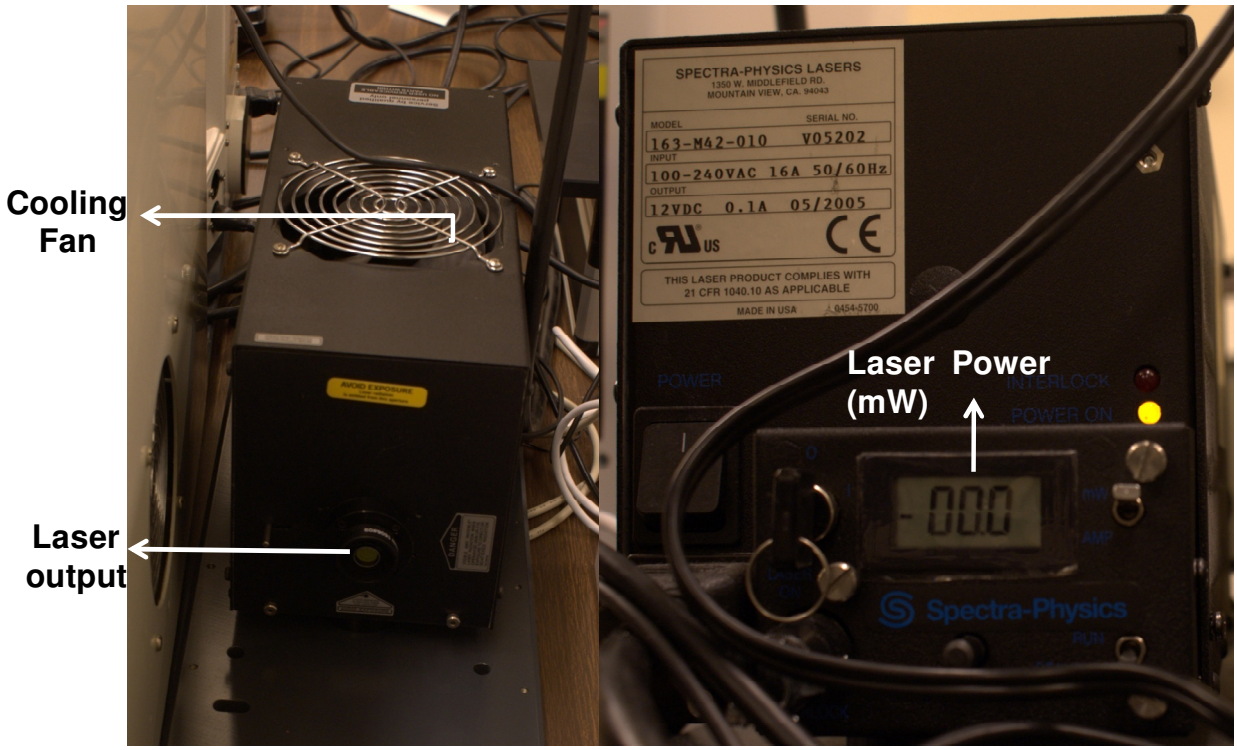

VITA

Kushagra Singhal

Candidate for the Degree of Master of Science

Title of Study: STRUCTURAL DYNAMICS OF SINGLE PHOTOACTIVE YELLOW PROTEIN MOLECULES MONITORED WITH SURFACE ENHANCED RAMAN SCATTERING SUBSTRATES

Major Field: Mechanical Engineering

Personal Data:
Sex: Male
DOB: 07/18/1985
Hometown: Agra, India

Education:

- Completed the requirements for the Master of Science in Mechanical Engineering at Oklahoma State University, Stillwater, Oklahoma in May, 2009.
- Completed the requirements for the Bachelor of Technology in Mechanical Engineering at Indian Institute of Technology, Kanpur, India in June, 2006.

Experience:

- Graduate Research Assistant, MAE, OSU Stillwater (Jan 2007 – Dec 2008)
- Lead Graduate Teaching Assistant, MAE, OSU Tulsa (Aug 2008 – Dec 2008)
- Lead Graduate Teaching Assistant, MAE, OSU Stillwater (Aug 2006 – Dec 2007)
- Visiting Researcher, University of Edinburgh, UK (May 2005 – July 2005)

Professional Memberships:

- Member of ASME, OSU chapter.
- Member of Materials Research Society.
- Member of Phi Kappa Phi honorary society.

Name: Kushagra Singhal
Institution: Oklahoma State University

Date of Degree: May, 2009
Location: Stillwater, Oklahoma

Title of Study: STRUCTURAL DYNAMICS OF SINGLE PHOTOACTIVE YELLOW PROTEIN MOLECULES MONITORED WITH SURFACE ENHANCED RAMAN SCATTERING SUBSTRATES

Pages in Study: 80
Major Field: Mechanical Engineering

Candidate for the Degree of Master of Science

Scope and Method of Study: Photoactive Yellow Protein (PYP) is a small blue-light (446 nm) photoreceptor protein that actuates the avoidance response in its host organism *Halorhodospira halophila*. We report our Surface-enhanced Raman Scattering (SERS) study on PYP at the single molecule level using "nanometal-on-semiconductor" SERS substrates under 514 nm excitation. The silver nanoparticle (AgNP) SERS substrates were prepared by redox technique on thin germanium films (coated on glass slides).

Findings and Conclusions: Single molecule SERS spectra were captured in terms of temporal appearance (jumps) of sharp discernable Raman peaks with significant spectral shifts/fluctuations. We associate these jumps with single PYP molecules diffusing in/out of high enhancement SERS sites ("hot-spots") on our SERS substrates. The single molecule spectra record the conformational changes in single PYP molecules during the scan integration time. These structural changes are homologous to the conformational steps that are instrumental in the photocycle of PYP. This observation suggests that single PYP molecules exhibit structural changes at the high enhancement sites during photo-excitation, suggesting a possibility of surface-enhanced photocycle in single PYP molecules.

At the single-molecule level, SERS yields well-resolved peaks, some of which were not reported earlier. These new modes along with variations in chemisorption configuration of PYP on AgNPs result in a broad spectrum upon statistical averaging of single-molecule spectra. Certain mutually exclusive peak pairs (and groups) have been identified, that can elucidate the molecular structure and configuration using the SERS selection rules. These observations indicate the significance of single-molecule SERS studies in allowing us to observe and analyze modes that are otherwise averaged out by high-enhancement modes in ensemble-averaged SERS. Thus, the present work establishes a framework for future analysis of the photocycle in PYP and scope for a greater insight into the biophysics of the molecule using single-molecule SERS studies with high structural sensitivity.

Dr. A. Kaan Kalkan